THESIS FOR THE DEGREE OF DOCTOR OF PHILOSOPHY (PHD)

Histones and histone modifying proteins in a biophysical aspect

by

Szabolcs Hetey

Supervisor: Dr. Lóránt Székvölgyi

UNIVERSITY OF DEBRECEN

DOCTORAL SCHOOL OF MOLECULAR CELL AND IMMUNE BIOLOGY

DEBRECEN, 2019

Table of Contents

1. ABBREVIATIONS

Act D	Actinomycin D
c-ChIP	Competition chromatin immunoprecipitation
CLSM	Confocal Laser Scanning Microscopy
COMPASS	Complex Proteins Associated with Set1
DIPG	Diffuse Intrinsic Pontine Glioma
DSB	Double-strand breaks
Ezh2	Enhancer Of Zeste Homolog 2
FCS	Fluorescence Correlation Spectroscopy
FRAP	Fluorescence Recovery After Photobleaching
GBM	Glioblastoma Multiforme
H3.3K27M	Lysine 27-to-methionine mutation of histone variant H3.3
H3K27M	Lysine 27-to-methionine mutation of histone H3
LSC	Laser Scanning Cytometry
MLL	Mixed lineage leukemia
NDR	Nucleosome depleted region
PcG	Polycomb-group proteins
PHD	Plant Homeodomain
PRC1	Polycomb Repressive Complex 1
PRC2	Polycomb Repressive Complex 2
SET	Su(var)3-9, Enhancer-of-zeste and Trithorax domain
spFRET	single-pair FRET
TrxG	Trithorax-group proteins
μpsFRET	microplate-scanning FRET

2. INTRODUCTION

2.1. Eukaryotic chromatin at the level of nucleosomes and histones

2.1.1. Basic chromatin organization

One remarkable difference between prokaryotes and eukaryotes is in their genome organization. In contrast to bacteria and archaea, eukaryotic cells fit their genetic material in a tiny microscopic space called nucleus. The DNA with structure proteins form a special complex called chromatin in this highly organized organelle and make up a nucleoprotein complex. The genomic DNA of different cells, from yeast to human, needs to be well compacted and functionally organized. The chromatin compactness and its hierarchy is considered in such processes as gene expression and its regulation.

The overall structure of the chromatin can influence protein-DNA interactions and play a role in transcriptional activation processes [1]. Through structural modifications, chromatin can be organized into a highly condensed structure known as heterochromatin that is inaccessible to chromatin binding factors. The chromatin can form a relatively uncondensed state as well referred to as euchromatin which is more accessible to these factors. Heterochromatin can be further subdivided into facultative heterochromatin and constitutive heterochromatin. Facultative heterochromatin has the potential to interconvert between euchromatic and heterochromatic states. Often it consists of genes that are expressed during development or differentiation and then it becomes silenced. In contrast, constitutive heterochromatin maintains a condensed form comprising permanently silenced genes and repetitive DNA elements, and is localized to centromeres and telomeres [2].

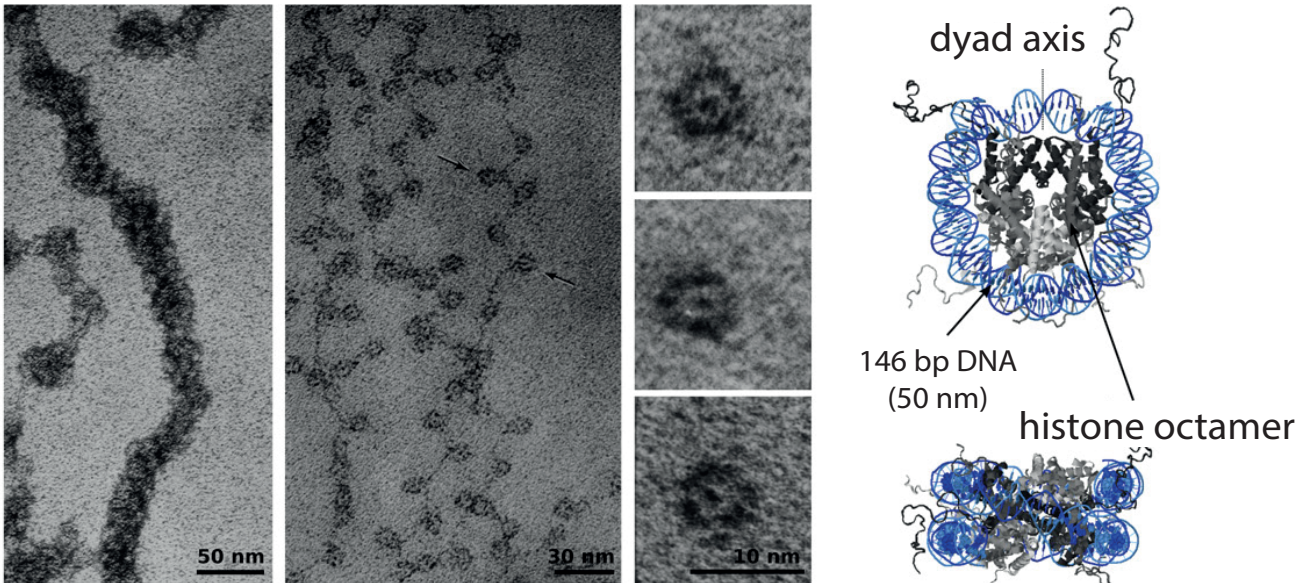

Figure 1. *Electron micrograph images and the crystal structure of the nucleosome core particle. Images show the nucleosome structure in different chromatin state. Left: low ionic chromatin spread, middle: high ionic chromatin spread, right: isolated mononucleosomes and the nucleosome core particle. Modified from ref.* [3]

In 1974, prominent studies of Kornberg and Olins & D. Olins [4], [5] proposed that the repeating units of chromatin are histone oligomers forming flexible chain with the DNA. It has been revealed that these units are nucleosomes consisting of two copies of histone H2A, H2B, H3 and H4 assembled into octamer and wrapped by 1.65 superhelical turns of 145-147 bp DNA [6], [7]. In the octamer, the core histones form an $(H3\text{-}H4)_2$ tetramer flanked by the H2A-H2B dimer. The repeating nucleosomes are connected with a 10-90 bp long linker DNA, and further assembled into higher-order structure of chromatin that is stabilized by linker histone H1. Hierarchical organization of the chromatin with the repeating nucleosomes is shown in **Figure 1**.

The structure of the nucleosome core particle (**Figure 2**) and the DNA organization around it was determined by X-ray crystallography in 1997 [6]. This study explained the interactions between the minor groove of the DNA double helix and the histone core in details. There are electrostatic interactions, hydrogen bonds and non-polar interactions between the histones and

the DNA backbone. A typical characteristics of the nucleosome core particle is the exposed histone tails passing over and between the gyres of superhelix. These flexible N-terminals of the nucleosome have regulatory roles through histone post-translational modifications and play mechanistic role in the regulation of DNA dynamics and nucleosome conformation [8].

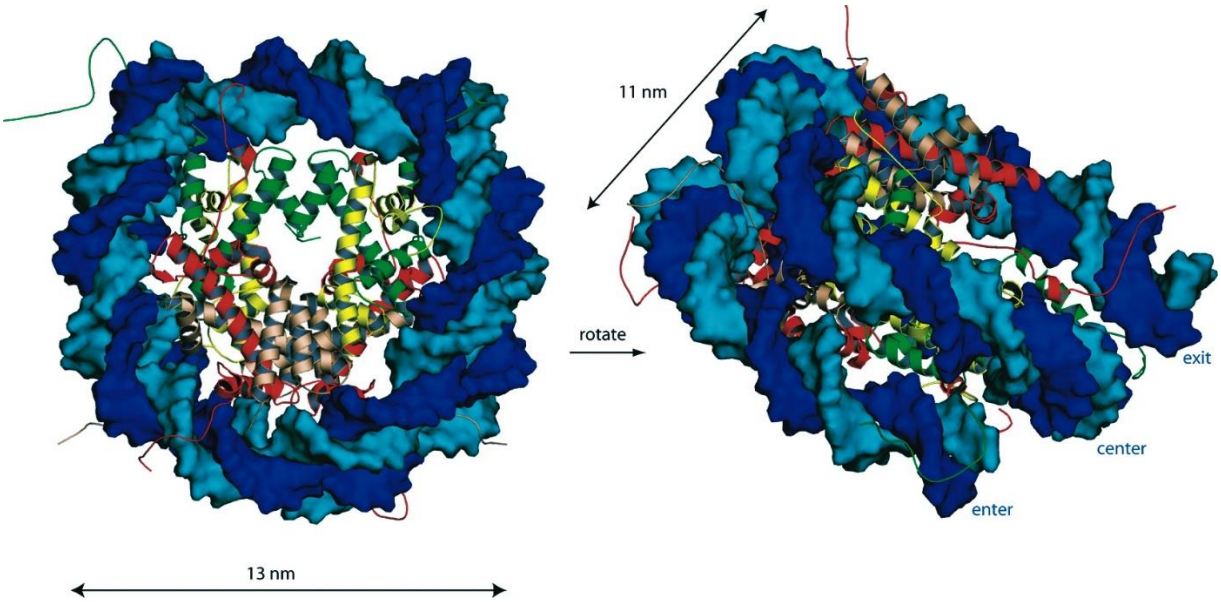

Figure 2. *Structure of the nucleosome core particle* [9]. *The DNA strands are indicated in different shades of blue. The DNA is wrapped in left-handed superhelical turns around the octamer. The enter and exit site of the DNA are labeled. H3 and H4 are in green and yellow, H2A and H2B are in red and pink.*

The organizing principle of nucleosomes follows the beads-on-a-string model, in which the repeating nucleosome particles are the beads along the length of the chromatin fiber as a string. Besides molecular crowding and DNA superhelicity nucleosomes play a special role in the condensation processes and chromatin formation as well [10]. Furthermore, they have dynamic properties in chromatin regulation and genome accessibility of DNA-templated reactions [11]. Alterations in nucleosome composition including incorporation of histone variants and post-translational modifications of histone tails change the stability and dynamics of the chromatin

[12]. Not least, mutations of histone tails involving defects in the chromatin architecture underlie tumor pathogenesis [13].

2.1.2. Investigation of the nucleosome conformation and dynamics

The nucleosomal DNA is able to unwrap temporarily from the nucleosomes. This unwrapping plays an essential role in the regulation of DNA accessibility. The criteria of this accessibility is the spontaneous fluctuations of the nucleosomes [14], [15]. The DNA breathing motion, which refers to these spontaneous local conformational fluctuations, results in transient unwrapping of nucleosomal DNA, H2A-H2B dimer releasing and thermal repositioning or sliding. In order to study these dynamics and conformations single molecule biophysics techniques have been applied in the last decades [3], [16], [17]. The advantage of these single molecule approaches is that they reveal the coexisting conformational subpopulations that would stay hidden in bulk techniques.

Förster resonance energy transfer-based (FRET) methods are widely accepted tools for measuring average distances and describing dynamics of biological molecules. In case of nucleosomes the dynamics have been quantified by FRET between dyes attached to the DNA and/or histone proteins [18], [19]. FRET analysis on single nucleosomes provides detailed information about structural diversity, particularly [20]. For instance, FRET on surface-tethered nucleosomes demonstrated spontaneous structure fluctuations [17], whereas confocal single-pair FRET (spFRET) experiments on freely diffusing single nucleosomes detected structural subpopulations under various conditions [21]. Structural intermediates of the nucleosome disassembly pathway have also been unraveled [22]–[24]. *Nurse et al.* elucidated the effect of the flexible tails of H3 and H4 histones on nucleosome structure and dynamics and concluded that the H3 N-terminal tail is involved in intranucleosomal interactions by influencing the DNA

breathing motion (**Figure 3**) and compacting the nucleosome [8]. Noteworthy, this study suggests a potential mechanism by which various combinations of histone tail modifications control or modify nucleosome accessibility.

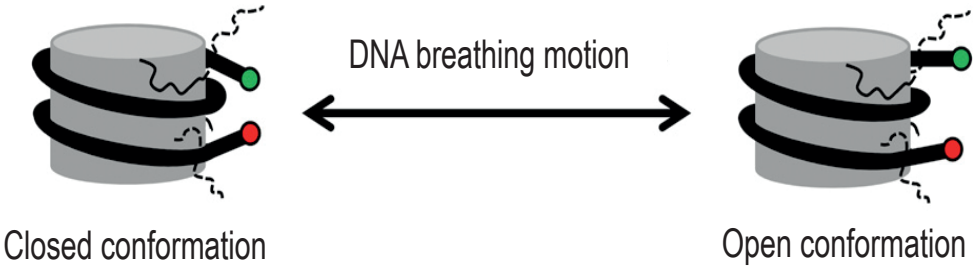

Figure 3. *In closed conformation, DNA ends are brought into close proximity and can undergo FRET. When DNA ends move apart during breathing motion, FRET signal is reduced. Modified from ref.* [8].

2.1.3. Canonical histone proteins and their variants

The existence of histones was discovered in the last millennium [25]. The first histone extraction was carried out from calf thymus under acidic conditions in 1965 and based on the subfractions of the stepwise precipitations, 5 histone subtypes were separated [26]. These subtypes are now designated as histone H1, H3, H4, H2A and H2B. Histones are highly invariant proteins across species [27] and show high stability and persist for long time in cultured cells [28].

Each of the histone proteins consists of a structured core and an unstructured tail domain. A common structural domain is the histone fold domain, which consists of three α-helices (α1, α2 and α3) connected by two short loops (L1, L2) seperating the α-helices. This structural domain promotes the heterodimerization of H2A with H2B and H3 with H4 [29]. An other structural

unit is the four-helix bundle, which helps to bring together the histone pairs [30] resulting in a stable H3-H4 tetramer core and two less stable H2A-H2B dimer [31], [32] that are altogether assembled into an octamer. Octameric nucleosomes occur in nearly all eukaryotes (dinoflagellates are exceptionals since they lost their histone proteins [33]).

Based on their proteomic and genomic characteristics, histone proteins are classified into two groups: canonical histones and histone variants. The so-called canonical histones are replication-dependent counterparts encoded by unique multigene family in metazoans [34]. Human canonical histone genes are grouped into one major *HIST1* cluster on chromosome 6 (6p21–p22) and two minor *HIST2* and *HIST3* clusters on human chromosome 1 (at 1q21 and 1q42). These genes encode mRNAs that lack introns and they possess a stem-loop sequence in the 3' end instead of a poly(A) tail [35]. The stem-loop end is conserved in all metazoans [36] and formed by endonucleolytic cleavage that is directed by a purine-rich sequence called histone downstream element. In *Saccharomyces cerevisiae* each of the four core histones are encoded by only two genes organized into four loci [37]. The *HHT1-HHF1* and *HHT2-HHF2* loci encode identical H3 and H4 proteins [38], while histone H2A and H2B are encoded by *HTA1-HTB1* and *HTA2-HTB2* loci [39]. Histone mRNAs in yeasts exist in polyadenylated form [40].

Canonical histone proteins include the major core histones: H2A, H2B, H3 (H3.1 and H3.2 in human) and H4. These histones are synthesized at high level during the brief S-phase tightly coupled to DNA replication [41][42]. This intensive expression allows their rapid deposition behind the replication fork. In contrast, histone variants are encoded by single or low copy genes, which are expressed in a replication-independent manner throughout the cell cycle. These variants show distinct regulatory mechanisms regarding their expression and incorporation resulting in nucleosomes with specific properties [43]. In most cases, the variants function as replacement histones contributing to dynamic chromatin formation during DNA-

based processes [44]. At protein levels, the differences between canonical histones and their variants can range from the few amino acids up to additional new structural domains. These differences can support various functions of variant specific chaperones (e.g. H3.3 assembly by HIRA [45]) or they can even alter nucleosome stability (e.g. H3.3 – H2A.Z coincorporation [46]). Some variants are considered as 'universal', being found in nearly all eukaryotic species. Universal variants have centromeric (CENP-A in humans, Cse4 in budding yeast, CID in *Drosophila melanogaster*) and non-centromeric histone H3 variants. The latter is present in all eukaryotes and can be considered as a common ancestor of the mammalian H3.1 (sequence alignment and features of human H3.1, H3.3 and yeast H3.3-like histones are reviewed in **Figure 4**). Conversely, some variants are lineage-specific representing distinct functions evolved with the complexity of the eukaryotic genome (e.g. testis specific H2B [47] and H3 variants [48]).

Inadequate incorporation of the histone variants are associated with various diseases. These events may affect the deposition pathways (e.g. implication of Atrx-Daxx-H3.3 pathway in pancreatic neuroendocrine tumors [49]) and arise from reduced or increased expression of certain histone variant [50][51].

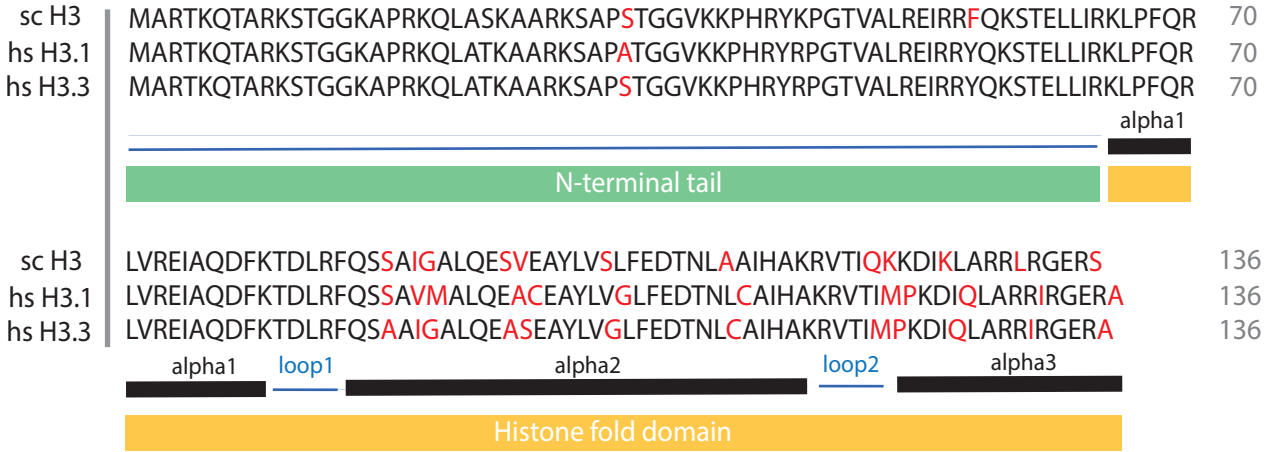

Figure 4. *Sequence alignment and domain structures of human (hs) H3.1, H3.3 and yeast (sc) H3.3-like histones. Amino acid differences are highlighted in red.*

2.1.4. *In vivo* dynamics properties of histone proteins

In vivo interactions of the chromatin proteins are highly dynamic. Photobleaching experiments show that most chromatin proteins are highly mobile within the mammalian cell nucleus and transiently interact with chromatin [52], [53]. The dynamic nature of non-histone proteins (transcription, replication, repair factors and chromatin modifying enzymes) and the short-term mobility of histones are extensively investigated. Phair and Mistelli's studies found that transient binding of many chromatin-associated proteins is common and the average residence times are typically between 2 to 20 seconds [53]. Their FRAP experiments over periods of several minutes show that H2A-GFP and H2B-GFP are persistently immobile in the chromatin, whereas H1-GFP exchanges rapidly [54]–[56].

Seminal series of studies examined the dynamic properties of core histones during replication and cell cycle [57]–[59]. In these studies, either the deposition of radiolabeled, newly formed histones were monitored or the *in vivo* stability of the nucleosomal histones were analyzed by FRAP experiments. The results suggested that H3.1 and H4 core histones remain bound to the chromatin after the incorporation during replication [58] and only a small fraction exchanges independently of transcription and replication [57]. In contrast to H3.1 and H4 histone, H2A and H2B have more rapid exchange rate (~3% mobile fraction within minutes based on FRAP experiments [57]). Presumably, this rapid component represents the euchromatin or transcriptionally active regions with histone chaperone activities [58], as the inhibition of transcription elongation eliminates this H2A-H2B fraction. This phenomenon is not observed in case of H3.1 and H4 histones. The kinetics of various histone variants, replication-

independent histone H3.3 in particular, is less known. Although genome-wide characterization of the H3.3-nucleosome dynamics with measurements of H3.3 turnover rate has been established [60], the diffusion properties of this variant have not been examined yet.

2.2. Histone post-translational modifications

2.2.1. Mechanism of histone modifications

Histone amino (N)-terminal tails protrude from the nucleosome core and comprise 25-30% of the mass of individual histones. They provide exposed surface for potential interactions with other proteins [60][61]. Different groups of these proteins have specific enzymatic activities and catalyze post-translational modifications of the histone tails. In this way, the modified residues can influence many DNA-related processes and can provide platform for other non-histone effector proteins (so-called chromatin readers) inducing nuclear signaling pathways [63]. Although these modifications occur mainly in the unstructured histone tails, there are modifications described on the residues of the histone core as well, where they have the potential to directly influence nucleosome dynamics and stability [64][65]. There are at least eight distinct types of modifications found on histones (acetylation, lysine methylation, arginine methylation, phosphorylation, ubiquitylation, sumoylation, ADP ribosylation, deimination and proline isomerization). The most informative ones are small covalent modifications: acetylation, methylation and phosphorylation [63]. There are over 60 residues where modifications have been observed (major histone tail modifications are reviewed in **Figure 5**). Further complexities are due to methylated forms (mono-, di-, or trimethyl for lysines and mono- or di- (asymmetric or symmetric) for arginines) and cross-talks between different modifications (e.g. ubiquitylation of H2B is required for the methylation of H3K4 and H3K79 [66]–[68]). Enzymes have been identified for acetylation [69], methylation [70],

phosphorylation [71], ubiquitination [72], sumoylation [73], ADP-ribosylation [74], deimination [75] and proline isomerization [76]. In most cases, these modifications have been found to be dynamic and specific enzymes are able to remove them. Preferences of these histones modifying enzymes may depend on the complex, where they are present. The proteins that operate with the enzyme complex may affect the residue to be modified [77] and the degree of the methylation status (mono-, di-, or tri-) [78]. They are able to influence the substrate preference (nucleosomal or free histones) of the enzyme complex as well [79].

Two distinct mechanisms can be distinguished based on the function of the modification. One is involved in the disruption of the DNA-histone interaction allowing the chromatin to get uncoiled and in turn influencing the overall chromatin structure. For instance, neutralization of the basic charge of lysines by acetylation allows the disruption of local interactions [80]. This effect correlates well with a class of enzymes functioning as transcriptional coactivators [81]. On the other hand, the local condensation of the chromatin is associated with H3S10 phosphorylation during both mitotic and meiotic processes [82]. The second mechanism is the recruitment of chromatin-modulating reader proteins, which is an indirect effect of the histone modifications resulting chromatin alteration through non-histone proteins with enzymatic activities (e.g. chromatin remodeling ATPases). This mechanism is indispensable in processes like transcription, repair or replication that require chromatin-remodeling activities. Chromatin reader proteins have specific domains that allow them to recognize histone modifications and other nucleosome features. Specific domain types including the bromodomains recognize the acetylated H3 or H4 tails [83] or distinct domain types recognize lysine methylation: PHD fingers and the so-called Tudor ‘royal’ family comprising chromodomains, Tudor, PWWP and MBT domains [84], [85].

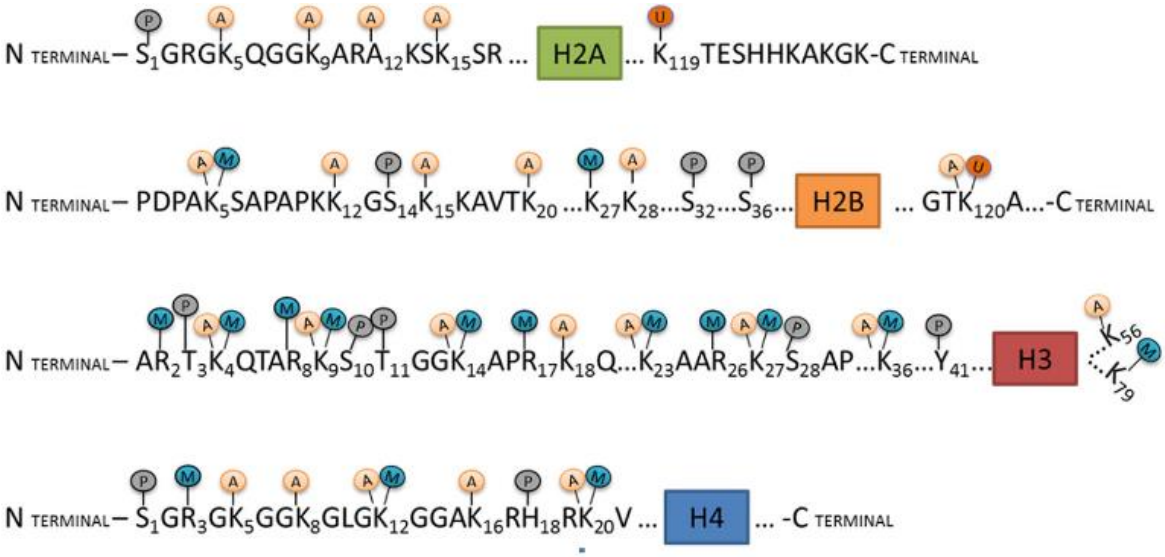

Figure 5. *Major histone modifications of the core histones include acetylation (A), methylation (M), phosphorylation (P) and ubiquitination (U). The figure was adapted from reference* [86].

2.2.2. Histone lysine methylation

Histone methylations occur on arginine and lysine side chains. In contrast to acetylation or phosphorylation, histone methylation does not involve the direct perturbation of chromatin structure through alteration of the charge. However, recruitment of proteins that are capable of identifying methylated sites (e.g. epigenetic readers) play a role in the biological outcome of the different methylation events.

In case of mammalian histones, evolutionarily conserved lysine methylation marks have been observed at multiple sites including K4, K9, K27, K36 and K79 of histone H3 and K20 of histone H4 [87]. Each of these positions can be methylated in four different ways: unmethylated, monomethylated (me1), dimethylated (me2) or trimethylated (me3) state. In almost all cases, lysine methylations are established by enzymes related to the SET-domain

protein methyltransferase superfamily [88]. One exception is the DOT1 family, its members methylate K79 in the globular region of histone H3 and they are structurally not related to SET-domain proteins [89]. Enzymatic removal of methyl-groups are generally catalyzed by the LSD1 (physically complexed with Co-REST repressor) and JARID1 family of histone demethylases [90]. Functional alternatives of enzymatic demethylations include histone replacement or histone tail cleavage [91], [92].

The distinct methylation states exhibit characteristics distribution patterns in the eukaryotic genome [93] and mark functionally distinct chromatin regions. In particular, methylation of histone H3K4, H3K36 and H3K79 is enriched in the active regions of the chromatin, whereas H3K9, H3K27 and H4K20 methylation are generally observed in silenced regions.

In the context of gene transcription, one of the most studied modification is the H3K4 methylation. Whereas H3K4me1 is associated with enhancer functions and gene repression in metazoans [94], both H3K4me2 and H3K4me3 are strongly correlated with transcriptionally active chromatin and are located near to the transcriptional start sites of highly expressed genes [95], [96]. H3K4me2 is generally distributed across the body of active genes and linked to ongoing transcription and gene expression in yeast [97]. H3K4me3 is localized at the 5′ end of the genes [98] and considered as a universal hallmark of active transcription from yeast to humans. Their occurrence around transcriptional start sites highly correlates with transcriptional activation [93]. H3K4me3 is supposed to facilitate transcription by the recruitment of nucleosome remodelling proteins and histone modifying enzymes [99]. Nevertheless, H3K4me3 is associated with the initiation of meiotic recombination in yeasts [100] and V(D)J recombination [101]. In *Saccharomyces cerevisiae* all methylation state of H3K4 is catalyzed by the trithorax-related Set1 within the COMPASS protein complex [102]. In turn, H3K4 methylation is catalyzed by the SET1 and KMT2 family of histone methyltransferases in human and diminished by the LSD1 and JARID1 family of histone

demethylases [90]. The composition and role of the COMPASS protein complex will be summarized in the next session.

As with H3K4me3, H3K36me3 might also be dedicated to the regulation of transcription. However, Setd2 enzyme which is responsible for K36 methylation, remains to be associated with the RNAPII resulting in H3K36me3 pattern throughout the gene body [67]. The reversal of H3K36me3 is catalyzed by Jmjd2 [103].

H3K79 methylation levels are also associated with transcriptional activity. In *Saccharomyces cerevisiae*, the H3K79me3 and Dot1 which mediates this modification, have been detected in the transcribed regions of active genes [98], [104]. In humans both H3K79me2 and H3K79me3 are strongly associated with active genes [105] and may influence developmentally regulated gene expression [106], [107].

Further examples of the distinct distribution of histone methylation are the methylations of H3K9 and H3K27. Recognition of these marks is largely associated with the formation of constitutive or facultative heterochromatin and gene silencing. H3K27me1 and H3K9me3 are found in pericentromeric heterochromatin regions [108] whereas H3K27me3 and H3K9me2 are distributed in the repressed euchromatin. H3K27me3 is also linked to silencing processes including homeotic gene silencing, genomic imprinting and X inactivation [109]. Both methylation marks are targets for chromodomain-containing proteins such as PcG proteins and Hp1 [110], [111]. H3K27me3 is present in *Drosophila melanogaster*, *Arabidopsis thaliana*, worms and mammals, but is absent from yeasts. It is frequently connected to gene silencing, particularly in the repression of unwanted differentiation pathways during lineage specification [93], [112]. H3K27me3 coexists with H3K4me3 active marks on developmentally crucial genes, particularly. The role of this so-called bivalent chromatin state tends to retain the chromatin and cellular plasticity at the early stages of the development with keeping poised the regulated genes during silencing [113]. H3K27me3 deposition is maintained by the Ezh2

methyltransferase within the PRC2 complex [114]. The mechanism and composition of the PRC2 complex and the role of Ezh2 in brain tumor progression will be detailed in the next section(s).

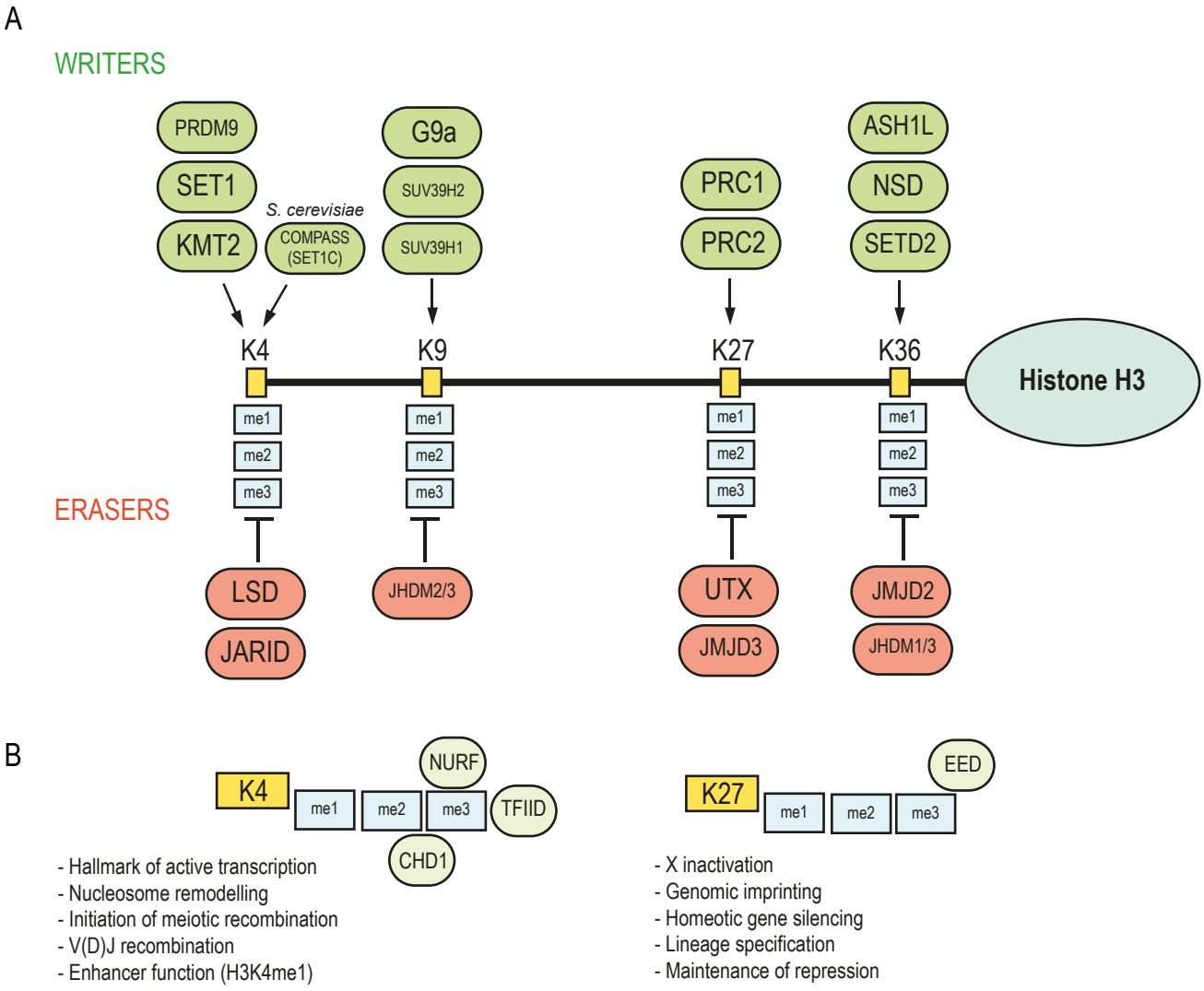

Figure 6. *A schematic depiction of histone H3 showing principal lysine methylation sites on the H3 N-terminal tail. (A) The writers and erasers show the main lysine methylases and demethylases in human. The yeast H3K4 methylase, COMPASS, is also depicted. (B) Downstream effects and chromatin readers of H3K4 and H3K27 methylations. The effector proteins participate in chromatin remodeling and regulate gene expression.*

2.3. Trithorax and polycomb group proteins

The TrxG and PcG protein families play a crucial role in cell commitment and differentiation during the development of metazoans. The first fundamental genetic studies identifying the TrxG and PcG genes were carried out in *Drosophila melanogaster* [115], [116]. These studies showed that TrxG and PcG genes have opposite roles in homeotic gene regulation and many of them encode proteins bearing the 130- to 140-amino acid motif called SET domain. Mutations in the TrxG genes propose their function as positive regulators of gene expression, whereas mutations in the PcG genes suggest their inhibitory role in transcription [117], [118]. Most of the TrxG and PcG proteins are evolutionarily conserved in mammals and function within similar pathways to those of their *Drosophila* counterparts. Both of these complexes have long been linked to the occurrence of different forms of cancer [119]–[121]. In the next sections, molecular mechanisms and clinical implications of TrxG and PcG proteins will be demonstrated.

2.3.1. Composition and molecular role of COMPASS histone H3K4 methylase

In budding yeast (*Saccharomyces cerevisiae),* all H3K4 methylation is established by a single Set1 complex called COMPASS (or Set1C) that is composed of the Set1 catalytic unit and seven other subunits (Swd1 [RbBP5], Swd2 [WDR82], Swd3 [WDR5], Bre2 [ASHL2], Sdc1 [DPY30], Spp1 [CFP1] and Shg1 [BOD1]) [122], [123]. COMPASS was identified as KMT2 homolog [102] (initially named as mixed-lineage leukaemia (MLL)). MLL fusion transcripts were originally identified at chromosome translocations in acute myeloid and lymphoid leukemia [124], [125]. In humans, Mll is found in a COMPASS-like complex and functions in a similar way as in yeasts [121], [126] (subunit composition from yeast to human is reviewed in **Figure 7**). The MLL genes are frequently mutated in the majority of cancer types [120].

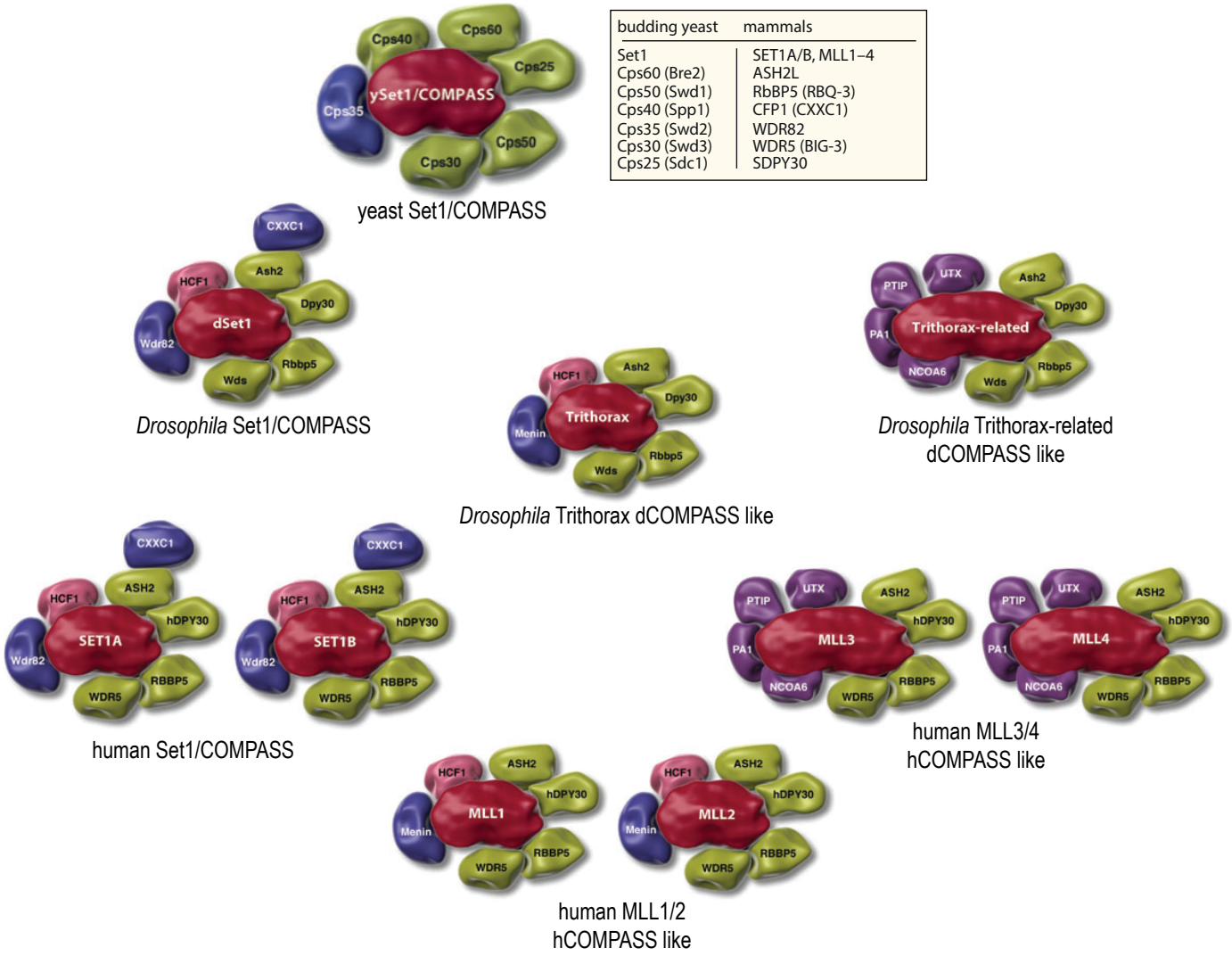

Figure 7. *Subunits of the COMPASS family from yeasts to humans. Modified from reference* [127]. *Budding yeast COMPASS subunits and their corresponding homologs in mammals are indicated in the table.*

COMPASS subunits are assembled around the catalytic unit Set1 acting as a scaffold. The complex can mono-, di-, and trimethylate H3K4, but transitioning to di- and trimethylation depends on the H2B monoubiquitination cross-talk followed by recruitment of the Swd2 subunit of COMPASS [128]. Recently, it has been described that Swd1 and Swd3 are responsible for all three methylation marks whereas Bre2, Sdc1, and Spp1 are required for trimethylation [129]. On the other hand, Bre2 and Sdc1 interact with the isolated SET domain as well and form SET-c [130]. In a similar way, Spp1, Swd2, and Shg1 directly interact with

the n-SET domain, the N-terminal domain, and the second RRM motif of Set1, respectively. The Spp1-Set1 interaction induces the SET catalytic domain to open and also read non-asymmetrically dimethylated H3R2 with its PHD-finger domain [131]. Spp1 is required for normal level of meiotic double-strand break (DSB) formation and interacts with the DSB specific proteins playing a role in cleavage activation [132], [133]. The role of COMPASS protein complex and H3K4me3 in DSB initiation will be discussed in detail in chapter 2.6.

2.3.2. The PcG complexes and the role of Ezh2 in PRC2

PcG proteins form conserved regulatory complexes suppressing genes through a variety of physiological roles and types of epigenetic patterning in higher organisms. They have been identified in *Drosophila melanogaster* as repressors and regulators of anterior-posterior body patterning through the maintenance of homeotic gene expression profile [134], [135]. In humans and vertebrates the polycomb family consists of structurally diverse set of proteins assembled into chromatin-associated complexes which participate in the establishment and maintenance of cell fates, in the regulation of Hox gene expression (antagonizing the function of TrxG protein family) and in the early steps of X-chromosome inactivation in women [136]. The PcG proteins assemble into functionally distinct complexes that belong to two protein families: PRC1 and PRC2. Both complexes have catalytic activity inducing histone modifications. PRC1 with its E3 ligase activity monoubiquitinate the histone H2A at lysine 119 (H2AK119u1) whereas PRC2 is involved in the mono/di/trimethylation of H3K27 (H3K27me2/3) through its Ezh2 catalytic unit. Classification of PcG complexes with their detailed composition is reviewed in **Figure 8**.

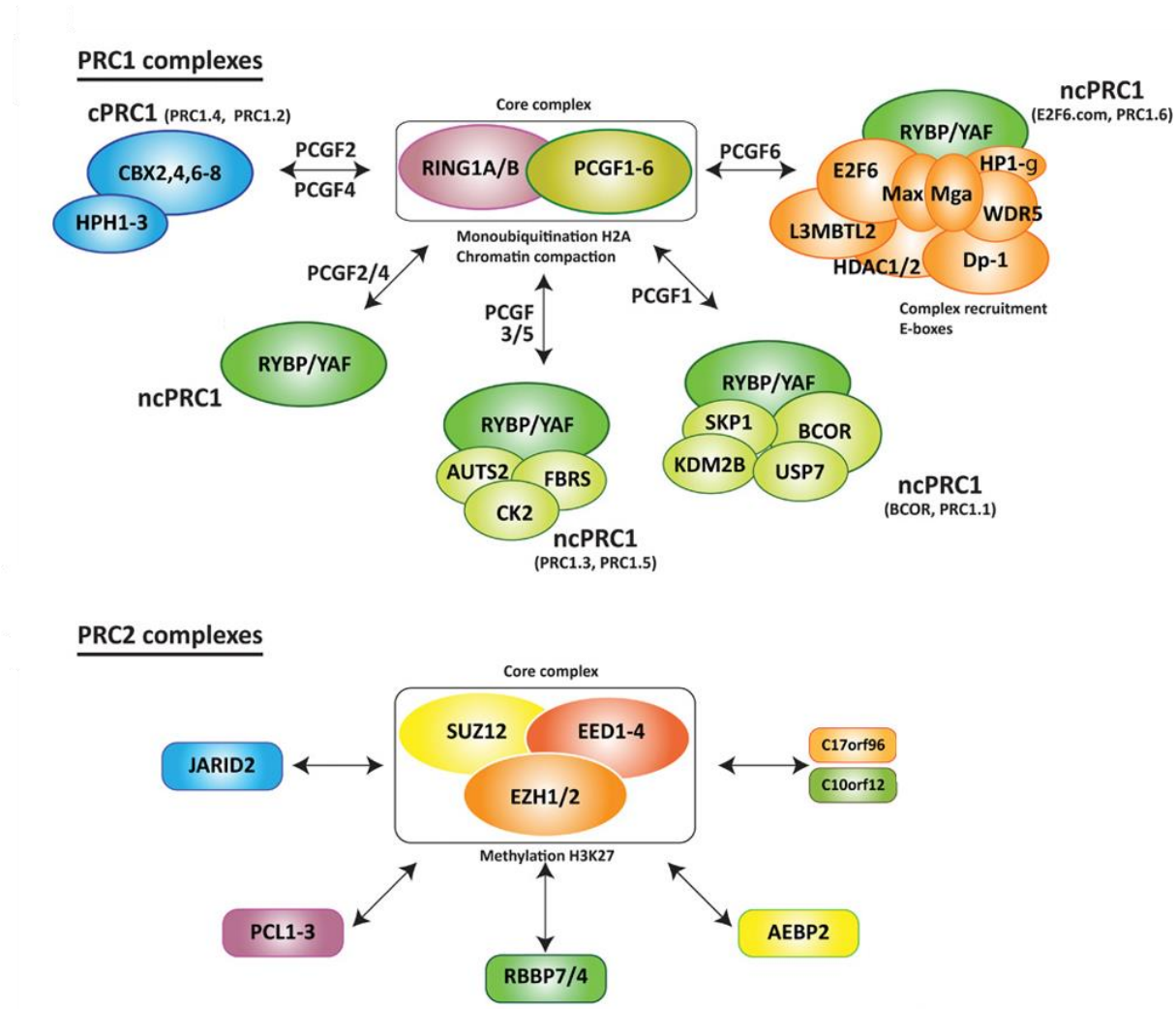

Figure 8. *Mammalian PcG complexes with the catalytic and regulatory subunits. The figure outlines the core subunits of the two major PcG families with their accessory proteins* [137].

The composition of PRC2 complex is dynamic, containing subunits responsible for the H3K27me3 mark and several accessory regulatory subunits controlling the enzymatic activity and holoenzyme function [138]. The core components of mammalian PRC2 complex include Suz12, Eed and Ezh2 (mutually exclusive with Ezh1 isotype). These three components are sufficient for methyltransferase activity *in vitro* [139]. The Aebp2, PCLs, Jarid2 and Rbbp4/7 proteins are other cofactors that facilitate the PRC2 function. In *Drosophila melanogaster*, polycomb-mediated silencing takes place through the recruitment of PcG proteins to the PRE

sequence locating upstream of the Hox transcription factor genes. Although, existence of similar DNA elements are under debate in mammals (PRE-like elements have been reported: [140], [141]), PRC2 recruitment through lncRNAs has been described in lineage-specific transcriptional silencing mechanisms [142].

One of the most important component of the PRC2 complex is the Ezh2 protein that plays a pivotal role in the formation of repressive epigenetic pattern. The human Ezh2 protein belongs to the histone-lysine methyltransferase family having the SET domain and the catalytic subunit of PRC2 being responsible for all the three types of H3K27 methylation. Ezh2 works together with PRC2 associated proteins mediating histone methylation in a spatially defined manner leading to different genomic functions [143]. For instance, H3K27me2 and H3K27me3 are linked to the facultative heterochromatin regions, whereas the H3K27me1 form is enriched in the constitutive heterochromatin [144]. Furthermore, the H3K27me3 may serve as a docking site facilitating the binding of PRC1 complex which catalyzes the monoubiquitylation of H2AK119 maintaining a repressed state of target genes. H3K27me3 may also regulate the transcription indirectly by pausing the RNA pol II transcription complex thus preventing the elongation stage at the PcG target sites [145]. Apart from the canonical repressive role of Ezh2, it has a PRC2-independent transcription inducer function as well. In breast cancer cells, it has been demonstrated that the interaction of Ezh2 with a mediator complex activates target genes through distinct mechanisms [146]. Growing body of evidence suggests that the overexpression of Ezh2 correlates with tumor progression and poor outcome in hematological and epithelial malignancies [147].

2.4. Implications of histone proteins and PRC2 in brain tumor progression

2.4.1. Histone gene mutations are involved in high-grade gliomas

Histones are related to cancer progression primarily due to alterations in histone post-translational modifications and the epigenetic pathways controlling these modifications. Recurrent mutations in the chromatin machinery and defected interplays between histone modifying enzymes and post-translational modifications are fundamental in tumorigenesis. These pathways and their misregulations are summarized in a number of studies [148]–[151] and they are involved in epigenetic drug investigations.

Although epigenetic histone modifications are well studied in cancer biology, somatic histone mutations and their manifestation in tumor progression are still not clear. The first exome sequencing study, in which recurrent somatic histone mutations have been identified, was carried out in 2012 and investigated genetic events of pediatric glioblastoma multiforme (GBM) [13]. It revealed mutations in the H3F3A gene encoding the histone variant H3.3 in 31% of the pediatric tumor samples. The mutations led to amino acid substitutions at two critical residues within the H3.3 histone tail (K27M and G34R/G34V) that were specific to GBM and highly prevalent in children and young adults. The presence of H3F3A mutations were strongly associated with alternative lengthening of telomers and specific gene expression profiles, particularly. More recently, these histone substitutions have also been described in diffuse pontine glioma (DIPG) [152] and lower-grade tumors such as pilocytic astrocytoma [153]. In DIPG, 78% of the sequenced samples carried mutations in the H3F3A or in the HIST1H3B gene encoding histone H3.1 (approximately 20% of K27M mutations were found in H3.1) [154]. Pontine gliomas affect very young children with a peak incidence at 6 years of age and 9 months median survival. In addition, DIPG histone mutations are associated with a clinically and biologically distinct subgroup of patients with a more aggressive clinical course and worse

prognosis [155]. All long-term survivors of these tumors are H3 wild type indicating prognostic and therapeutic implications of H3 [155].

In high-grade brain tumor samples, the identified K27M and G34R/V mutations are heterozygously expressed and mutually exclusive. They exhibit distinct gene expression profiles, DNA methylation patterns and age dependency [13], [156]. K27M mutations are more frequent in younger patients (5–29 years) while G34R/V mutations occur in slightly older patients (9–42 years). Tumors with mutated histones exhibit different localization patterns within the central nervous system. K27M tumors are primarily found in the midline locations (spinal cord, thalamus, pons, brainstem) and G34R/V tumors are mostly located in the cerebral hemispheres (frontal, parietal, occipital, and temporal lobes) [157], [158]. In addition, H3.3 mutations show simultaneous overlapping with other specific mutations within the same tumor (e.g. ATRX/DAXX, TP53, PDGFRA [13], [155]) acting as driver mutations. Co-occurrence of H3.3 with ATRX or TP53 mutations is accompanied with higher abundance of copy number alterations, particularly [13]. Of note, the chromatin remodeler Atrx is specially involved in nucleosomal deposition of the H3.3 variant at telomers and pericentric heterochromatin [159], [160]. The localization and characteristics of the K27M and G34R/V mutations are summarized in **Figure 9**.

2.4.2. The link between K27M mutations and the Polycomb pathway

Both H3K27M and H3G34R/V affect histone posttranslational modifications. G34R/V mutations are supposed to influence K36me2/3 levels on the same H3.3 tail, presumably through the inhibition of methyltransferase Setd2 [161] whereas K27M plays a dominant role in blocking the accumulation of repressive H3K27 methyl marks [161]–[164].

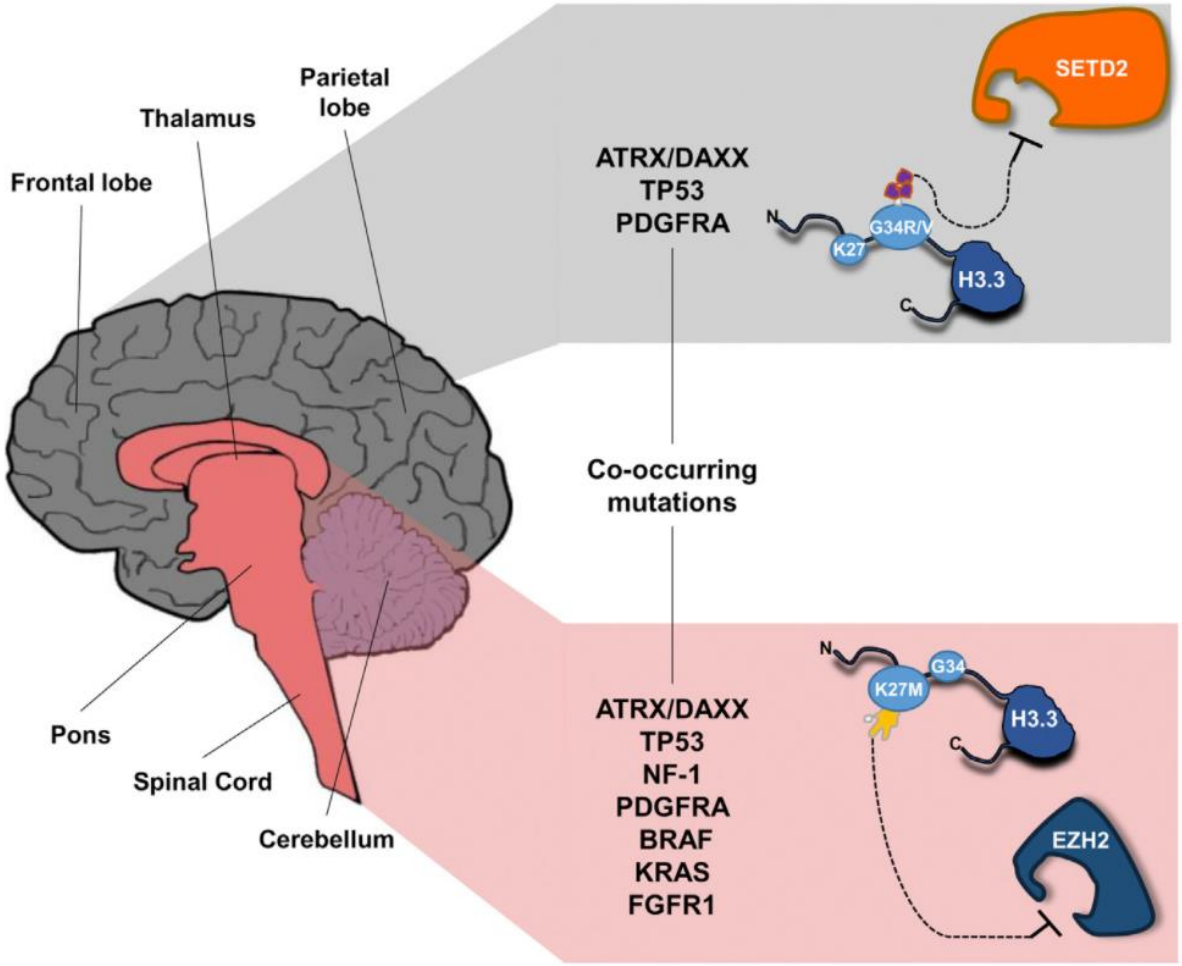

Figure 9. *Neuroanatomic and molecular consequence of H3.3K27M and H3.3G34R/V in gliomas. H3K27M mutations are predominantly found in midline locations. G34V or G34R*

are found in cerebral cortical tumors. Gene alterations co-existing with histone mutations are listed. [165].

This dominant effect of the K27M mutation is irrespective of whether found in histone H3.1 or H3.3 and one mutant allele among 30 alleles encoding histone isoforms is already enough for the global H3K27 hypomethylation [161], [163], [166]. Moreover, quantitative mass spectrometry by *Lewis et al.* proved that the H3.3/H3.1 K27M protein is 3.63% (± 0.33) to 17.61% (± 1.11) of total H3 in human DIPG samples [161] and this small population of mutant histones is sufficient for the loss of H3K27me2/me3. The explanation of this phenomenon is that methionine binds and stabilizes PRC2 thus it prevents the deposition of methyl groups [161], [167]. The binding and interaction between H3K27M and Ezh2 catalytic subunit of PRC2 is proved by immunoprecipitation [166] and binding partner analysis of photoreactive K27M containing peptides [161]. The biochemical background of this inhibition is the long, unbranched hydrophobic side chains of the methionine, which is capable of functioning as orthosteric inhibitor against Ezh2 SET domain. Consequently, transgenes containing K-to-M mutations at other known methylated lysines (H3K9M and H3K36M) are also sufficient to cause specific reduction in methylation through the inhibition of SET-domain enzymes [161], [168]. In this way, the gain-of-function effect of H3K27M contributes to transcriptional dysregulation indirectly through the alteration of the epigenetics landscape: genes, where H3K27me3 marks are reduced, are transcriptionally upregulated. The activation of the gliomapromoting candidate neural restricted transcription factor Olig2 is a good example of that upregulation [162], [166]. Surprisingly, aside from the global K27me3 hypomethylation H3K27M expressing cells show remaining K27me3 domains associated with gene silencing. Genes in this group also include cancer-associated genes, for instance p16INK4A and CDK6 [162], [166].

As discussed above, these studies described the epigenetic consequences of H3K27M missense mutation including perturbated H3K27me3 modification and decreased DNA methylation on oncogenic regions [162]. Recently it has also been found that special cell-of-origin condition with cooperating driver mutations (e.g. loss of p53 or active PDGFRA) is prerequisite for gliomagenesis [169]. Additional questions remain open regarding K27M histone mutations. Some of these connect to the biophysical properties of H3K27M histones and to the structural effect of substitution on the nucleosome architecture.

2.5. Implications of Mll complex in brain tumor progression

Although the novel studies of malignant brain tumors have mostly focused on oncohistones and proteins belonging to the Polycomb group [170], Mll proteins are also involved in the neoplastic phenotype. Inactivating mutations in MLL2 and MLL3 have been identified in 16% of pediatric medulloblastoma patients [171]. The majority of these mutations (nonsense mutations, out-of-frame indels, or splice site mutations) results in protein products lacking the key methyltransferase domain. *Parsons et al.* have demonstrated that the Mll pathways are important to medulloblastomas and that Mll2 and Mll3 play a tumor suppressor role. Additionally, there is an identified Mll-Homeobox axis that significantly contributes to tumorigenic behavior of glioblastoma cancer stem cells [172]. Mll directly activates the Homeobox gene HOXA10 that activates a downstream Homeobox network and other genes previously characterized by playing a role in tumorigenesis. Expression level of MLL1 has also been found higher in glioma stem cells than matched non-stem tumor cells. Loss of MLL1 reduces the expression of HIF transcripts and Hif2α protein and reduces glioma stem cell self-renewal, growth, and tumorigenicity [173].

2.6. Major determinants of the meiotic double-strand breaks in yeasts and humans

A unique feature of the meiosis is the generation of DSBs during the early prophase I [174]. DSBs initiate the process of homologous recombination which is responsible for the maintenance of genetic diversity and the segregation of homologous chromosomes during the first meiotic nuclear division [175]. Meiotic DSBs across the genome are not randomly distributed but concentrate within discrete regions described as DSB hotspots. In *Saccharomyces cerevisiae*, these hotspots correlate with intergenic nucleosome depleted regions (NDR) near promoters and overlap with DSB-associated proteins such as Spo11 [176] and its subcomplexes like RMM (coalescence of Rec114, Mer2, and Mei4 proteins) [174]. Within this structural arrangement of meiotic chromosomes, hotspots reside in the chromatin loop regions, while the DSB machinery essential for the regulation and enzymatic induction of DSBs is bound to the axis [177], [178].

In *Saccharomyces cerevisiae*, potential candidate for the selection of DSB sites is the COMPASS histone methylase complex [100], [133]. Inactivation of the Set1 COMPASS subunit severely reduced the level and distribution of meiotic DNA breaks [179] similarly to reduced H3K4 trimethylation mark [180]. However, the H3K4me3 by itself has modest predictive power for determining hotspot strength and DSB frequency [181]. The link between the H3K4me3 and recombination initation might be the Spp1 subunit of COMPASS which is able to interact with both H3K4me2/3 and Mer2 (RMM complex) at the meiotic chromosomal axis [132], [133]. Tethering of Gal4BD-Spo11 fusion constructs (Spo11 fused to the DNA-binding domain of Gal4) to cold regions within the genome of *Saccharomyces cerevisiae* promotes DSB formation and induces a repressive, distance-dependent effect affecting DSB distribution over a considerable margin [182], [183].

Somewhat differently from *Saccharomyces cerevisiae*, hotspot designation in mammals (*H. sapiens and M. musculus*) relies greatly upon the meiosis specific histone H3 methylase Prdm9 [184]–[186]. Prdm9 is a histone methyltransferase expressed particularly in oocytes and spermatocytes [186], [187]. Knocking out of PRDM9 results in sterility in both sexes [187]. It binds a specific DNA motif through its highly polymorphic multi-Zn-finger domain and activates recombination by trimethylating histone H3K4 and H3K36 on adjacent nucleosomes [188]. Levels of H3K4me3 and H3K36me3 are highly correlated with DSB hotspots and presumably through recruiting chromatin modifying proteins H3K4me3 and H3K36me3 play a role in NDR formation [186], [189]. Most frequently, DSBs are created at these H3K4me3- and H3K36me3-marked NDRs [190], [191]. Genome-wide mapping of Prdm9 in mouse spermatocytes [192], [193] proved that both histone modifications are associated with Prdm9 activity [188], the formation of DNA breaks by Spo11 [194] and the presence of DSB repair proteins such as Dmc1 and Rad51 [191].

In addition to histone modifications, the regulation of DSB formation is also connected to the three-dimensional organization of the meiotic chromosomes. Sister chromatids in the early meiotic prophase are organized into a series of loops that are anchored to the proteinaceous chromosome axes [195]. Similarly to *Saccharomyces cerevisiae*, the mammalian DSB machinery, such as Mei4, Rec114, and Iho1 (orthologs of the RMM complex) are found in the chromosome axes [196], [197] and they are required for the Spo11-dependent DSB formation. In contrast, Prdm9 is mostly localized at the chromatin loops modifying the surrounding nucleosomes and generating a proper chromatin environment with the modifications [193], [198]. Presumably, following histone mark deposition, the Prdm9-bound hotspot DNA is brought to the chromosomal axis by the action of Prdm9-interacting proteins (e.g. Cxxc1, Ewsr1, Ehmt2 or Cdyl) [184], [198]. This event would ensure suitable spatial environment for

subsequent recombination events. This Prdm9-dependent mammalian model is comparable to the previously mentioned Spp1-dependent anchoring in *Saccharomyces cerevisiae*.

3. AIMS OF THE STUDY

The objectives were related to relevant topics of polycomb and trithorax field. One hand, I wanted to study the H3K27M oncohistone which is a newly described key player of the pediatric brain stem glioma and a less-characterized driver mutation. The role of Ezh2 (PRC2 catalytic subunit) in tumor promoting mechanism of K27M is crucial, therefore my aims were to examine the transcriptional interference of H3K27M with Ezh2, respectively. On the other hand, I raised the question how Spp1 behaves differently from Set1 protein at the level of nuclear diffusion and what chromatin binding characteristics it has in terms of turnover and residence time. Here, the main goal was to prove that Spp1 has a COMPASS-independent subpopulation in meiosis that manifests in altered nuclear dynamics and diffusion properties.

My major goals were the followings:

- *In vitro* reconstitution of H3K27M containing nucleosomes and study the methionine mutation and Ezh2 effect on nucleosome conformation using Förster resonance energy transfer-based approaches.
- Analysis of H3.3K27M nuclear distribution in living cells and describe the salt-dependent elution profile of chromatin incorporated H3.3K27M using laser-scanning cytometry (LSC).
- Test the viability of *Saccharomyces cerevisiae* strains expressing H3K27M histones.
- Study the diffusional properties of H3.3 wild type and H3.3K27M histones using FCS and FRAP techniques, and describe the transcriptional relationships of mutant histones and Ezh2 protein.

- Diffusional characterization of Spp1 and Set1 COMPASS subunits with FCS and FRAP techniques.
- Quantitative analysis of Spp1 residence dynamics and turnover rate in meiosis using competition ChIP-Seq.

4. MATERIALS AND METHODS

4.1. *In vitro* nucleosome reconstitution

Mononucleosomes were reconstituted using the modified salt-dialysis protocol of *Luger et al.* [199]. A schematic workflow is summarized in **Figure 10**. Briefly, fluorescently labeled Widom-601 positioning PCR amplicon (with length of 170 bp) [200] and recombinant *Xenopus laevis* histones were reconstituted into nucleosomes containing histone H3 wild type or H3K27M constructed by site-directed mutagenesis. Histone octamers were mixed with positioning DNA fragment in 2 M NaCl-TE buffer and reconstituted into nucleosomes with slow dialysis down to 5 mM NaCl-TE using Slyde-A-Lyzer Mini dialysis tube (7K MWCO, Thermo Scientific) and a second dialysis bag (Spectrapor 7K MWCO). In our energy transfer experiments the positioning DNA fragment was labelled at thymine nucleobases via C6-linker at -53 (Alexa 594) and +41 positions (Alexa 488) with respect to the dyad axis. In case of Ezh2/nucleosomes, the nucleosomes reconstituted by end-labeled DNA fragments were also analysed. Where needed, positioning DNA to histone octamer ratio was optimized between 1:1.5 and 1:1.8 molar ratios in order to avoid aggregation. The ratio was adjusted in a way that less than 5% free DNA was visible after reconstitution. Nucleosome concentration following reconstitution was determined using a Cary 4E spectrophotometer. Nucleosome quality was validated on native PAGE, where a remarkable shift could be observed between free DNA and reconstituted nucleosomes.

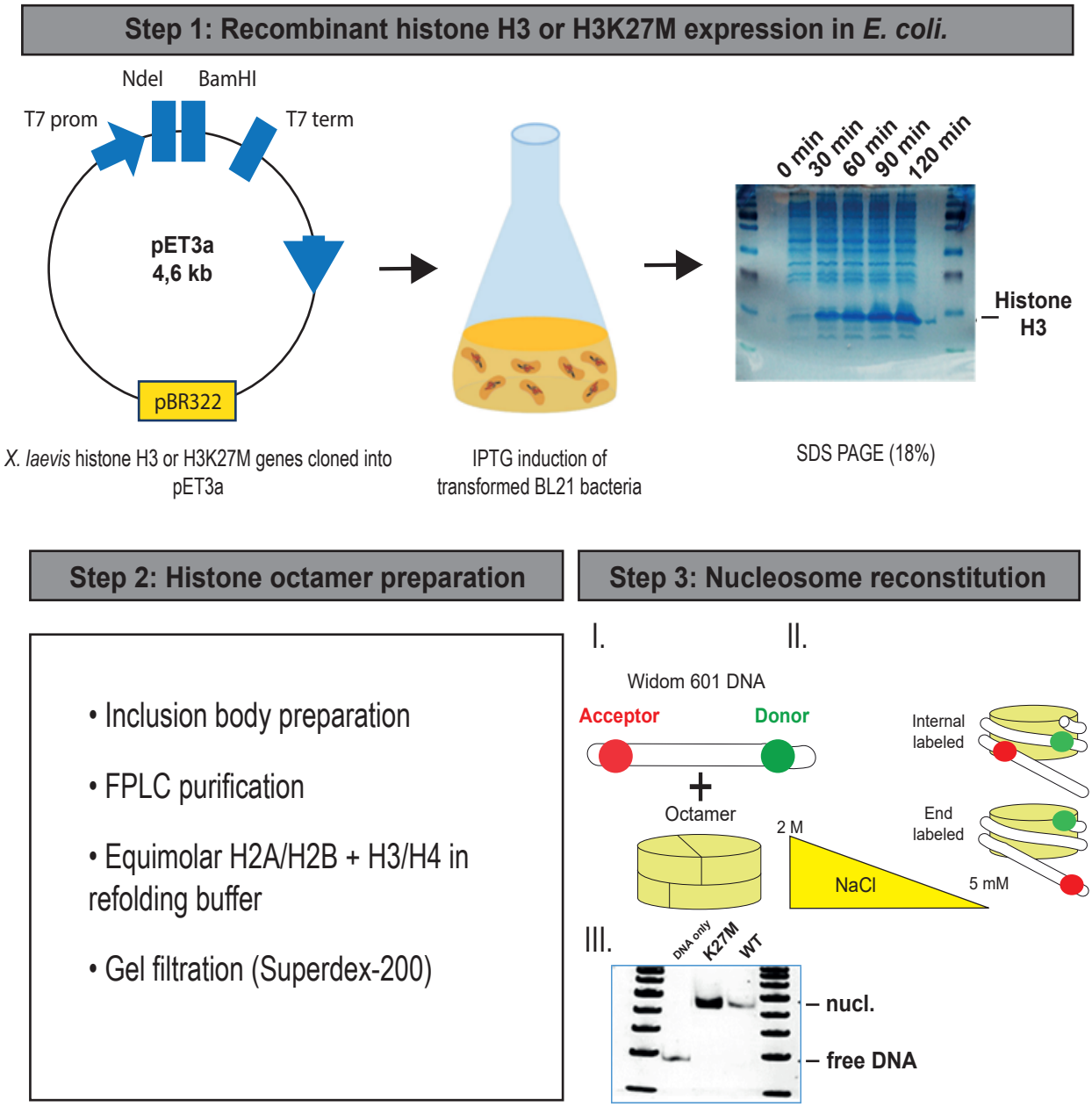

Figure 10. *Main steps of nucleosome reconstitution: Step 1: wild type or K27M mutant form of histone H3 gene was subcloned into pET-3a expression vector and induced by the addition of isopropyl-β-D-thiogalactopyranoside (IPTG) in BL21 (DE3) E. coli strain. Expression levels were analyzed by denaturing gel electrophoresis. Step 2: This step included the purification of histone proteins with inclusion body preparation and gel filtration under denaturing conditions. Purified recombinant histones in equimolar concentration were*

refolded into histone octamers and separated in Superdex-200 column. Step 3: Reconstitution of purified octamer and positioning DNA sequence into nucleosome core partice using salt gradient method. During reconstitution either end-labeled or internal-labeled dye positions were used. Different migration of free DNA and nucleosomes (nucl) was validated on non-denaturing polyacrylamide gels.

4.2. Bulk FRET (μpsFRET) analysis using microplate scanning

Since the radius of the nucleosome is ~5 nm, energy transfer efficiency (also known as proximity ratio in the ratiometric FRET methods) between labels attached to the DNA decreases from one to zero during the salt-induced dissociation (**Figure 11)**.

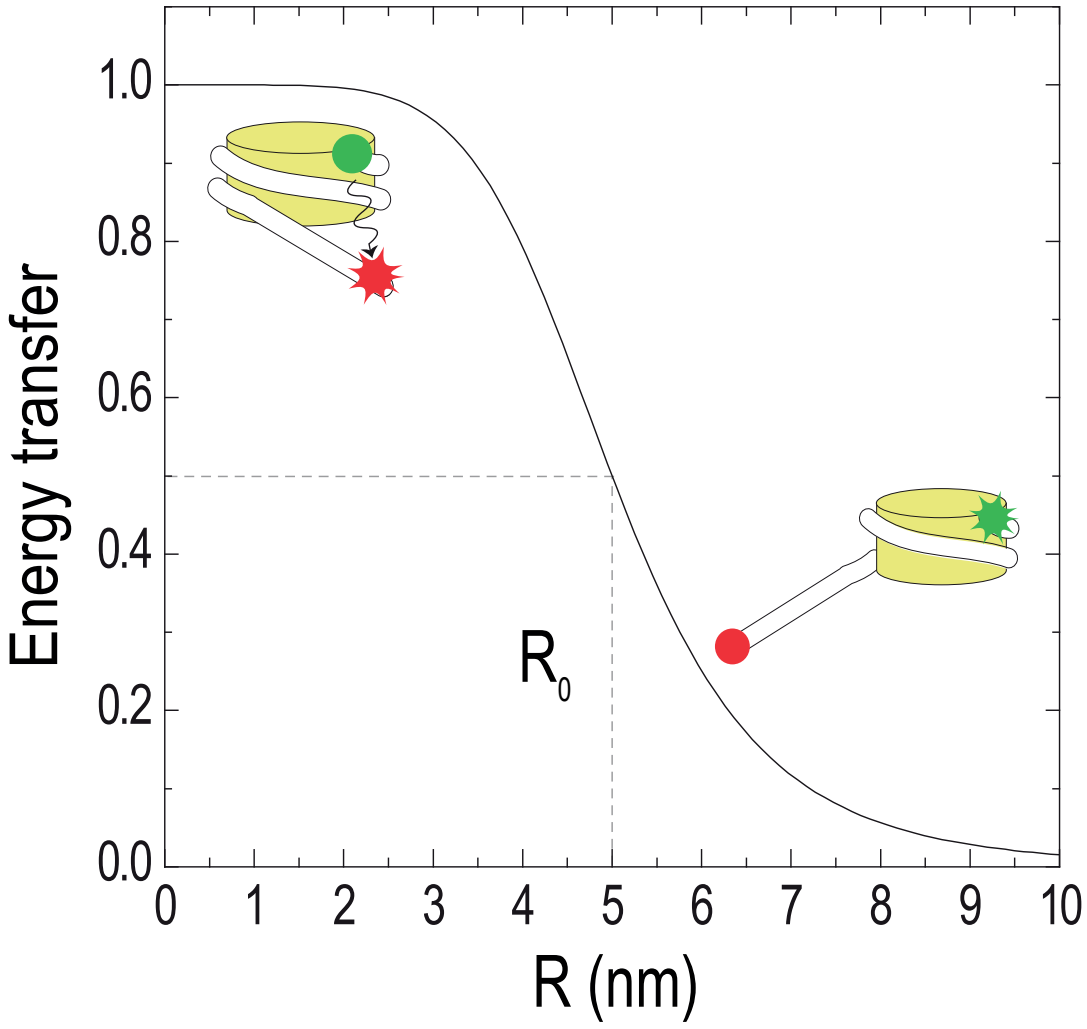

Figure 11. *Energy transfer efficiency as a function of the distance between the dyes with Förster radius R_0 of 5 nm.*

In order to determine the average proximity ratios at the level of nucleosome populations Typhoon 9400 (GE Healthcare) variable mode fluorescence scanner was used. Samples in experimental buffer with different NaCl concentrations were incubated in 384-well microplates prior to the measurement (μpsFRET). The final concentration of labeled nucleosomes was approximately 1 nM. All images were acquired with 100 μm pixel resolution in a way that the image plane was set 3 mm above the scanner surface. Fluorescent emission was detected in three spectral channels: donor channel (excitation at 488 nm, detection at 500-540 nm); acceptor channel (excitation at 532 nm, detection at 595-625 nm); energy transfer channel (excitation at 488 nm, detection at 595-625 nm). Detection voltages of the two photomultiplier tubes (PMT) were set between 600 V and 700 V. Proximity ratios were calculated based on intensity values of each acquired image and plotted against the increasing NaCl concentration using the Image Quant software. As with spFRET measurements, correction factors were determined prior to each measurement.

4.3. Single-pair FRET experiments

For spFRET measurements intact nucleosomes were freshly diluted in a 0.02 μm-filtered experimental buffer with different concentrations of NaCl in 10 mM Tris-HCl, 0.1 mM EDTA, pH 7.5, supplemented with 0.01% Nonidet P40 and 1 mM ascorbic acid in order to avoid photobleaching. Nucleosomes were placed into 384-well microplates (SensoPlate Plus, Greiner Bio-One) previously passivated with Sigmacote® (Sigma-Aldrich). The final concentration of labeled nucleosomes was approximately 50 pM supplemented with 250 pM of unlabeled

nucleosomes to prevent dissociations caused by low nucleosome concentration. Experiments were carried out using a specific confocal system [201] illuminated continuously with a 491 nm laser (Cobolt) for excitation. Prior to burst analysis the nucleosomes were incubated with or without the Ezh2 complex (Active Motif, containing Ezh2, Eed1, Suz12 proteins) for 60 minutes at room temperature in experimental buffer. The confocal volume was calibrated with Alexa 488 fluorophore using an ALV5000/E autocorrelator (ALV-Laser GmbH., Langen, Germany), and autocorrelation curves were fitted. After donor excitation fluorescent emission was separated into two detection windows for donor (520-560 nm) and acceptor (>600 nm). Emitted photons were collected by two avalanche photodiodes (APD, Perkin Elmer Optoelectronics). Single molecule bursts were collected by TimeHarp2000 (PicoQuant), and analyzed by the software Frettchen [201], [202] where one burst was defined as a group of at least 50 photons with a mutual separation of less than 120 μs. Proximity ratio (P) histograms were plotted based on the selected single events and analyzed by IGOR Pro software (WaveMetrics). P is related to the energy transfer efficiency depending on the distance between the fluorophores:

$$P = \frac{N_A}{N_A + N_D}$$

Equation 1.

where N_A and N_D represent the number of detected photons in the respective channels. In both spFRET and bulk systems the correction factors (background and cross talk) needed for P determination were defined in independent measurements.

4.4. *In situ* salt elution assay using laser scanning cytometry

Embedding of live HeLa cells constitutively expressing pEGFP-N1-H3.3 or pEGFP-N1-H3.3K27M into 8-well chambers (Ibidi, Martinsried, Germany) and their quantitative microscopy after salt treatment were based on the protocol of *Imre et al.* [203]. Briefly, cell suspension containing 6×10^6 cells/ml was mixed with 1% LMP (low melting point) agarose diluted in 1x PBS and was dispensed onto agarose pre-coated Ibidi wells at 37 °C. Embedded cells were covered and left to sediment on the well surface for 4 minutes at 37 °C, then they were left to polymerize on ice for 2 minutes. After washing with 500 µl ice cold 1x PBS (three times, three minutes), permeabilization was carried out with 500 µl ice cold 1% (v/v) Triton X-100 dissolved in 1x PBS/EDTA (5 mM EDTA in PBS) for 10 minutes. Aſter permeabilization, nuclei were washed again with 500 µl ice cold 1x PBS/EDTA (three times, three minutes) and were treated with different concentrations of NaCl. NaCl solutions were diluted in 1x PBS/EDTA supplemented with X mM NaCl. The salt elution range was 0 mM-1400 mM NaCl in histone eviction assay and 0-400 mM NaCl in Ezh2 assay. Intensity of the remaining EGFP-tagged histones or immunolabeled Ezh2 aſter treatment with increasing concentration of NaCl was quantitatively analyzed by LSC. The workflow of the protocol is summarized in **Figure 12**.

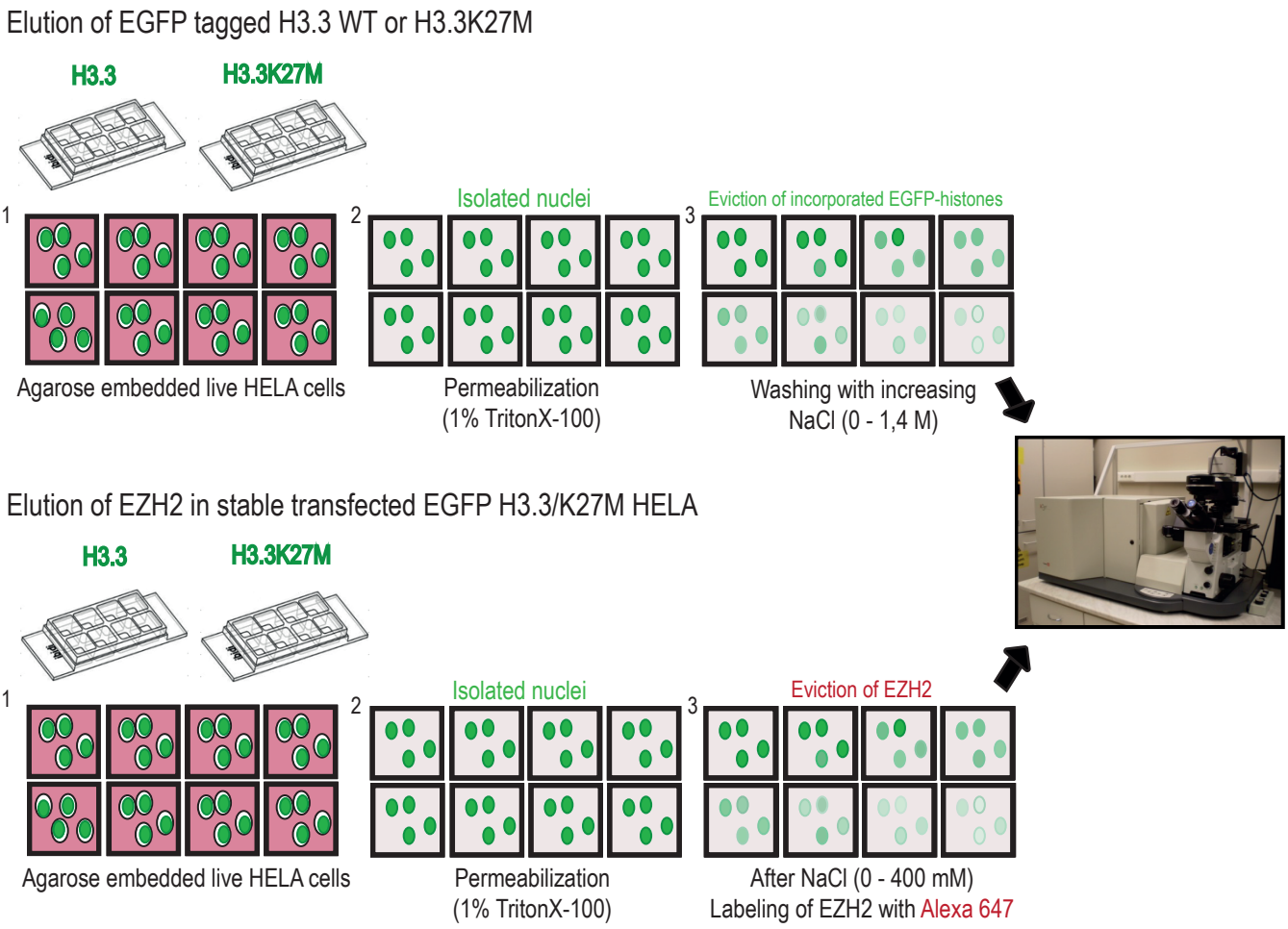

Figure 12. *Flowchart of the salt elution method. EGFP-tagged histones remaining in the nuclei after treatment with increasing NaCl concentration. Histones were detected and quantitatively analyzed by laser scanning cytometry (LSC). Similar workflow was applied in the Ezh2 assay, where the remaining Ezh2 was analyzed using indirect immunofluorescent labeling.*

4.5. Growth and viability of control and H3K27M mutant *Saccharomyces cerevisiae*

Control (H3 wild type), H3K27M, and K27R/Q mutant budding yeast cells were established in the SK1 genomic background by plasmid shuffling technique [204]. Cells were grown to an optical density (OD600) of 0.7-1.0 and ten-fold serial dilutions were spotted onto fresh plates of various metabolite and drug composition. Colony sizes were checked after two days of

growth at 30 ºC. Kinetic growth measurements were performed in various liquid cultures, and optical densities were tracked for 24 hours. OD600 values higher than 1.5 were extrapolated from diluted cultures, corrected with the dilution factor. Sporulation was induced in diploid plasmid shuffle strains using 1% (w/v) potassium acetate as non-fermentable carbon source. After 24 hours of sporulation at 30 ºC, ascus sacs were digested by Zymolyase 20T (MP Biomedicals) at 30 ºC for 10 minutes, and tetrads were dissected using a micromanipulator. Fertility (spore viability) was determined by counting the number of viable spores after two days of growth on YPD plates.

4.6. Cell culture and transfection

HeLa cells were grown in RPMI-1640 (Sigma, R5886) supplemented with 10% (v/v) fetal calf serum, 2 mM glutamine, penicillin and streptomycin, in 5% CO_2 humidified chamber. H3.3K27M point-mutation was introduced into a pEGFP-N1-H3.3 and pmCherry-N1-H3.3 plasmid [205], using the quick change mutagenesis technique. EZH2 was PCR amplified from the NM_004456 (EZH2) Human cDNA ORF Clone (OriGene), and the amplicon was cloned into a pEGFP-N1 and pmCherry-N1 plasmid, respectively. Transient and stable transfections of pEGFP-N1-H3.3 / H3K27M, pmCherry-N1-H3.3 / H3K27M, alone or in combination with pEGFP-N1-EZH2 or pmCherry-N1-EZH2, were carried out by Lipofectamine 2000 (Invitrogen) or polyethylenimine PEI-B [206] according to the manufacturer's recommendations. Single- and co-transfected cells were analyzed by FRAP, FCS and CLSM, respectively. Prior to FRAP and FCS measurements, RPMI-1640 was changed to phenol-red free RPMI or Hank's balanced salt solution (HBSS). Where indicated, cells were pre-treated for 60 minutes before each measurement with actinomycin D (act D, 5 μg/ml), cycloheximide (CHX, 20 μg/ml) and flavopiridol (flav, 100 nM).

4.7. Confocal laser scanning microscopic (CLSM) analysis

HeLa cells were fixed with 1% formaldehyde prior to each measurement. CLSM images were acquired using Olympus FluoView 1000 confocal microscope supplied with a 60x oil immersion objective (NA 1.35). Excitation and emission filters were as follows: EGFP, 488 nm excitation, 500-540 nm detection; mCherry, 543 nm excitation, 600-680 nm detection. Ten optical slices having a thickness of 0.7-1.1 μm were collected from each nucleus, applying the Kalman filter mode to reduce noise and alternative excitation to exclude crosstalk. Colocalization between Ezh2-mCherry and H3.3-EGFP or H3.3K27M-EGFP was computed by the JACoP plugin in ImageJ [207].

4.8. Fluorescence recovery after photobleaching

4.8.1. Recovery of histone H3.3/H3.3K27M-EGFP and Ezh2-EGFP in HeLa cells

FRAP measurements were performed in HeLa cells using Olympus FluoView 1000 confocal microscope, based on an inverted IX-81 stand with an UPlanAPO 60x (NA 1.2) water immersion objective. EGFP was excited by the 488 nm Argon-ion laser line and fluorescence was detected through a 500-550 nm band-pass filter. In the histone FRAP measurements, H3.3-EGFP or H3.3K27M-EGFP HeLa cells were randomly selected and five pre-bleach images were taken (256×256-pixel area, 10x zoom, ~9 μW laser power at the objective) which was followed by a 500 ms bleach period of 100% laser power (900 μW). Rectangular areas were selected as bleach ROIs. In the first 90 minutes, images were acquired every ten minutes and then every 30 minutes, up to 420 minutes (7 hours). Transcription was inhibited by flavopiridol

(100 nM) or actinomycin D (5 μg/ml), while translation was repressed by cycloheximide (20 μg/ml). Drugs were added 60 minutes before the onset of measurements. Actinomycin D caused a significant (~90%) loss of the initial (pre-bleach) EGFP signal, preventing the long-term tracking of fluorescence recoveries. At these timepoints, FRAP recoveries were estimated by extrapolation (applying logistic regression) that allowed us to approximate the immobile fractions of histones H3.3 / H3.3K27M. FRAP experiments on Ezh2-EGFP was performed under similar conditions to those on histones (photobleaching parameters and confocal setup were the same), except that the fast-recovering Ezh2-EGFP fluorescent signal was tracked for only ten seconds.

4.8.2. Recovery of Set1-GFP or Spp1-GFP in *Saccharomyces cerevisiae*

FRAP measurements were performed in sporulating yeast cells (between 0-6 hrs in SPM) using an Olympus FluoView 1000 confocal microscope, based on an inverted IX-81 stand with an UPlanAPO 60x (NA 1.2) water immersion objective. Samples were taken every hour from standard liquid sporulation cultures and measurements were carried out on microscope slides covered with 1% potassium acetate pad. GFP was excited by the 488 nm Argon-ion laser line and fluorescence was detected through a 500-550 nm band-pass filter. Cells expressing the Set1-GFP or Spp1-GFP proteins were randomly selected after $CuSO_4$ induction (100 μM) and five pre-bleach images were taken (256 × 256-pixel area, 15x zoom, ~9 μW laser power at the objective) followed by a 500 ms bleach period of 100% laser power (900 μW). Images were taken every second up to 1 minute.

4.9. Fluorescence correlation spectroscopy

4.9.1. H3.3 and H3.3K27M measurements in HeLa cells

HeLa cells were transfected by H3.3-EGFP or H3.3K27M-EGFP and analysed by a special fluorescence fluctuation microscope (FFM) [208] that combines fluorescence correlation spectroscopy (FCS) and confocal laser scanning microscopy (CLSM). The FFM consists of an FCS module combined with inverted IX-70 microscope (Olympus, Hamburg, Germany), supplied with an UplanApo / IR 606 water immersion objective lens (NA 1.2) and a 5% CO_2 humidified, constant temperature chamber. Fluorescence excitation of EGFP was elicited by a Cobolt laser (at 491 nm, 5-15 μW outgoing power, 1 μW excitation power at the objective). EGFP emission was detected through a 515-545 nm band-pass filter using an avalanche photodiode (APD). Measurements were conducted at 37 °C.

4.9.2. Ezh2 measurements in HeLa cells

HeLa cells were transiently transfected with Ezh2-EGFP and analysed by Olympus FluoView 1000 confocal microscope (described in the FRAP experiments). Autocorrelation curves were calculated by an ALV-5000E correlation card at three randomly selected points of the nucleus of each cell, with 10 × 8 s runs. All measurements were performed at room temperature (22 °C).

4.9.3. Set1 and Spp1 measurements in *Saccharomyces cerevisiae*

Set1 and Spp1 FCS measurements were all performed at room temperature (22 °C) using Olympus FluoView 1000 confocal microscope. Sporulating yeast cells were taken every hour from liquid sporulation cultures and FCS was performed on microscope slides covered with 1% potassium acetate pad. Autocorrelation curves were calculated by an ALV-5000E correlation card at three randomly selected points of each nuclei, with 10 × 8 s runs. In case of rich medium, cells were grown in YPD medium up to A260 = 1.0 and were measured on pre-coated microscope slide covered with YPD agar following induction (workflow of FCS and FRAP experiments carried out in yeasts is summarized in **Figure 13**).

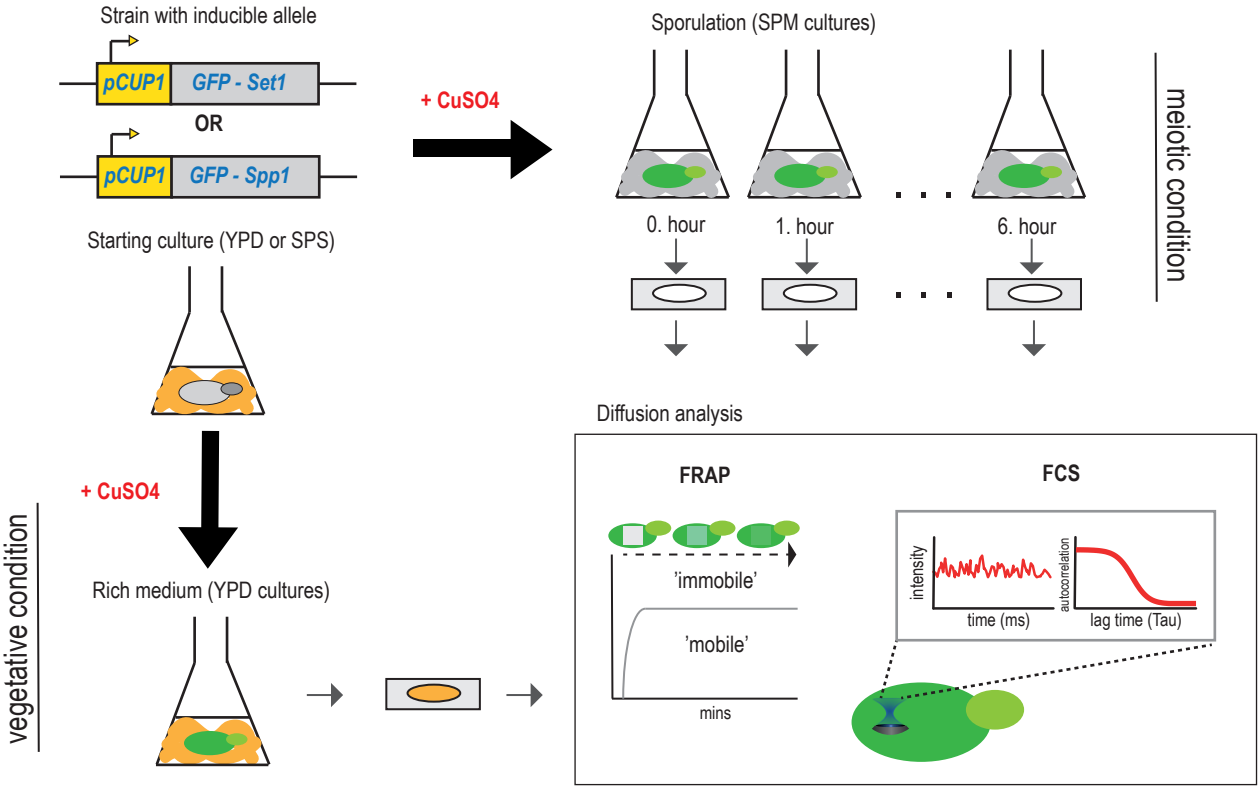

Figure 13. *Schematic diagram of yeast experiments. Strains with inducible GFP-Set1 or GFP-Spp1 construct were grown in starting culture to early exponential phase and following $CuSO_4$ treatment were further incubated either in SPM (meiotic measurements) or YPD*

(vegetative measurements). In SPM, cells were dropped onto potassium acetate pad in every hour. Diffusion properties of induced Spp1 or Set1 were studied with FRAP and FCS.

4.9.4. FCS data processing

FCS data processing and autocorrelation curve fitting were performed by the QuickFit 3.0 software (Krieger, Jan; http://www.dkfz.de/Macromol/quickfit/) applying a 3D normal diffusion model for two-component fitting as follows:

$$G(\tau) = \frac{1}{N}\left[\rho_1\left(1+\frac{\tau}{\tau_1}\right)^{-1}\left(1+\frac{\tau}{\gamma^2\tau_1}\right)^{-\frac{1}{2}} + \rho_2\left(1+\frac{\tau}{\tau_2}\right)^{-1}\left(1+\frac{\tau}{\gamma^2\tau_2}\right)^{-\frac{1}{2}}\right]$$

Equation 2.

where τ is the lag time, τ_1 and τ_2 are the diffusion times of the fast and slow species, ρ_1 and $\rho_2 = 1-\rho_1$ are the fractional amplitudes of the two components, N is the average number of molecules in the detection volume, and γ is the aspect ratio of the ellipsoidal detection volume. Autocorrelation curves distorted by aggregates floating through the focus were excluded from the analysis.

4.10. Spp1 c-ChIP experiments in *Saccharomyces cerevisiae*

4.10.1. c-ChIP protocol

50 mL of meiotic yeast cells (4×10^7 cells/ml) were collected at the indicated timepoints and crosslinked with 1% formaldehyde for 20 min at room temperature. Formaldehyde was quenched with 125 mM glycine for 5 min at room temperature, and cells were washed three times with ice-cold 1x TBS, pH 7.5 (20 mM Tris HCl at pH 7.5, 150 mM NaCl). Cells were resuspended in 500 µL of lysis buffer (50 mM Hepes KOH at pH 7.5, 140 mM NaCl, 1 mM

EDTA, 1% Triton X-100, 0.1% Na-deoxycholate, 1 tablet of complete inhibitor cocktail (Roche) in 50 mL solution) and lysed with acid-washed glass beads for 10 min in a FastPrep bead beater machine. Chromatin samples were fragmented to an average size of 300 bp by sonication (Bioruptor, Diagenode). In order to obtain whole-cell extract (WCE), a 50 µL pre-IP sample was removed and centrifuged at full speed for 10 sec to separate cell debris (supernatant = WCE). The rest of the samples was also centrifuged at 12,000 rpm (4 °C) for 20 sec to separate cell debris. IP was performed by adding the 450-µl extract to a pellet of magnetic protein G dynabeads (Dynal), corresponding to 50 µl or 2×10^7 beads, which were preincubated with 9E11 (monoclonal mouse anti-myc, ab56, Abcam) or anti-GFP (polyclonal rabbit, ab290, Abcam) antibodies overnight at 4 °C. IP samples were washed twice with lysis buffer, twice with lysis buffer supplemented with 360 mM NaCl, twice with washing buffer (10 mM Tris HCl at pH 8.0, 250 mM LiCl, 0.5% NP-40, 0.5% Na-deoxycholate, 1 mM EDTA), and finally once with 1x TE at pH 7.5, using the magnetic device supplied by Dynal. Cross-linking was reversed by heating in TE-1% SDS overnight at 65 °C. Afterwards, proteins were digested with proteinase K (12 µl of 20 mg/ml stock) for 3 h at 65 °C. Nucleic acids were purified using a PCR clean up kit and RNA digestion (10 µg RNase) was carried out for 1 h at 37 °C. DNA was finally resuspended in 50 µl nuclease-free dH_2O. ChIP protocol was carried out with help of Ibolya Fürtös.

4.10.2. c-ChIP sequencing library preparation

Sequencing libraries were prepared according to the Illumina's TruSeq ChIP Sample Preparation protocol. Briefly, the enriched ChIP DNA was end-repaired and indexed adapters were ligated to the inserts. Purified ligation products were then amplified by PCR. Amplified libraries were prepared at the Genomic Medicine and Bioinformatics Core Facility of the

University of Debrecen, Hungary [209]. The libraries were sequenced using 50 bp single end reads with Illumina HiScan SQ (Genomic Medicine and Bioinformatics Core Facility of the University of Debrecen); or with Illumina HiSeq 2500 (EMBL Genomics Core Facility, Heidelberg, Germany).

4.10.3. Turnover rate estimation from c-ChIP data

Average coverage (i.e. the occupancy) of the Spp1 binding sites were calculated using both the GFP- and MYC competition ChIP-seq data for each timepoint separately. Next, GFP/MYC occupancy ratios were calculated and the same exponential model was fitted according to *Deal et al*. [210]:

$$\frac{GFP}{MYC} = 1 - e^{-\lambda t}$$

Equation 3.

where $\frac{GFP}{MYC}$ is the GFP/MYC occupancy ratio, e is the mathematical constant ~2.72, t is the time in minutes measured from the induction of the GFP-tagged Spp1 gene and λ is the turnover rate. This model is identical to the model used by others [211], [212]. After fitting the model, the standard error of the estimates was calculated and a t-test was performed to evaluate the goodness of fit of the model. In total, 977 binding sites could be described with the model (p-value < 0.05).

5. RESULTS

5.1. Characterization of the structure of K27M nucleosomes by Förster resonance energy transfer (FRET)

In order to determine how lysine 27 to methionine substitution affects the stability of nucleosomes carrying this mutation, Förster resonance energy transfer method was applied to analyze nucleosome conformation and dynamics. K27M point mutation was introduced into a recombinant histone H3 using *in vitro* mutagenesis protocol and it was expressed in BL21 (DE3) *E. coli* in order to obtain H3K27M mutant nucleosomes. The expression protocol was based on a pET3a IPTG inducible expression system optimized for the individual histone proteins. The expression and purification of H3K27M histones resulted in similar efficiency and yield to canonical histones and did not show sensitivity to the introduced amino acid substitution. We successfully applied this protocol for the canonical histones as well and assembled the purified histones into wild type (containing two copies of H2A, H2B, H3, H4) or mutant octamers (containing two copies of H2A, H2B, H3K27M, H4). Then, we combined and reconstituted these octamers into nucleosomes with a Selex 601 (Widom 601) positioning DNA. In order to apply the downstream FRET analyses we incorporated fluorescent tags into the Widom 601 sequence creating suitable donor/acceptor fluorophore pairs. The K27M mutation did not perturbate the reconstitution protocol and the mutant nucleosomes produce similar migration profile on native gel as their wild type counterparts (**Figure 14**).

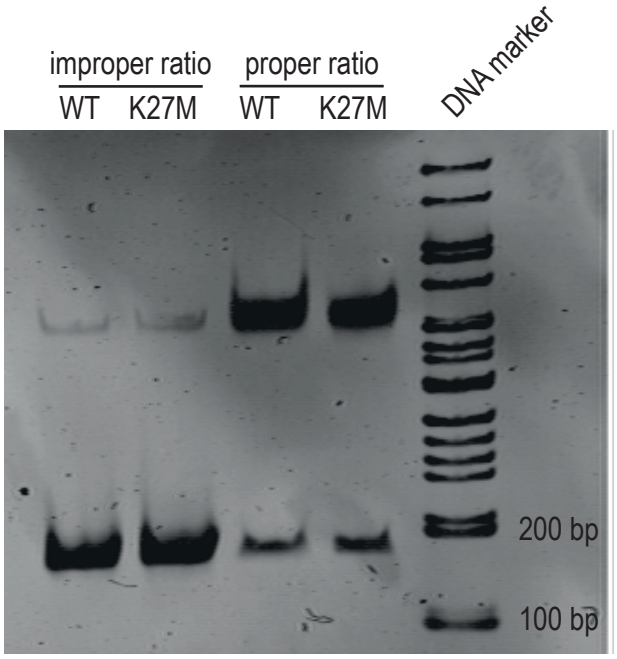

Figure 14. *Validation of reconstituted wild type and mutant nucleosomes on native 6% polyacrylamide gel. The molar ratio between DNA and octamer was optimized between 1:1.6 and 1:2. The gel demonstrates the improper (excess 170 bp Widom-601 DNA) and proper ratio, respectively.*

Then, we measured the equilibrium stability of wild type nucleosomes and nucleosomes with histone H3K27M by microplate-scanning FRET (μpsFRET) (**Figure 15**). This method allows to analyze the nucleosome structure under bulk conditions and it applies a commercial multimode scanner to image fluorescence from a section of a microplate filled with the labeled wild type or mutant nucleosomes. Energy transfer proximity ratios (P) were computed at gradually increasing salt concentrations that elicited nucleosome disassembly in well-controlled way. The comparison of the dissociation kinetics of wild type and mutant samples showed a small reduction in salt-dependent stability of K27M nucleosomes; however, the difference was not statistically significant.

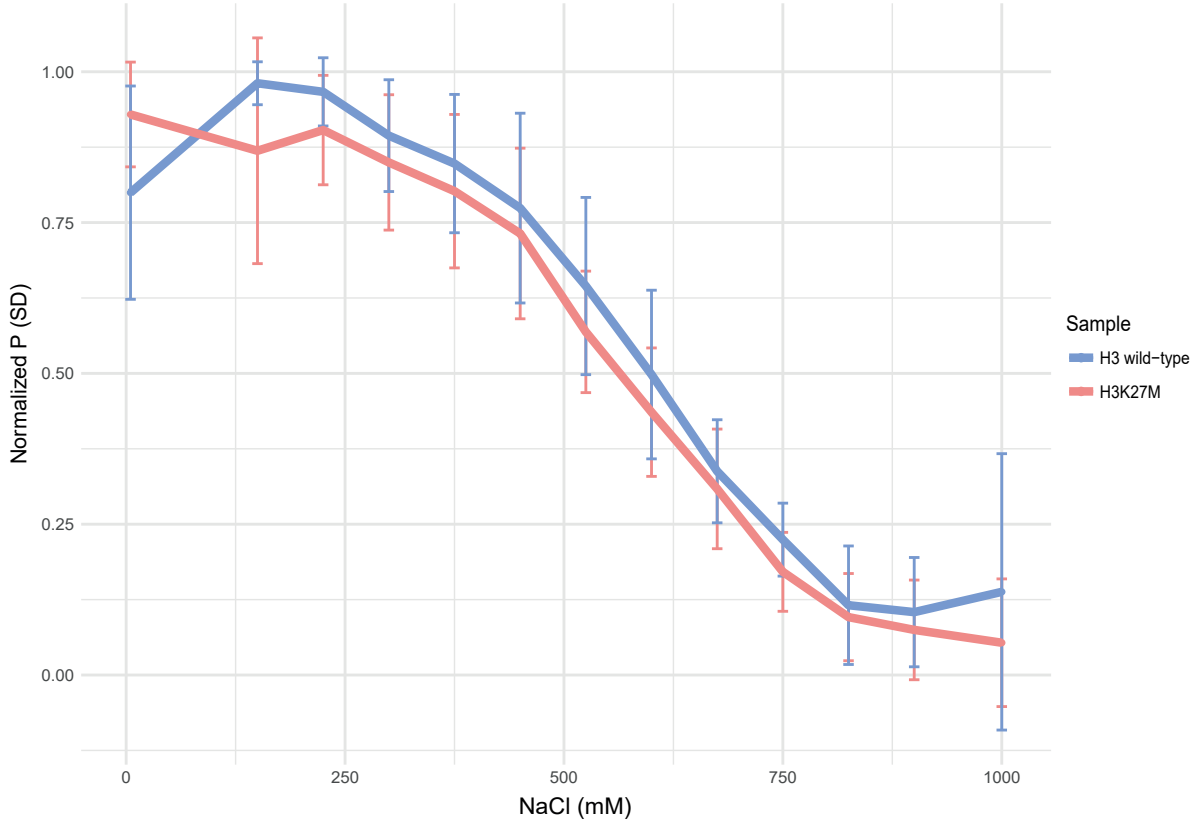

Figure 15. *Salt-dependent destabilization of wild type (blue) and H3K27M (red) nucleosomes measured by bulk µpsFRET. The decrease of proximity ratios (P) reflects nucleosome dissociation. Curves represent the mean of five independent experiments (± SD).*

Next, supplementation of the reconstituted nucleosomes with a recombinant Ezh2-complex (contains Ezh2, Eed and Suz12 proteins) resulted in no detectable changes regarding nucleosome stability (**Figure 16**). In these experiments the question was whether the Ezh2 is able to bind to the methionine residue under this condition and how the interaction of the Ezh2 complex influences the stability of the nucleosome [161], [213].

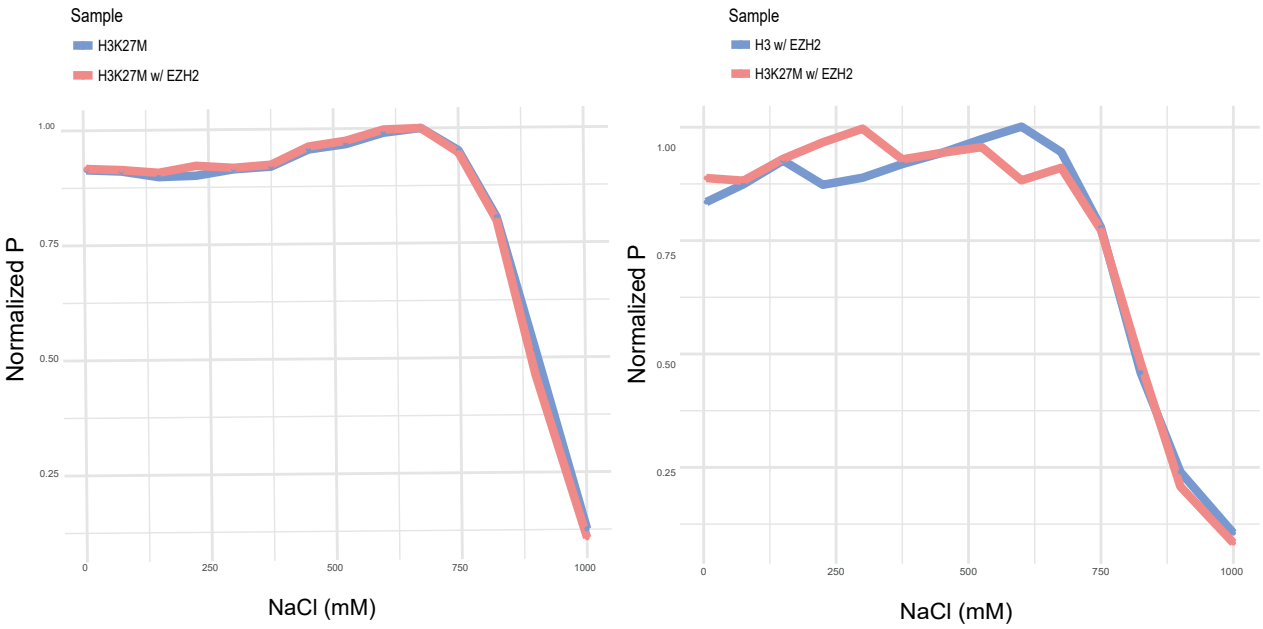

Figure 16. *Left: Salt-dependent destabilization of H3K27M nucleosomes with (red) or without (blue) Ezh2 complex. Right: Wild type (blue) or H3K27M (red) nucleosome stability in the vicinity of Ezh2 complex. The curves demonstrates the dissociation of end-labeled nucleosomes*

Since the properties of individual nucleosomes are averaged in these bulk FRET measurements, subtle differences might remain undetected over the whole molecular assembly process. Therefore, we repeated the salt dissociation measurements using spFRET that allows us to track potential subpopulations of nucleosomes. In the spFRET setup, 50 pM fluorescent nucleosomes were mixed with 250 nM of unlabeled nucleosomes, and proximity ratio histograms were recorded for a range of salt concentrations (**Figure 17**). At the level of individual nucleosomes, the disassembly process did not reveal a significant difference or structural heterogeneity between wild type and H3K27M nucleosomes. This implies that nucleosomes with H3K27M histones maintain a canonical molecular architecture.

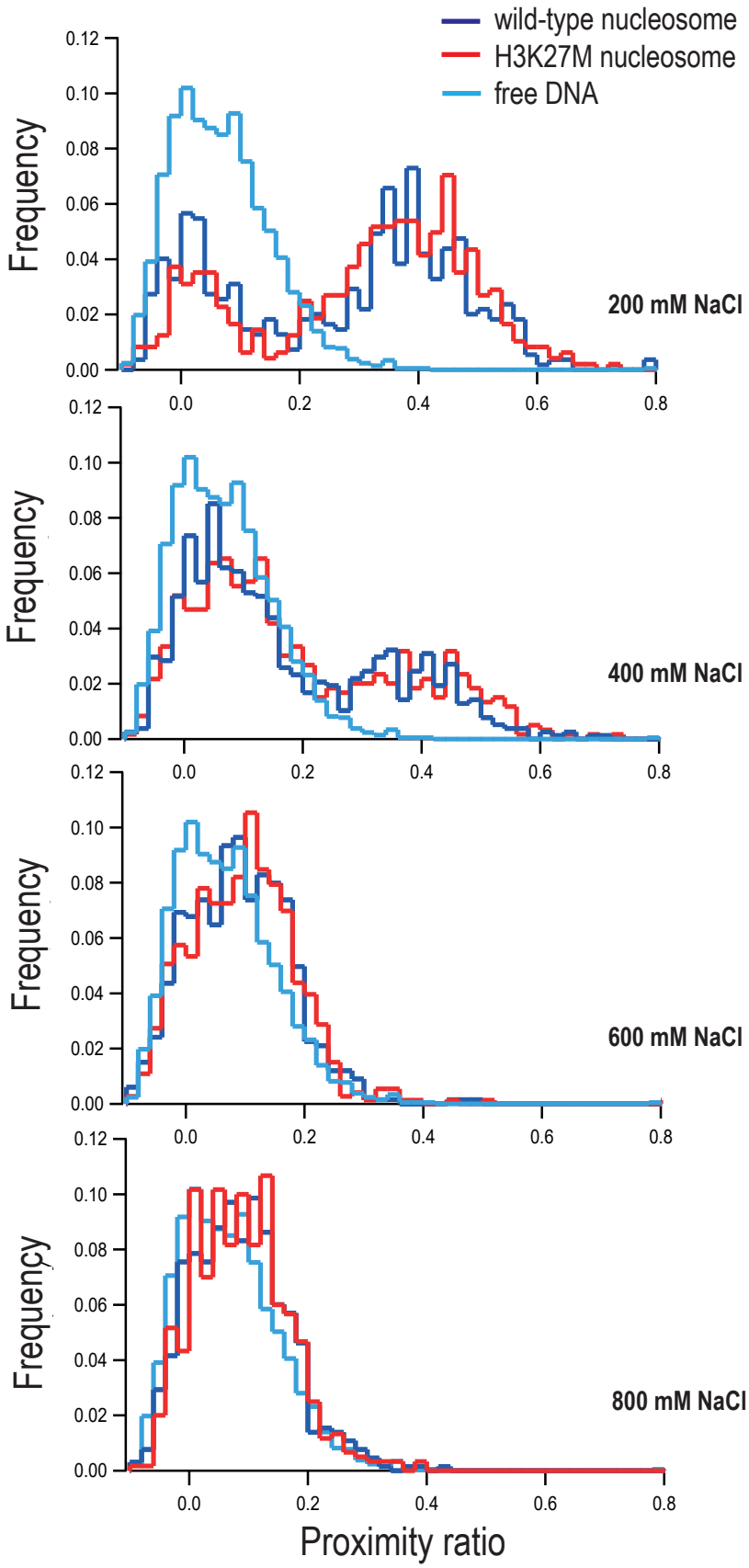

Figure 17. *Structural analysis of wild type and H3K27M nucleosomes at single molecule level with spFRET. The figure shows the distribution of P on single nucleosomes. Wild type*

(dark blue), H3K27M (red) nucleosomes, and free DNA (light blue) were measured in parallel at various salt concentrations. Intact nucleosomes appear at a P of ~0.4.

5.2. *In situ* salt elution assay of H3.3K27M and Ezh2

The *in situ* salt elution assay protocol (described and optimized by *Imre et al.* [203]) allowed us to examine nucleosome stability in close to native chromatin context. With this current approach, we were able to compare the stability of chromatin-incorporated nucleosomes containing the H3.3K27M histones to the incorporated wild type nucleosomes. Moreover, in a modified salt range we observed the elution profile of Ezh2 in HeLa cells transfected with H3.3 wild type or H3.3K27M transgene.

Based on three independent experiments we concluded that K27M substitution did not alter the incorporation property of the H3.3 histone. Similarly, the Ezh2 elution profile was not affected by the K27M mutation either (**Figure 18**). Our assay implies that the interaction between Ezh2 and methionine [161] does not influence the chromatin incorporation of H3.3K27M histones. Surprisingly, we could reproduce the same difference in 1100 mM NaCl concentration (**Figure 18**, right).

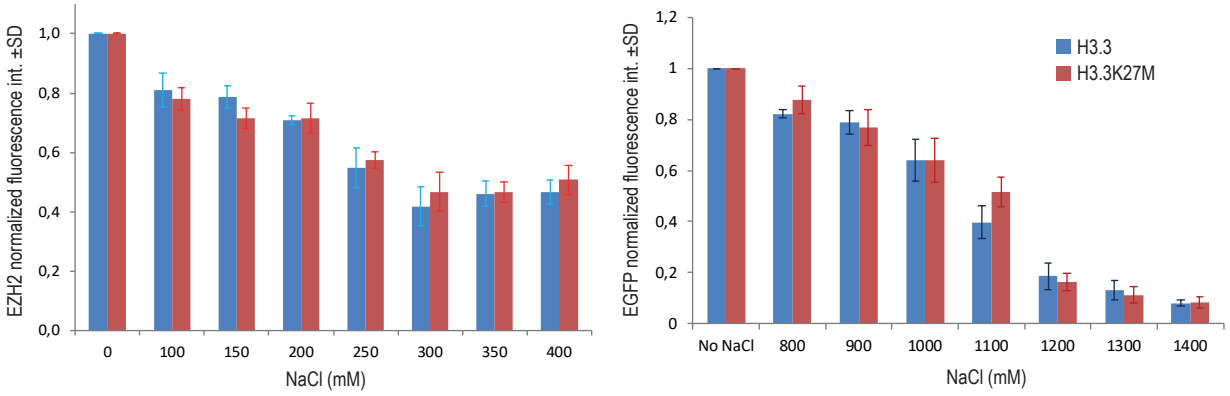

Figure 18. *Salt elution profiles of Ezh2 after H3.3-EGFP or H3.3K27M-EGFP transfection (left) and H3.3-EGFP, H3.3K27M-EGFP (right). The decreasing fluorescent signal indicates the eluting proteins due to increasing ionic strength. The columns were plotted based on three independent experiments and were normalized to the no-salt (maximum intensity) control. Error bars represent SD of the mean.*

5.3. The effect of K27M mutation on the proliferative capacity and stress tolerance of H3K27M-expressing budding yeast cells

Since *Saccharomyces cerevisiae* encodes only two copies of each histone gene (HHT1 / HHT2: histone H3; HHF1 / HHF2: histone H4; HTA1 / HTA2: histone H2A; HTB1 / HTB2: histone H2B), therefore the construction and genetic analysis of homozygote H3K27M mutants could be feasible. We introduced the K27M point mutation into the HHT2 gene (coded by a pCEN-ARS-hht2K27M-HHF2-TRP1 plasmid), and transformed it into an hht1Δ recipient strain expressing histone H3 (Hht2) from a URA3 plasmid (pCEN-ARS-HHT2-HHF2-URA3). Wild type ura+ and mutant trp+ plasmids were exchanged by plasmid shuffling [214], and trp+/ura+ colonies were selected and validated by Sanger sequencing for the presence of the homozygous mutation. As budding yeasts lack the polycomb repression and H3K27 methylation system, H3K27R and H3K27Q mutants were also built as controls for K27M (having different

molecular weights and charge compared to methionine). Genotypes of the shuffle strains are listed in **Table 1**.

Strain	Ploidy	Backgr.	Genotype
AND1640	2n	SK1	*MatA/ Matα, DMC1/ DMC1, leu2/ leu2, hhf1::HphMX/ hhf1::HphMX, hhf2::G418/ hhf2::G418, trp1/ trp1, his4/ his4, ura3/ ura3, p(HHT2, HHF2, URA3)*
AND1640-K27Q	2n	SK1	*AND1640, p(hht2-K27Q, HHF2, TRP1)*
AND1640-K27R	2n	SK1	*AND1640, p(hht2-K27R, HHF2, TRP1)*
AND1640-K27M	2n	SK1	*AND1640, p(hht2-K27M, HHF2, TRP1)*
ANT1318-10C	n	SK1	*MatA, DMC1, leu2, hht1::HphMX, hht2::G418, trp1, his4, ura3, p(HHT2, HHF2, URA3)*
ANT1318-10C-K27Q	n	SK1	*MatA, DMC1, leu2, hht1::HphMX, hht2::G418, trp1, his4, ura3, p(hht2-K27Q, HHF2, URA3)*
ANT1318-10C-K27R	n	SK1	*MatA, DMC1, leu2, hht1::HphMX, hht2::G418, trp1, his4, ura3, p(hht2-K27R, HHF2, URA3)*
ANT1318-10C-K27M	n	SK1	*MatA, DMC1, leu2, hht1::HphMX, hht2::G418, trp1, his4, ura3, p(hht2-K27M, HHF2, URA3)*

Table 1. *Genotypes of the yeast strains used for proliferation and sporulation assays. Each histone mutation was introduced by plasmid shuffle technique and validated by Sanger sequencing.*

Growth and survival of the test strains were monitored in kinetic and end-point growth assays that were performed under various metabolic and stress conditions (**Figure 19/A** and **Figure 19/B**). The process of sporulation and meiosis were tested in diploid K27M strains to assess differentiation capacity and fertility (**Figure 19/C**). We found similar growth characteristics and stress tolerance in all tested conditions, suggesting that the basic metabolic processes, repair mechanisms and meiotic differentiation of yeast cells were not perturbed by the homozygous expression of histone H3K27M.

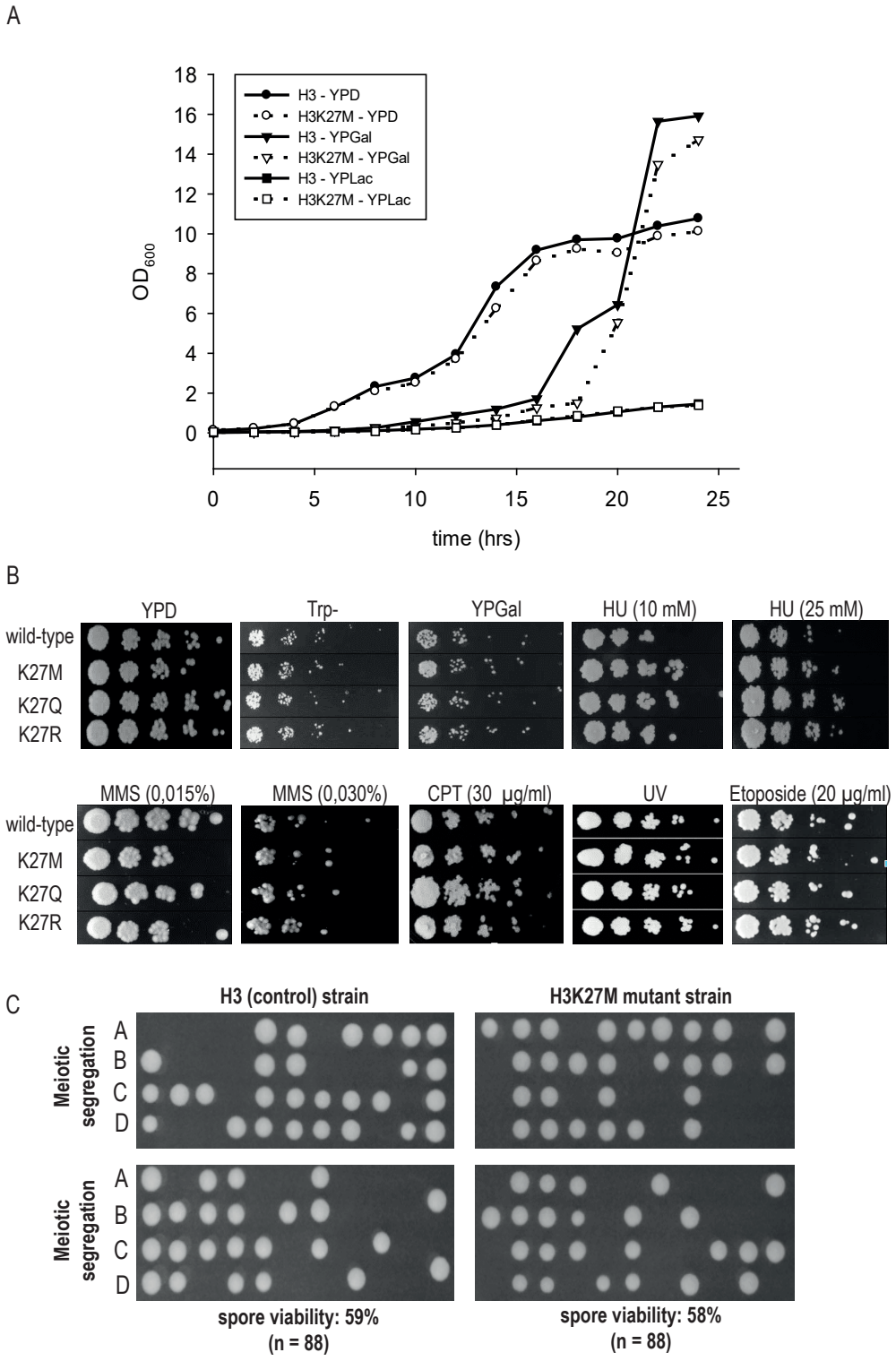

Figure 19. *(A) The growth of Saccharomyces cerevisiae in liquid cultures was monitored by measuring the absorbance (OD600) in rich medium (YPD), YP-galactose (YPGal) and YP-lactate (YPLac) over 24 hours. Similar growth curves were obtained for the control and H3K27M cells, independent from the metabolic condition. (B) End-point growth measurement (spot assay) of different H3K27 mutant strains (H3K27M, H3K27Q and*

H3K27R) in various metabolic and stress conditions. Overnight cultures were serially diluted and spotted on the indicated plates. The mutant strains did not show any growth defects under the tested conditions. (C) Wild type and H3K27M diploid strains were passed through the germline by meiosis and sporulation. There was no significant difference between the fertility of wild type and K27M strains assessed by the number of viable spores. MMS: Methyl methanesulfonate; HU: Hydroxyurea; CPT: Camptothecin.

5.4. Microscopic analysis of the nuclear distribution of wild type and H3K27M nucleosomes in relation to Ezh2

As opposed to yeasts, H3.3K27M mutation has a dominant negative character in humans that makes functional studies possible in the genetic context of endogenous (wild type) H3.3 expression. We tagged Ezh2 with mCherry and co-expressed the fusion protein with H3.3-EGFP or H3.3K27M-EGFP in live HeLa cells. We used confocal laser scanning microscopy (CLSM) to analyze the subcellular distribution of Ezh2-mCherry in relation to H3.3-EGFP and H3.3K27M-EGFP (**Figure 20**).

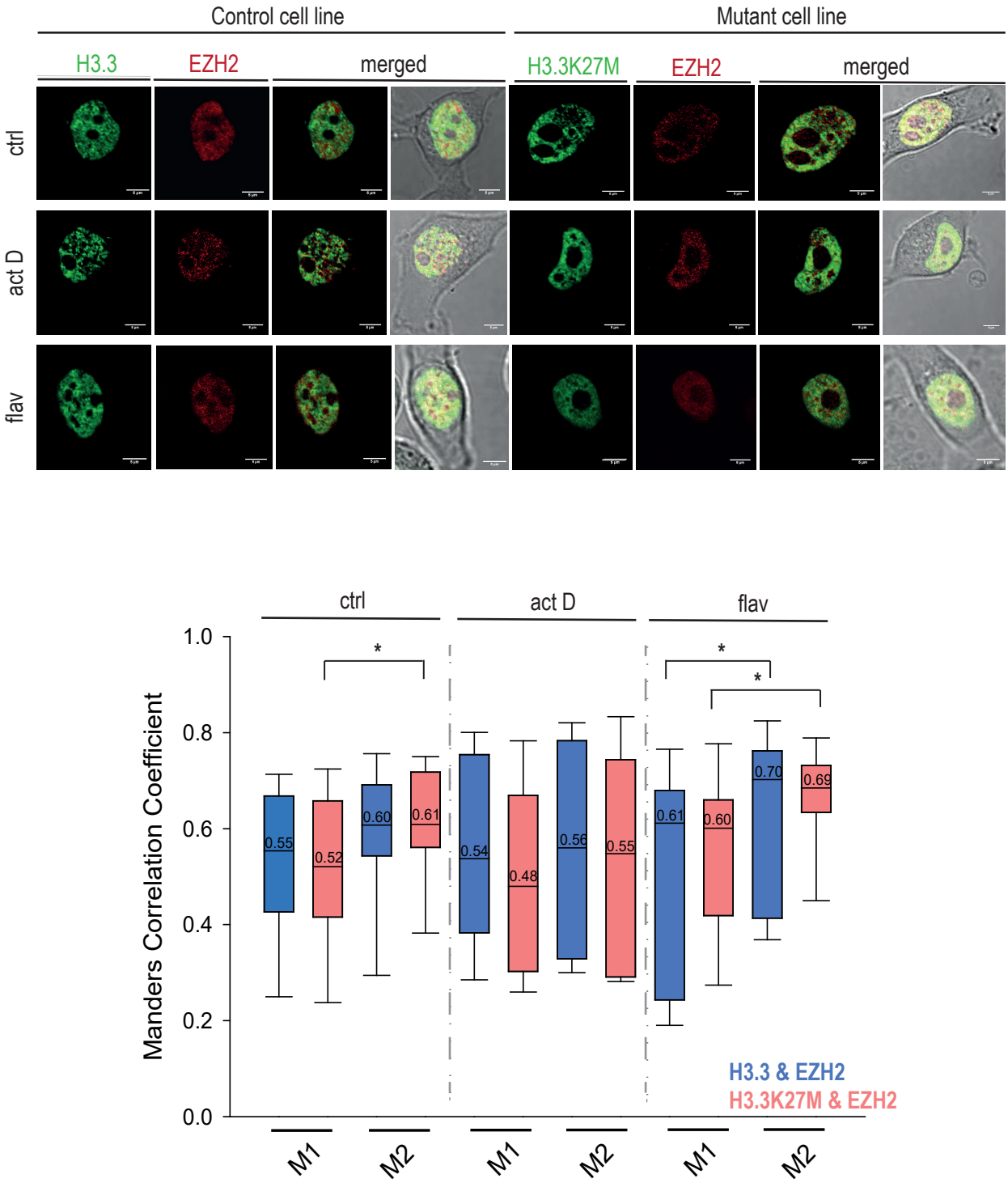

Figure 20. *Confocal laser scanning microscopy was performed in HeLa cells expressing H3.3-EGFP or H3.3K27M-EGFP (green) and Ezh2-mCherry (red). Representative optical stacks are shown. Scale bar: 5 µm. Top: Nuclear distribution of H3.3-EGFP / H3.3K27M-EGFP and Ezh2-mCherry under normal growth condition (ctrl) and after transcriptional*

inhibition induced by actinomycin D (act D, 5 µg/ml, 60 min) or flavopiridol (flav, 100 nM, 60 min). Bottom: Quantification of colocalization between H3.3-EGFP / H3.3K27M-EGFP and Ezh2-mCherry based on the Manders correlation coefficient. The Manders 1 (M1) parameter represents the fraction of H3.3-EGFP or H3.3K27M-EGFP overlapping with Ezh2-mCherry. The Manders 2 (M2) parameter corresponds to the fraction of Ezh2-mCherry overlapping with H3.3-EGFP or H3.3K27M-EGFP. For statistical analysis, two-tailed t-tests were performed at a level of significance of 0.05 ($p<0.05$). The number of cases (N) was ≥ 60. Median values are indicated in the boxplots.*

Based on the Manders' colocalization coefficients [215], [216], about half of the Ezh2 pool overlapped with histone H3.3 or H3.3K27M, while the other half occupied distinct nuclear compartments (**Figure 20** and **Figure 21**). K27M mutation or transcriptional inhibition elicited by actinomycin D and flavopiridol treatments did not change significantly the pattern of colocalization and genomic distribution of Ezh2.

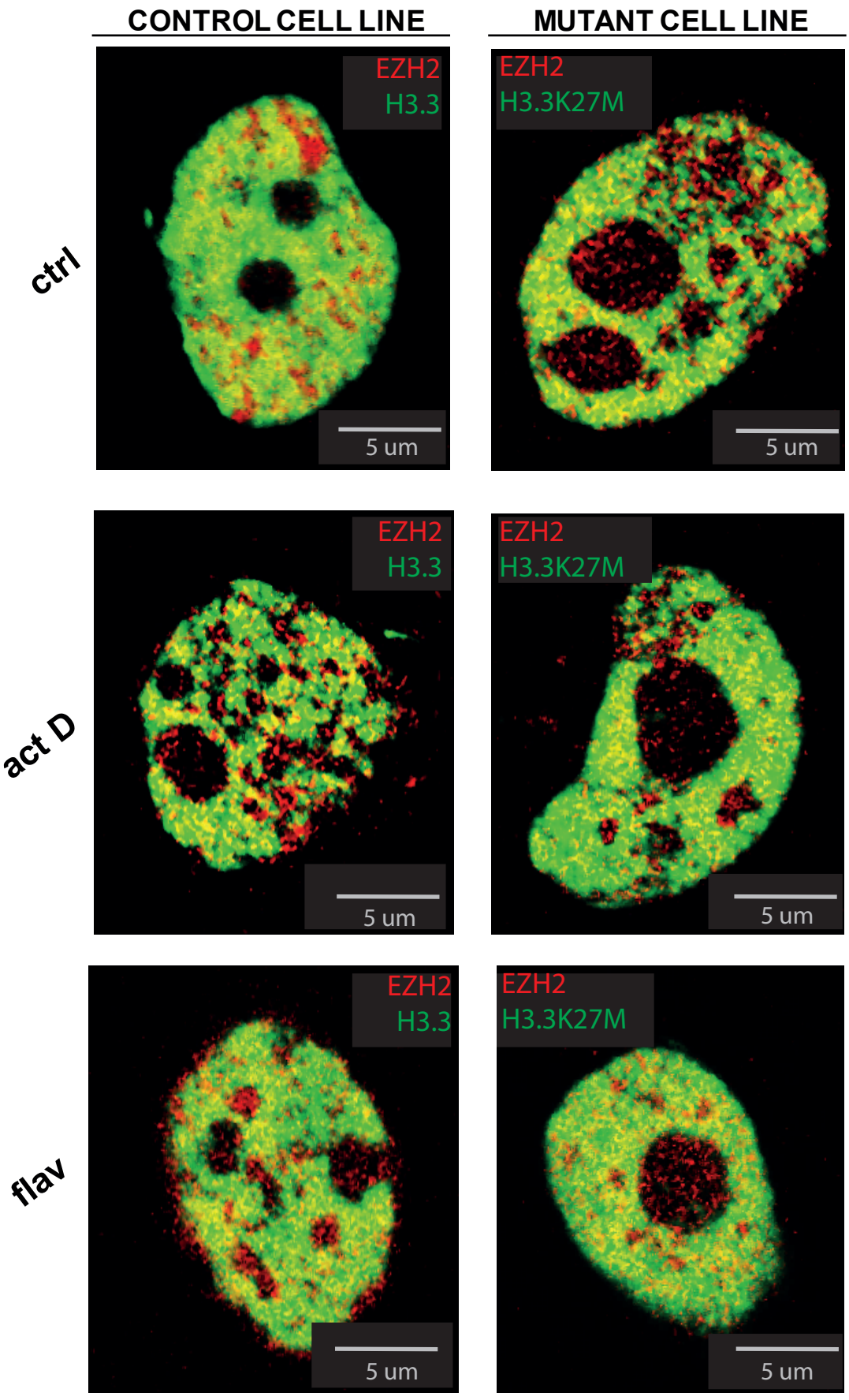
CONTROL CELL LINE
MUTANT CELL LINE
ctrl
act D
flav
EZH2
H3.3
EZH2
H3.3K27M
5 um

Figure 21. *Representative optical stacks of H3.3/H3.3K27M-EGFP and Ezh2 nuclear distribution in higher magnification.*

5.5. Kinetics study of Ezh2 and H3.3K27M at various spatial and temporal resolutions

5.5.1. Measuring the kinetics of H3.3K27M nucleosomes and Ezh2 in live cells using FRAP

We performed kinetics measurements to assess the diffusional properties of Ezh2, H3.3 and H3.3K27M histones at various spatial and temporal resolutions. We studied HeLa cells stably expressing histone H3.3-EGFP or H3.3K27M-EGFP and Ezh2-EGFP in the presence of wild type or K27M mutant histones by FRAP analysis. Transcription dependence of H3.3/H3.3K27M-EGFP and Ezh2-EGFP mobility was assessed by comparing control and transcriptionally stressed HeLa cells. Different time course was used for the measurements; long-term - up to eight hours - for the core histone molecules and short-term - seconds - for the fast Ezh2 molecules that recovers as fast as most transcription factors [217], [218]. In the histone FRAP experiments, nascent protein synthesis was inhibited by cycloheximide (CHX) to avoid the perturbing effect of newly translated histone-EGFP molecules. In each measurement, EGFP fluorescence was bleached with a high intensity laser pulse and intensity changes were tracked within the bleached regions, in the total nuclei and in randomly selected regions outside of the nuclei that were used for background subtraction. FRAP curves were obtained by normalizing the background subtracted signal with the mean pre-bleach signal and at the same time, correcting for the decrease of total fluorescence due to the initial high-intensity laser pulse and bleaching upon post-bleach imaging [218], [219]. We found that recovery of

H3.3/H3.3K27M-EGFP and Ezh2-EGFP fluorescence was independent from K27M mutation status, but it was transcription dependent (**Figure 22**).

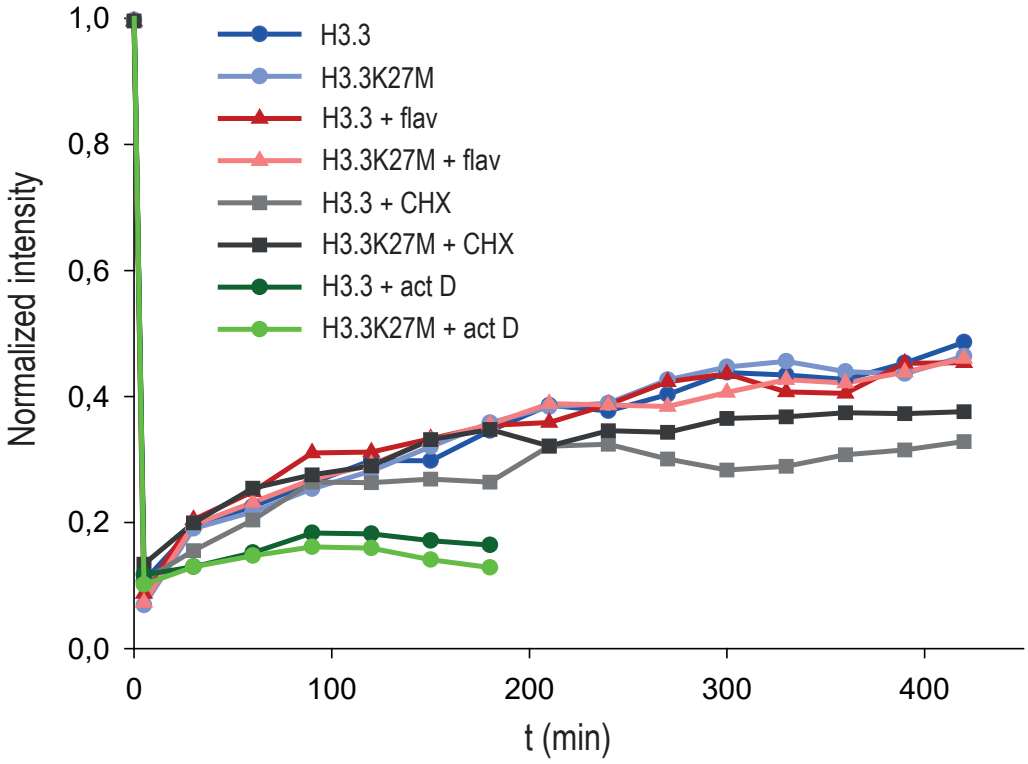

Figure 22. *FRAP recovery curves of histone measurements.*

The recovery of H3.3/H3.3K27M-EGFP fluorescence did not reach the initial pre-bleach value since most histone molecules remained in the slowly exchanging fraction. Actinomycin D increased the immobile (unrecovered) fraction of H3.3 and H3.3K27M (from 55% to 85%), suggesting strong and direct chromatin binding depending on the process of transcription. However, it is worth mentioning that actinomycin D had a fading effect on histone-EGFP expressing cells in the long-term measurements. Therefore, in contrast to 8 hours long flavopiridol experiments, actinomycin D treated cells were monitored for only 180 minutes. We observed that 5 g/ml actinomycin D treatment results in a continous decrease of EGFP signal even in low laser intensity (**Figure 23**). Since histone repopulation was examined over 8 hours

in optimal case, this phenomenon prevented the complete quantification of kinetics and allowed monitoring for 180 minutes. After the third hour, nuclei became too faded for further evaluation.

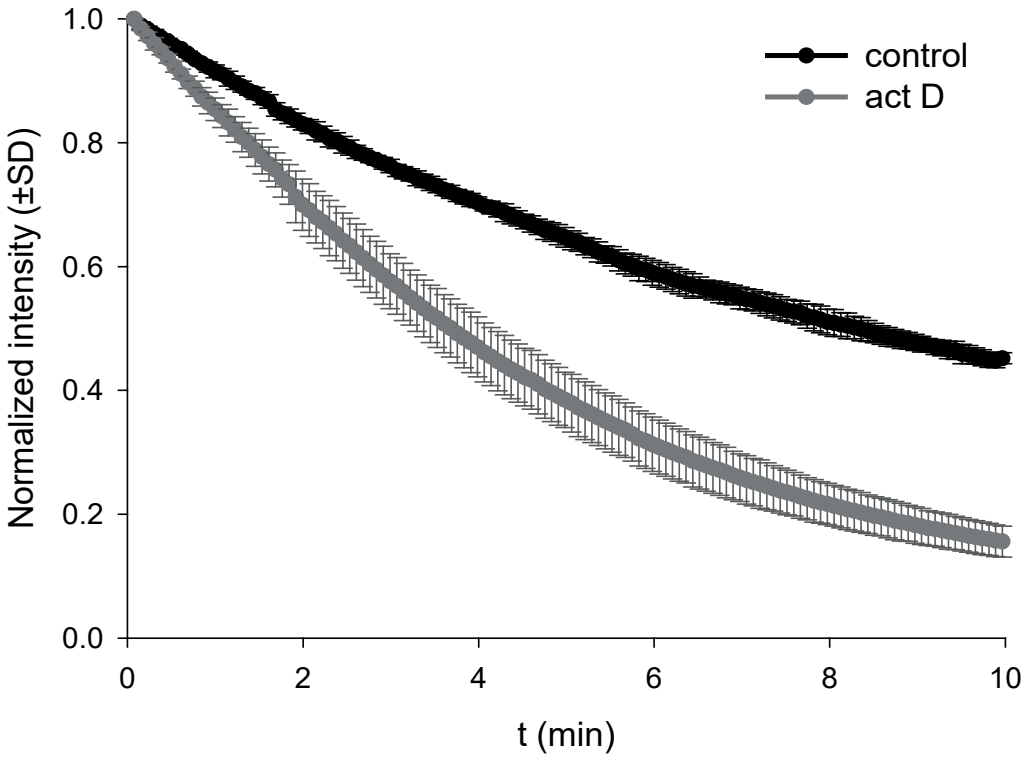

Figure 23. *EGFP fading effect of actinomycin D during long-term FRAP measurements. The curve shows a faster decay in the histone-EGFP signal compared to the control (non-treated) sample.*

Interestingly, the pTEFb (transcriptional elongation factor) inhibitor flavopiridol [220] did not change significantly the repopulation rate of H3.3/H3.3K27M histones implicating that nascent RNA elongation was nonessential for the chromatin binding of H3.3. The same general pattern was observed after cycloheximide treatment, i.e. most recovery events involved pre-existing histones.

Contrary to more static histone molecules, Ezh2-EGFP fully recovered in less than ten seconds under normal growth conditions, lacking an apparent immobile fraction. Flavopiridol and

actinomycin D treatments induced the formation of a stable immobile fraction of Ezh2 (15% and 35%, respectively). These results suggest that Ezh2 has a non-canonical cellular pool that is associated with active transcription, but it is independent from H3.3K27M mutation (**Figure 24**).

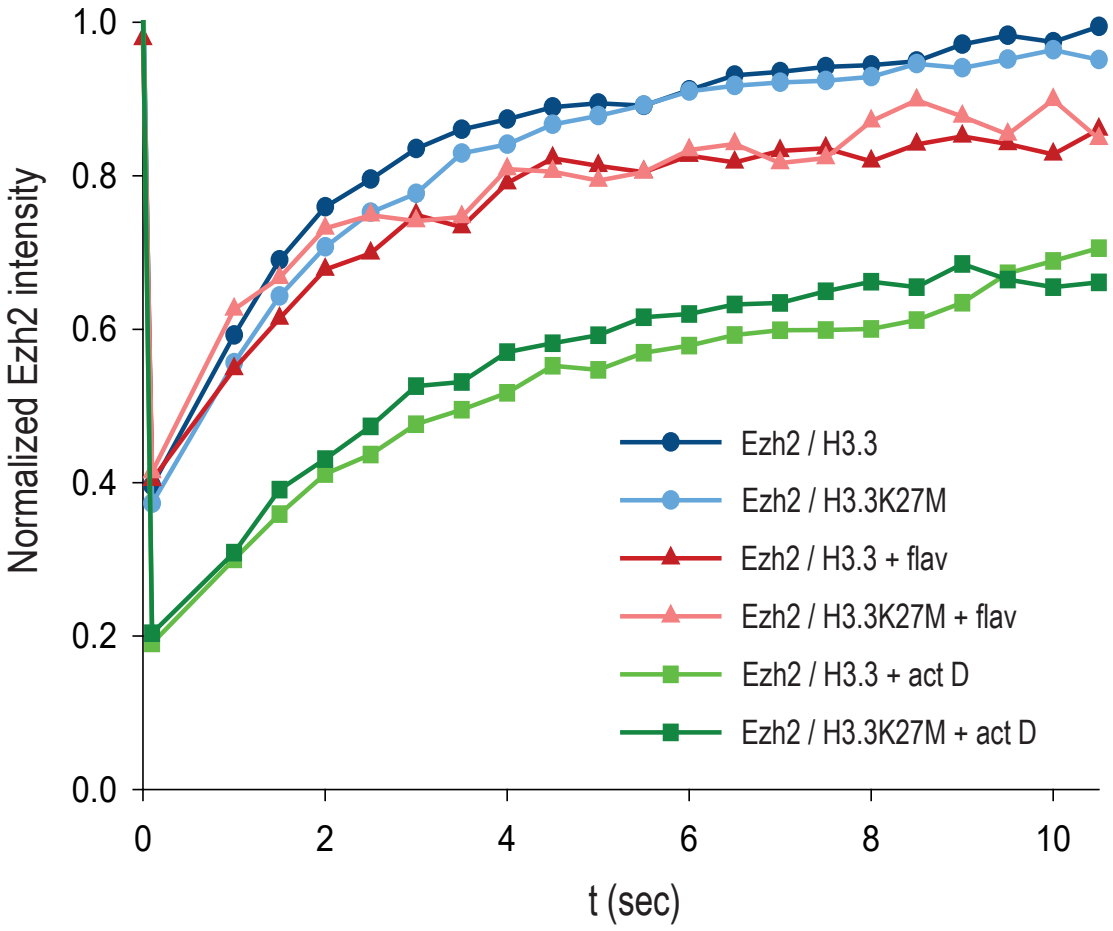

Figure 24. *Recovery curves of Ezh2-EGFP in the presence of wild type (H3.3-mCherry) or mutant (H3.3K27M-mCherry) nucleosomes.*

5.5.2. Measuring the kinetics of H3.3K27M nucleosomes and Ezh2 in live cells using FCS

To scale up the temporal and spatial resolution of our measurements and gain kinetic information in sub-second time frame and sub-micrometer distance range, we applied fluorescence correlation spectroscopy (FCS) allowing us to quantify a number of diffusion parameters (e.g. diffusion time, effective diffusion constant, fast and slow diffusion components). From the rate and frequency of fluorescence intensity fluctuations we computed the time-dependent autocorrelation function ($G(\tau)$), fitted with a 3D normal diffusion model, indicating two autonomous diffusing components (representative fitting with parameters are presented in **Figure 25,** normalized autocorrelation curves are presented in **Figure 26/A**).

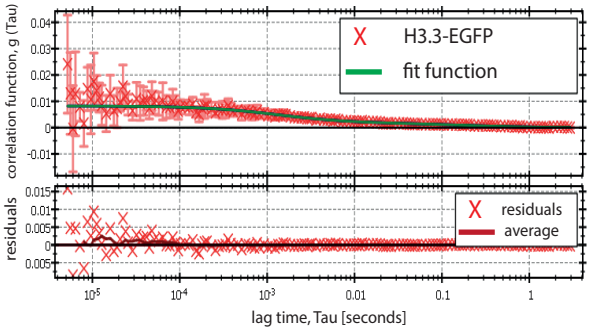

ρ1	0.69
$\tau_{D,1}$[µs]	732.95
ρ2	0.31
$\tau_{D,2}$[µs]	200000
γ	8
V_{eff}[fl]	1.09
D_2[µm²/s]	20.70
Temp. [°C]	37

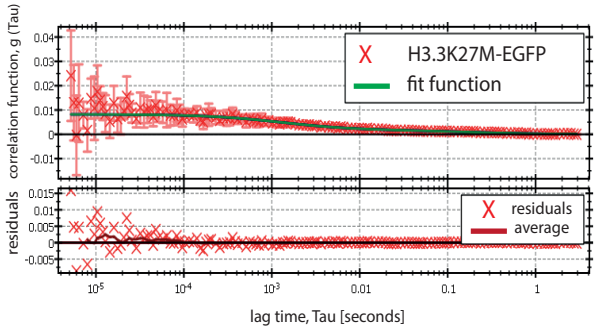

ρ1	0.70
$\tau_{D,1}$[µs]	1266.07
ρ2	0.31
$\tau_{D,2}$[µs]	200000
γ	8
V_{eff}[fl]	1.1
D_2[µm²/s]	16.85
Temp. [°C]	37

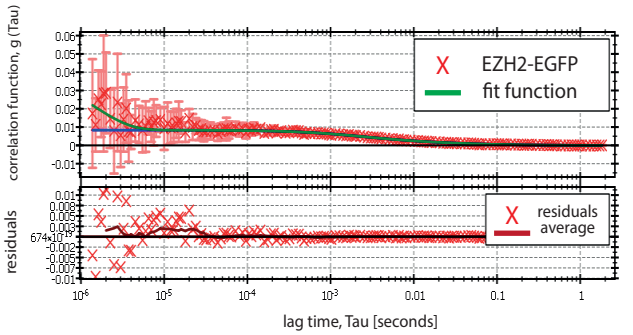

ρ1	0.63
$\tau_{D,1}$[µs]	2963
ρ2	0.37
$\tau_{D,2}$[µs]	79000
γ	9
V_{eff}[fl]	0.80
D_2[µm²/s]	5.2
Temp. [°C]	23

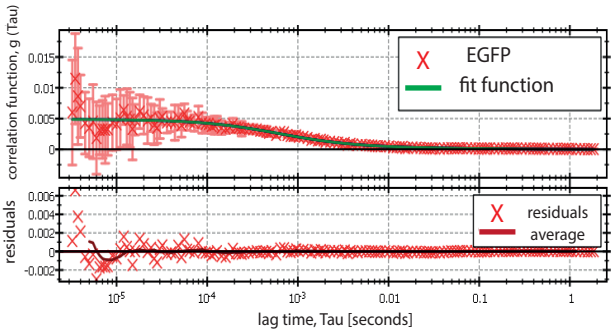

ρ1	0.95
$\tau_{D,1}$[µs]	645.3
ρ2	0.05
$\tau_{D,2}$[µs]	100000
γ	8
V_{eff}[fl]	0.53
D_2[µm²/s]	21
Temp. [°C]	23

Figure 25. *Representative autocorrelation curves fitted with a two-component 3D normal diffusion model using a simulated annealing algorithm. Analysis of fluorescence intensity fluctuations of H3.3/H3.3K27M-EGFP, Ezh2-EGFP and a monomer EGFP upon passing through a confocal volume resulted in diffusional parameters. Fitted autocorrelation curves with the residuals are shown.*

The average ratio of fast components, corresponding to the fraction of molecules freely diffusing across the nucleoplasm, was 61% (SD±19) for H3.3-EGFP and 56% (SD±20) for H3.3K27M-EGFP, respectively (**Figure 26/B,** middle). The proportion of mobile pool increased by 10% after actinomycin D treatment ($p<0.05$) in case of H3.3K27M. The average diffusion coefficient (D) was the same for wild type and K27M mutant histones (31±19 $\mu m^2/s$ and 29±16 $\mu m^2/s$, measured at 37 ºC) and it was not affected by transcription inhibition (act D) or impaired protein synthesis (CHX) (**Figure 26/B**, left). The average fraction of the fast component was approximately 60% for Ezh2-EGFP (**Figure 26/C,** middle), which slightly increased in the presence of H3.3K27M-mCherry ($p<0.05$) and after transcription inhibition by flavopiridol ($p<0.05$). The latter pool of Ezh2-EGFP also had a higher mobility (**Figure 26/C,** left), reflected by the increased diffusion coefficients of flavopiridol inhibited cells ($p<0.05$).

When the diffusion coefficients of the fast populations were converted into apparent molecular masses (based on the Stokes-Einstein equation for spherical objects [221]), there was no significant difference between the real and apparent masses of H3.3/H3.3K27M-EGFP molecules (55.9 kDa / 49.26 kDa vs. 42.26 kDa) (**Figure 26/B**, right). However, Ezh2-EGFP gave ~10-fold larger average molecular mass than the real molecular mass of the fusion protein (1.221 kDa / 1.900 kDa vs. 102.36 kDa, **Figure 26/C,** right). This difference reflects that Ezh2 is a part of large protein complexes. The apparent molecular masses were not affected by the presence of K27M mutation.

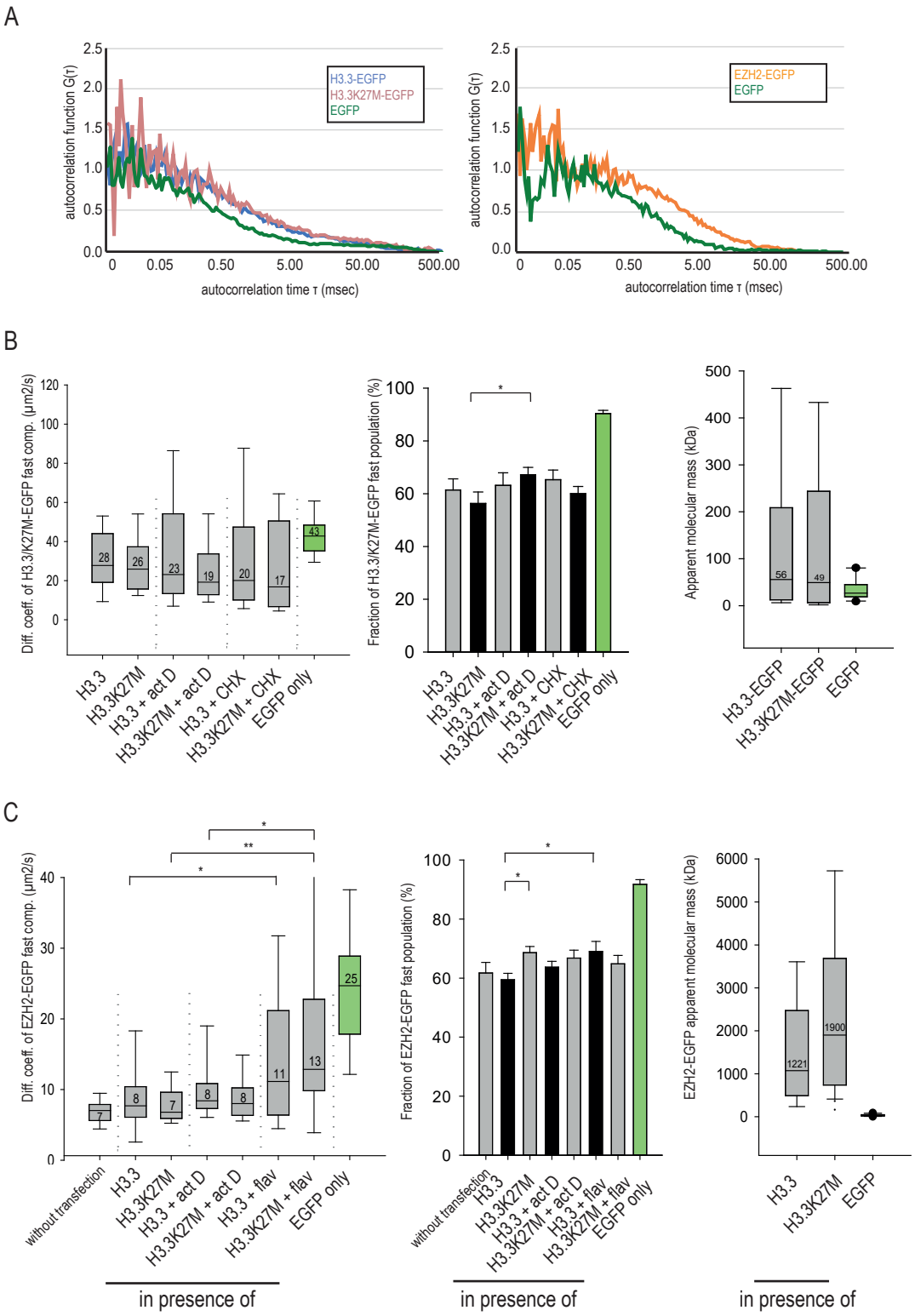

Figure 26. *Summary of the H3.3/H3.3K27M and Ezh2 FCS results. (A) Representative time-dependent autocorrelation curves after amplitude normalization. (B) Left Panel: Distribution of diffusion coefficients of H3.3-EGFP and H3.3K27M-EGFP. Middle Panel: Average fractions of fast components are shown under normal metabolic conditions and upon transcription and translation inhibition. Significant difference is indicated (* p<0.05). Data*

*were analyzed by two-tailed t-test. A p value *<0.05 was considered to be statistically significant. The number of cases (N) analyzed was ≥ 28. Error bar: SEM. Median values are indicated in the boxplots. Right Panel: Distribution of apparent molecular masses of H3.3-EGFP, H3.3K27M-EGFP, and EGFP. (C) Left Panel: Distribution of diffusion coefficients of Ezh2-EGFP in the presence of wild type (H3.3-mCherry) or mutant (H3.3K27M-mCherry) histones. Data were analyzed by Mann-Whitney rank sum test. A p value *<0.05 was considered to be statistically significant; a p value **< 0.001: highly significant,). Middle Panel: The average fraction of fast diffusion components of Ezh2-EGFP in the presence of wild type (H3.3-mCherry) or mutant (H3.3K27M-mCherry) histone. Statistical significance is indicated (* p < 0.05). Right Panel: Distribution of apparent molecular masses of Ezh2-EGFP in the presence of wild type (H3.3-mCherry) or mutant (H3.3K27M-mCherry) histones, or EGFP.*

5.6. Quantitative microscopic analysis of Spp1 and Set1 chromatin binding by FRAP and FCS

During studying the dynamics of Ezh2 Polycomb protein, we expanded our diffusional characterization to an additional, highly conserved histone methylase. The budding yeast Set1-complex called COMPASS has been proved to be an excellent model to study the SET1/MLL family complexes which play central role in the regulation of gene expression through deposition of H3K4me3 mark and contribute to malignancies of the brain, respectively [171], [172]. On the other hand, the role of Spp1 subunit in the promotion of normal DSB level is not clear. We assume that Spp1 has a COMPASS-independent role in meiotic DSB formation and it manifests in altered diffusional properties.

Thus, we carried out kinetics analysis on two COMPASS subunits, Spp1 and Set1, involving FRAP and FCS techniques. The measurements were performed under meiotic and vegetative conditions controlled by the inducible pCUP1 promoter. The successful induction of GFP-Spp1 or GFP-Set1 allele is shown in ***Figure 27.***

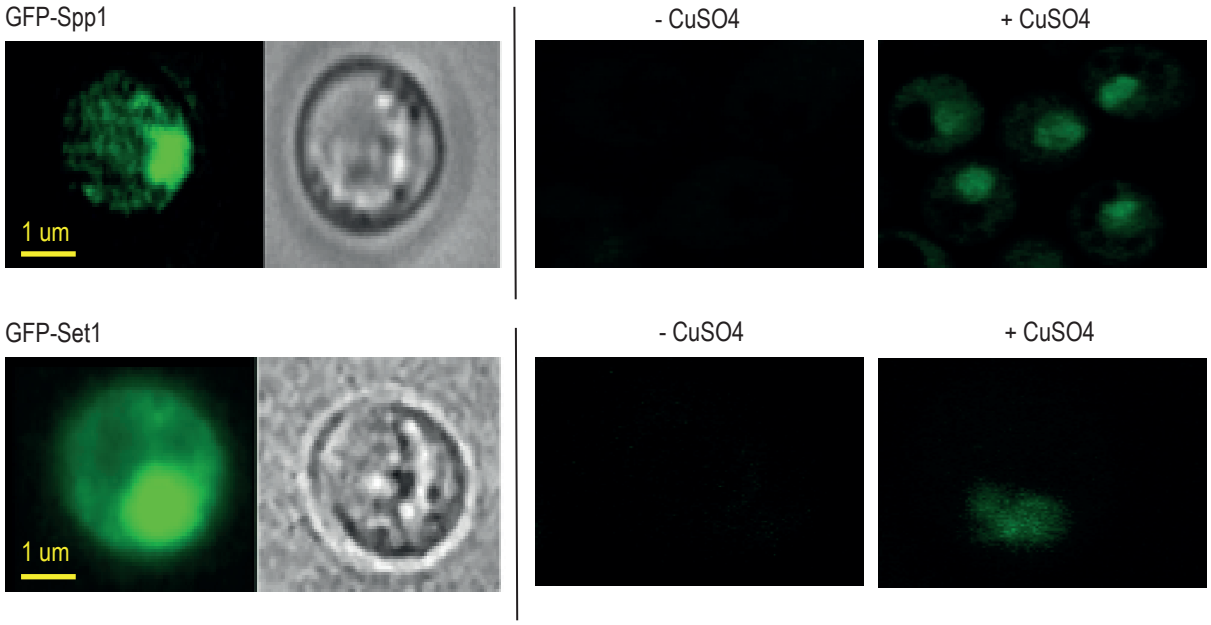

Figure 27. *N-terminally tagged fluorescent Spp1 and Set1 proteins were induced in sporulating or vegetative yeast cells by adding 100 µM $CuSO_4$. Expression was driven by a pCUP1 promoter. Increased nuclear level of GFP signal became easily detectable following copper treatment.*

Using FRAP, whole live-cell nuclei were bleached and fluorescence recovery was examined in the first five hours of meiosis (**Figure 28/A**) in SPM and in the exponential phase in YPD rich medium (**Figure 28/B**). The recovery of the fluorescent signal in the bleached area as the consequence of movement of the GFP-Spp1 and GFP-Set1 is recorded by sequential imaging scans. GFP-Spp1 and GFP-Set1 recoveries reached the plateau within less than 50 seconds. The recorded mobility suggests that they are highly dynamic within the nucleoplasm. However,

about half of the FRAP signal did not return after the initial bleach pulse, indicating that ~50% of Spp1 and Set1 remained tightly bound to chromatin representing the immobile fraction.

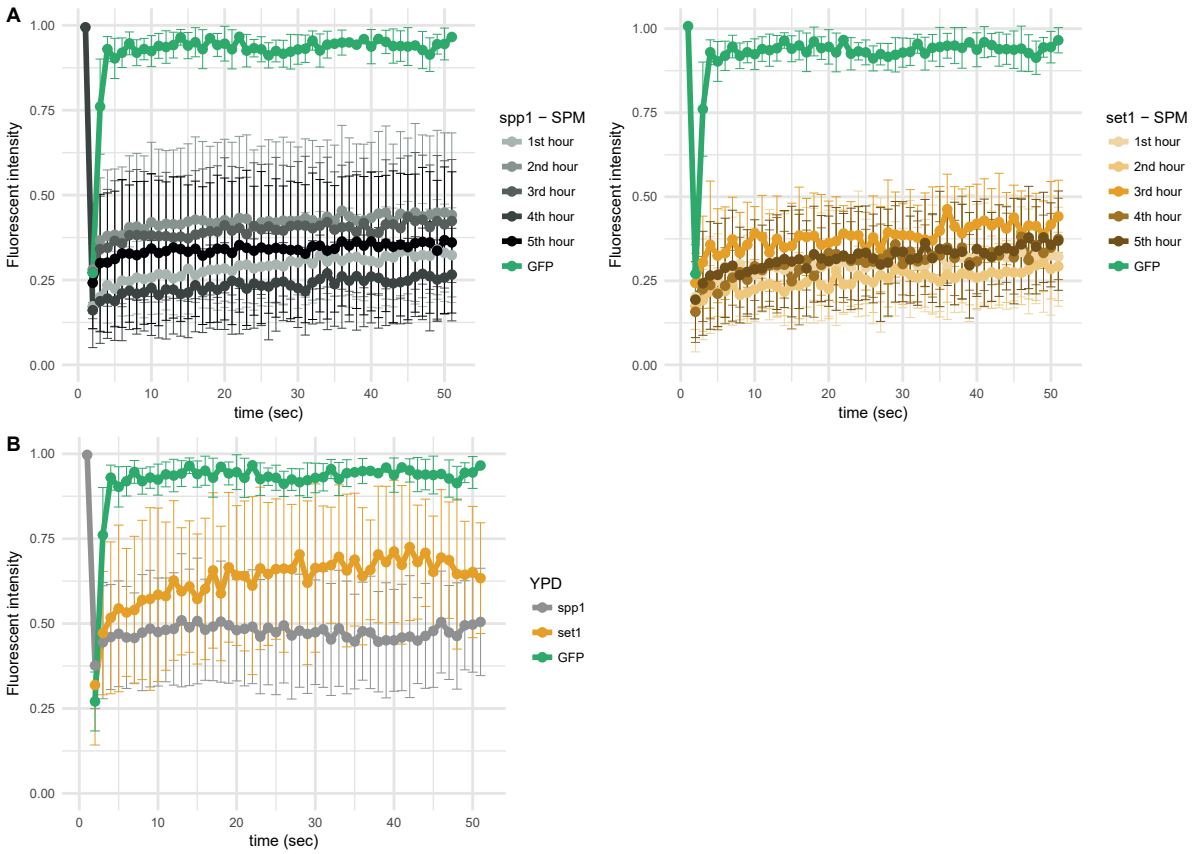

Figure 28. *FRAP recovery curves of GFP-Spp1 and GFP-Set1 in meiotic (SPM) and standard (YPD) condition. (A) The curves show the retrieval of GFP-Spp1 (grey), GFP-Set1 (orange), and GFP only (green) signals at various meiotic timepoints. Plateau phase was reached within 50 seconds in both Spp1 and Set1 measurements (error bar: SD). (B) Slight, but not significant difference between Set1 and Spp1 recovery in rich medium.*

Next, similarly to our experiments with histones and Ezh2, we reduced the time and spatial range and estimated the diffusional parameters of GFP-Spp1 and GFP-Set1 by monitoring the Brownian movement of individual proteins. Time-dependent autocorrelation functions were fitted in the same way as described previously *(Equation 2)*. The distribution of fast and slow components did not show any differences between Spp1 and Set1 (**Figure 29**, left), however,

the average diffusion coefficient (D) of Spp1 was significantly slower compared to Set1 (**Figure 29**, middle). The altered diffusion coefficient highlights the reduced nuclear mobility of Spp1. When diffusion times were converted into apparent molecular mass, GFP-Set1 was equal to the expected molecular mass of COMPASS (379 kDa) while GFP-Spp1 gave an approximately 43-fold higher value (1764 kDa) compared to the real molecular mass of the fusion protein (**Figure 29**, right). This can be related to the anchoring of Spp1 protein to a huge macromolecular complex that was different from COMPASS.

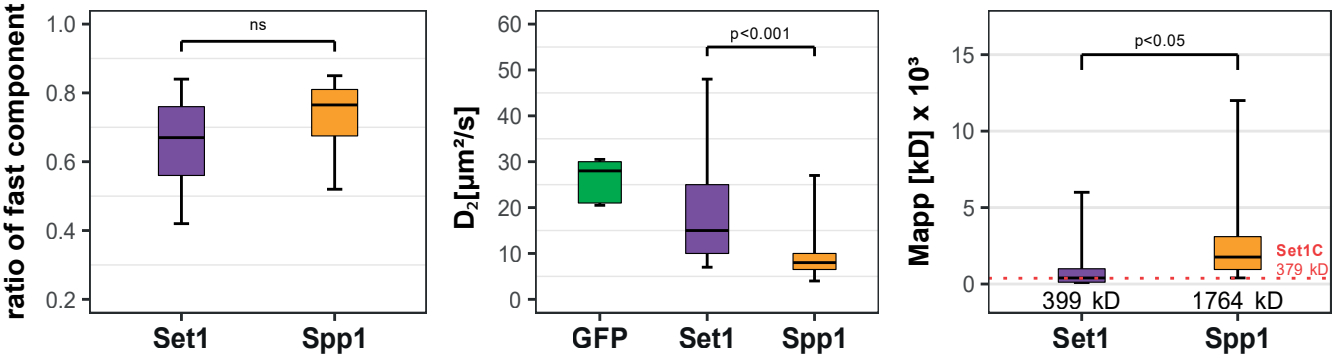

Figure 29. *Interpretation of the collected autocorrelation curves shows significant differences between GFP-Spp1 and GFP-Set1 diffusion coefficients (D) and apparent molecular mass (M_{app}) with similar fast component distribution in meiotic condition. Left panel: Average fraction of fast components after two-component fitting. (ns: no statistically significant difference between GFP-Spp1 and GFP-Set1) Middle panel: Distribution of diffusion coefficients. Significant difference is indicated (*p<0.001, Mann-Whitney rank sum test). Right panel: Distribution of apparent molecular masses (M_{app}) of the mobile complexes comprising GFP-Spp1 and GFP-Set1. Numbers show median M_{app} values in kDa. Significant difference is indicated (*p<0.001, Mann-Whitney rank sum test). Molecular mass of the full Set1 complex is also shown at the right side of the figure.*

5.7. Quantitative analysis of Spp1 chromatin binding by competition ChIP

To quantify the binding characteristics of Spp1 in terms of turnover and residence time, we performed dynamic chromatin mapping using c-ChIP, which allowed estimation of *bona fide* turnover rates at Spp1 binding sites [212]. We differentially tagged a constitutive and an inducible isoform of Spp1 with myc and GFP epitopes, respectively (**Figure 31/A**), and turned on the expression of the inducible allele (driven by a pCUP1 promoter similarly to FCS and FRAP experiments) with copper addition during the meiotic time course. The induced Spp1 protein isoform could be detected as early as 30 minutes after copper induction. Genotypes of the c-ChIP strains are listed in **Table 2.**

Strain	Ploidy	Backgr.	Genotype
LV21	2n	SK1	*Mata/Matα, leu2/LEU2, HIS4/his4, trp1/trp1, ura3/ura3, set1Δcter-9xmyc-SET1::LEU2/NatMX4-pCUP1-1-yGFP-SET1*
LV22	2n	SK1	*Mata/Matα, leu2/LEU2, HIS4/his4, trp1/trp1, ura3/ura3, SPP1-13xmyc::KanMX4/NatMX4-pCUP1-1-yGFP-SPP1*

Table 2. *Genotypes of the c-ChIP yeast strains. Strains were created by Lóránt Székvölgyi.*

The GFP-Spp1 level increased exponentially during the time course and reached its maximum after 6 hrs in SPM (**Figure 31/B**). Then, Myc and GFP ChIP experiments were performed corresponding to dense meiotic timepoints (4.5, 5.0, 5.5, 6.0, 6.5 hrs in SPM, with the kind/great help of Éva Nagy, Beáta Boros-Oláh and Ibolya Fürtös). Binding sites were determined similarly to conventional ChIP-Seq pipelines. Then, Spp1 turnover rates were calculated by determining the ratio of GFP (new Spp1) and myc (old Spp1) ChIP signal and fitting the data with an exponential model. The fitting was based on the model published in [222] and [212]. The ratio of Spp1 isoforms provided an estimate of the nucleoplasmic pool of Spp1 molecules. An example fit of our turnover rate model is demonstrated in **Figure 30.**

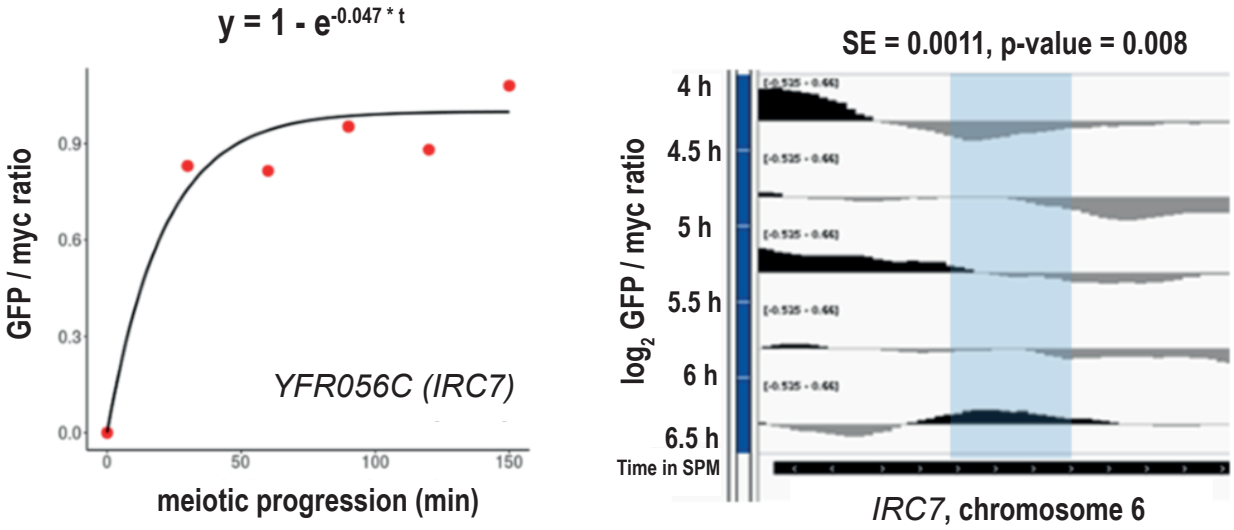

Figure 30. *Representative Spp1 turnover estimation on the IRC7 locus. Model equation (with standard error (SE) and p-value) and temporal changes of GFP / myc ratios are shown on the left panel. Genome browser snapshot is shown on the right.*

In these computational steps, the workflow was optimized and performed by Zsolt Karányi. Our analysis revealed that Spp1-binding sites (that could not be associated with COMPASS) exhibited different replacement dynamics compared to common (Spp1 & Bre2) binding sites. Spp1-only sites were significantly slower than canonical (COMPASS-associated) sites over gene bodies, TTS, RPG/Ribi genes, and Mer2/Red1 sites (**Figure 31/C**). This suggests that Spp1 binding is more stable at these genomic elements. If Spp1 binding sites were grouped by their kinetic behaviour (disappearing, appearing, and constant fractions, **Figure 31/D-H**), disappearing and appearing Spp1 sites would sharply stood apart based on the distribution of turnover rates and occupancies like disappearing Spp1 sites tended to have higher turnover rates and higher occupancies compared to appearing sites (**Figure 31/D**). Appearing Spp1 sites with longer residence times were strongly associated with high Mer2 occupancy, low H3K4me3 and Bre2 occupancies whereas disappearing Spp1 sites showed low Mer2 occupancy, high H3K4me3 and Bre2 occupancies and high turnover rates (**Figure 31/E-G**).

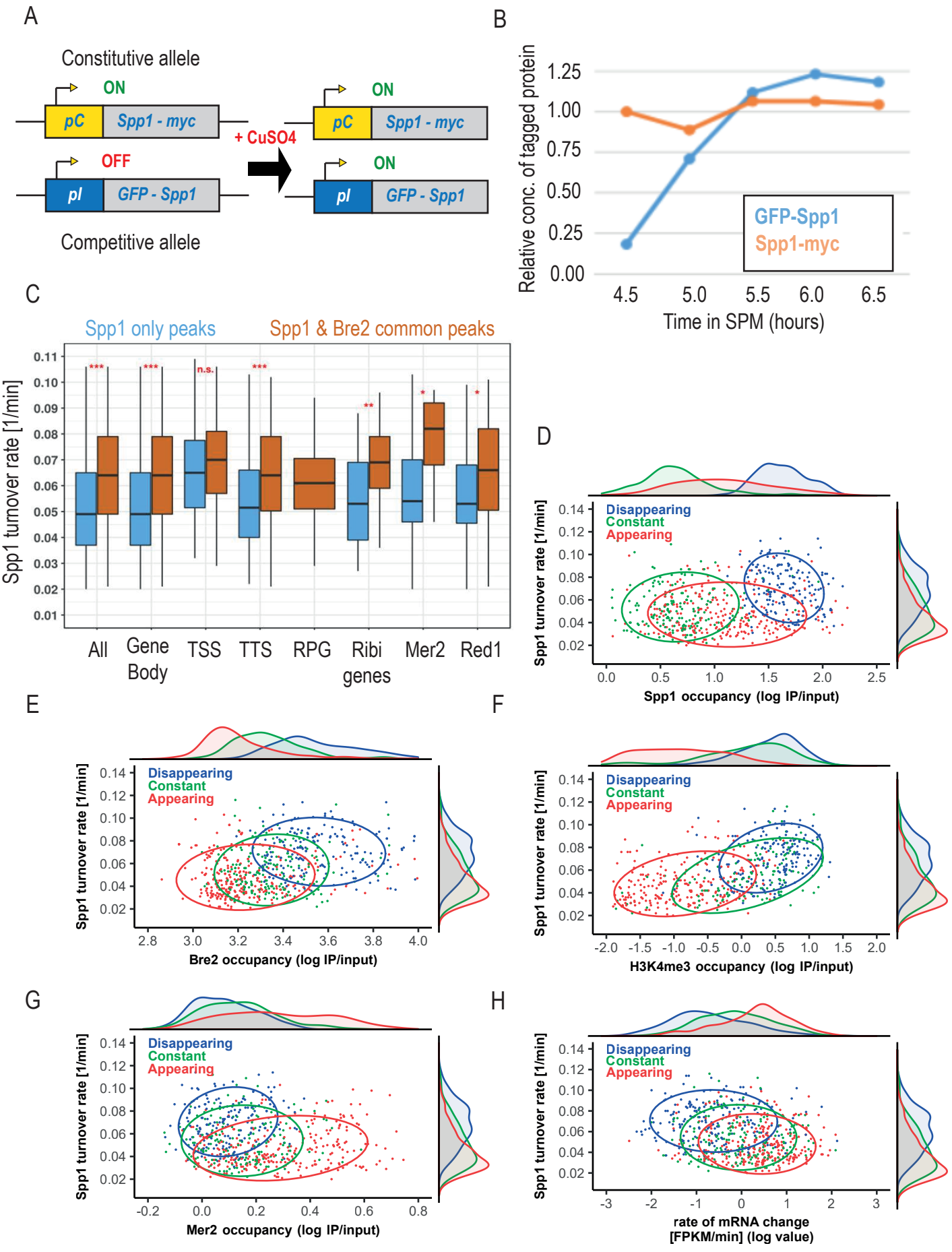
A
Constitutive allele
ON
pC
Spp1 - myc
+ CuSO4
ON
pC
Spp1 - myc
OFF
pI
GFP - Spp1
ON
pI
GFP - Spp1
Competitive allele
B
Relative conc. of tagged protein
1.25
1.00
0.75
0.50
0.25
0.00
4.5
5.0
5.5
6.0
6.5
Time in SPM (hours)
GFP-Spp1
Spp1-myc
C
Spp1 only peaks
Spp1 & Bre2 common peaks
Spp1 turnover rate [1/min]
0.11
0.10
0.09
0.08
0.07
0.06
0.05
0.04
0.03
0.02
0.01
***
***
n.s.
***
**
*
*
All
Gene Body
TSS
TTS
RPG
Ribi genes
Mer2
Red1
D
Spp1 turnover rate [1/min]
Disappearing
Constant
Appearing
0.14
0.12
0.10
0.08
0.06
0.04
0.02
0.0
0.5
1.0
1.5
2.0
2.5
Spp1 occupancy (log IP/input)
E
Spp1 turnover rate [1/min]
Disappearing
Constant
Appearing
0.14
0.12
0.10
0.08
0.06
0.04
0.02
2.8
3.0
3.2
3.4
3.6
3.8
4.0
Bre2 occupancy (log IP/input)
F
Spp1 turnover rate [1/min]
Disappearing
Constant
Appearing
0.14
0.12
0.10
0.08
0.06
0.04
0.02
-2.0
-1.5
-1.0
-0.5
0.0
0.5
1.0
1.5
2.0
H3K4me3 occupancy (log IP/input)
G
Spp1 turnover rate [1/min]
Disappearing
Constant
Appearing
0.14
0.12
0.10
0.08
0.06
0.04
0.02
-0.2
0.0
0.2
0.4
0.6
0.8
Mer2 occupancy (log IP/input)
H
Spp1 turnover rate [1/min]
Disappearing
Constant
Appearing
0.14
0.12
0.10
0.08
0.06
0.04
0.02
-3
-2
-1
0
1
2
3
rate of mRNA change
[FPKM/min] (log value)

Figure 31. *Competition ChIP unravels bona fide turnover rates of Spp1 chromatin binding. (A) Scheme of the c-ChIP yeast strain. Differentially tagged Spp1 isoforms are expressed from allelic positions in a diploid cell. The constitutive allele (Spp1-myc) is driven by an endogenous SPP1 promoter while the inducible allele (GFP-Spp1) is controlled by a copper-inducible (pCUP1) promoter. Expression of GFP-Spp1 was induced by addition of 200 μM of* $CuSO_4$*. (B) Relative protein levels of induced GFP-Spp1 and constitutive Spp1-myc as a function of time. Copper induction was initiated at 4.5 hrs in SPM and cells were collected in every 30 min until 6.5 hrs in SPM to perform c-ChIP analyses. (C) Turnover rate of Spp1 over functional genomic elements for Spp1-bound sites (that are not associated with Bre2) and common (Spp1&Bre2) binding sites. The turnover rate of Spp1-only sites is significantly slower than the turnover rate of common (Spp1&Bre2) sites (Student's t-test, * $p < 0.001$; ** $p < 0.0001$; *** $p < 0.00001$). Ribosome protein genes (RPG) are not associated with Spp1-only peaks, therefore, there is no turnover rate estimation for this peak category. TSS: transcription start site; TTS: transcription termination site. (D-G) Turnover rate vs. occupancy plots reveal differential chromatin binding dynamics among the three kinetic classes of Spp1 peaks. y axis: Spp1 turnover rate; x axis: Spp1/Bre2/H3K4me3/Mer2 occupancy. Disappearing, appearing, and constant Spp1 peaks are highlighted in blue, red, and green, respectively. On the top and the right side of scatter plots, histograms show the distribution of the measured parameters. Circles denote the confidence interval (q10-q90) of the point distributions. (H) Spp1 turnover rate as a function of meiotic gene expression. Three kinetic classes of Spp1 binding sites cannot be distinguished based on these parameters.*

6. DISCUSSION

Histone tails play an important role in nucleosome structure and dynamics. Selective changes of histone tail residues, particularly the residues of H3 N-terminal tail, are able to alter the stability and dynamic properties of nucleosome core particles [223], [224]. The first aim of our study was to examine whether the H3K27M histone mutation affects nucleosome structure or perturbs chromatin incorporation of the mutant histone. In order to accurately answer these questions, we successfully performed FRET-based experiments at single-molecule and bulk level to study nucleosome architecture, and carried out *in situ* salt elution assay to estimate the stability of chromatin incorporated histone H3K27M.

Based on the performed spFRET and μpsFRET experiments, we found that dissociation mechanism of nucleosomes containing H3K27M histones is the same as dissociation of wild type nucleosomes. These results suggest that H3K27M nucleosomes maintain their wild type molecular architecture and stability, indicating that this single amino acid substitution of the N-terminal H3 tail domain does not cause detectable rearrangements in the structure of nucleosome core particle. Beyond the scope of this thesis, but the intra-molecular similarity between wild type and mutant nucleosomes was also revealed by Replica-Exchange Molecular Dynamics (REMD) simulation using Gromacs 4.5 software (collaboration with Jörg Langowski's workgroup, Biophysics of Macromolecule, DKFZ Heidelberg). The salt elution profile of incorporated H3.3K27M histones serves a good evidence that these mutant nucleosomes show similar structural features in the native chromatin as their wild type counterparts.

During structural analysis of H3K27M nucleosomes, we raised the question whether Ezh2 affects the architecture of mutant nucleosomes. Including Ezh2 into FRET experiments was relevant as its binding to methionine residue of the K27M mutation [161] plays a crucial role

in the epigenetic dysregulation of pediatric glioma. We assumed that the collaboration between Ezh2 and H3K27M nucleosomes results in structural alterations. In order to test this hypothesis we repeated the μpsFRET experiments supplemented the reconstituted nucleosomes with Ezh2 complex. Although we probed various conditions including the optimalization of Ezh2/nucleosome molecular ratio, incubation time and fluorophore position, we could not find any nucleosome alteration caused by the Ezh2 complex. This result was confirmed by EMSA experiments showing no convincing difference in the electrophoretic mobility between nucleosomes and nucleosomes treated with Ezh2 complex. We also quantified the remaining Ezh2 in salt treated HeLa nuclei in vicinity of H3.3K27M-EGFP and concluded that the mutant histone does not affect the elution profile of Ezh2 in the range of 0-400 mM NaCl.

In summary, the structural analysis of nucleosomes bearing H3K27M provides impressive evidence that neither K27M missense mutation nor Ezh2 complex do not alter dramatically the nucleosome architecture and rather nuclear biochemical processes cause the gain-of-function mechanism.

To examine the impact of H3K27M on cell viability and chromatin-templated processes we engineered H3K27 mutant yeast strains and carried out a genetic screen with a growth assay under various stress and metabolic conditions. The aim of this assay was to gain a mechanistic insight how H3K27M mutation may promote genomic instability in glioma. An advantage of the system was that the chromosomal H3 and H4 histone genes were deleted in these strains, and they were kept alive by plasmid expressing wild type H4 histone and H3 histone bearing the particular mutation. Thus, the H3 histone pool of the mutant strains carried exclusively mutant H3 histones. The experiments demonstrated that *Saccharomyces cerevisiae* cells with the mutant form of histone H3 did not show any growth defect and stress sensitivity neither in vegetative nor in meiotic conditions. As the PRC2 complex does not exist in budding yeasts, these results might suggest that the involvement of PRC2 pathway is a crucial point of the

K27M phenotype and the mutation alone cannot account for remarkable alteration in nuclear processes. Interestingly, a similar experimental system was used to study the H3G34R effect in fission yeast by *Yadav et al.* [225], in which the mutant histone pool caused increased sensitivity to chemicals and resulted in chromosomal instability.

Our further aim regarding H3K27M was to accomplish an *in vivo* functional analysis in human cells, in which we image the nuclear distribution of mutant histones in relation to wild type histones and Ezh2, and probe the diffusional properties of these proteins at various spatial and temporal resolutions using FRAP and FCS. In these studies, we also examined the transcription dependency of H3.3K27M and Ezh2 using actinomycin D and flavopiridol to inhibit transcription.

The nuclear distribution of Ezh2 and H3.3 / H3.3K27M based on CLSM analysis did not show convincing differences in the colocalization patterns neither in non-treated nor in transcription inhibited condition. Manders' coefficient was a good indicator that Ezh2 was not changed much by the K27M mutation or due to transcription inhibition. However, Ezh2 distribution (e.g. Ezh2 accumulation near K27M nucleosomes) seemed to be different likely due to Ezh2-K27M methionine binding. Considering the limitations of the confocal microscopy and the homogenous distribution of histone H3.3 our assumption was not further investigated.

In live human cells, H3.3K27M histones followed similar diffusion kinetics to their wild type counterparts and fully recapitulated the slow kinetics and tight chromosome binding of canonical (replication-dependent) H3 molecules. Here, the novelty was the understanding of long-term nuclear kinetics of histone variant H3.3 which is a least-studied part of the field [58]. Furthermore, we found that act D treatment (but not flavopiridol) significantly increased the immobile fraction of H3.3 histones suggesting transcription-dependent H3.3 mobile component. Although, the EGFP fading effect of actinomycin D may contribute to slower H3.3 recovery.

By FRAP and FCS we found a remarkable differential recovery of Ezh2 in response to transcriptional stress that was accompanied by a significantly increased immobile fraction and faster diffusion rate of the mobile fraction. The differential recovery of Ezh2 was rather dependent on transcription than K27M mutation status. Except the significant difference between Ezh2 fast component ratio of H3.3 and H3.3K27M co-transfected cells, the transcription inhibition perturbed the Ezh2 kinetics in each case. The results suggest that the nuclear mobility of Ezh2 is significantly restrained by transcription elongation, independently from the presence of H3.3K27M mutation. An explanation for the faster Ezh2 diffusional rate observed by FCS might be that the inhibited transcription allows a more mobile, possibly a PRC2-independent function for Ezh2 [226]. A remaining and interesting question regarding this finding is the well reproducible, slower recovery curve after inhibition. The Ezh2 recovery without transcriptional stress was in accordance with previously published data presenting high mobility properties of numerous nuclear proteins [53]. Noteworthy, the similar Ezh2 diffusional coefficients between H3.3 and H3.3K27M co-transfected cells are consistent with the results of a recent study [227] in which *Tatavosian et. al* did not find any alteration in Ezh2 diffusional coefficient in HEK293T cells expressing H3.3K27M-FLAG or H3.3-FLAG transgene.

The estimation of the apparent molecular weight of Ezh2 showed a slight, but not significant, increased molecular weight in H3.3K27M-EGFP transfected cells. This increase might be a result of the “gluelike” property of methionine resulting in non-specific bindings between the PRC2 subunit and nucleosomes bearing H3.3K27M.

Moreover, the COMPASS histone modifying complex was introduced into our experimental system utilizing our FCS and FRAP knowledge. We were particularly interested how the Spp1 protein diffusional behaviour differs from the Set1 catalytic subunit in meiotic conditions. First of all, this study was relevant regarding the described diffusional parameters. The results raised the possibility, that Spp1 has a COMPASS-independent function on chromosome axial sites

and contributes to chromatin changes preparing potential recombination initiation sites for meiotic DNA break formation. On the other hand, the diffusional properties of the COMPASS protein complex, similarly to mobility of TrxG and PcG proteins was unexplored so far. Since TrxG and PcG proteins are conserved in eukaryotes and they function within similar pathways, the biophysical experiments performed in this study might shed light on the diffusion properties of Mll proteins as well. Considering that homologous recombination plays an important role in the evolution of eukaryotic genomes, unraveling the process of DSB initiation becomes particularly interesting. However, the prevailing molecular model of meiotic DSB formation is based mainly on studies performed in yeasts and we have also studied the underlying mechanisms of DSB initiation in *Saccharomyces cerevisiae*, several steps have been shown to be evolutionarily conserved in mammals. For instance, in mammalian meiotic cells, H3K4me3 marks are conserved on the chromosome axes near DSB hotspots. [228]. Similarly to Spp1, a mammalian protein (e.g. one of the numerous PHD finger-containing proteins) may read the H3K4me3 mark and allow molecular interactions with DSB proteins. Potential candidates might be the interaction partners of the Prdm9 H3K4 methylase [198]. Based on this, following writing of H3K4me3 on the nearest nucleosome (or nucleosomes), Prdm9 promotes the recruitment and activation of the Spo11-containing recombination initiation complex through protein interactions.

Regarding nuclear mobility, we observed a similar recovery kinetics in both Spp1 and Set1 using FRAP. The intensity curves reached the plateau phase within 50 seconds during the measurements without significant differences. The estimated, approximately 50% immobile fraction indicates that the half of the whole fraction is tightly bound either to the chromatin or to another high molecular weight complex. These experiments were repeated in YPD medium and the profile showed high similarity. We detected a modest difference between Spp1 and Set1 recovery in this condition, however, it was not significant. These results also showed that the

difference between vegetative and meiotic conditions did not alter the nuclear mobility at this timescale.

Moreover, in order to characterize these two subunits, we applied FCS in the first six hours of sporulation. This period overlaps with the early prophase of the first meiotic division, when the homologous recombinations occur. We analyzed the fluorescence autocorrelation functions with a two-component model of normal diffusion. Following fittings we observed similar amount of fast component distribution, but distinct diffusion coefficient between Spp1 and Set1. The reduced diffusion coefficient of Spp1 is a good indicator of Spp1 binding to the chromosome in this phase of sporulation. Furthermore, to better understand the mechanism behind slower Spp1 mobility, we estimated the apparent molecular weight of GFP-Spp1 and GFP-Set1 using a similar method as in our Ezh2 and H3.3 experiments. Based on our results, the apparent molecular weight of GFP-Spp1 was increased and resulted in a remarkable difference between the expected and observed molecular weight of Spp1. This difference cannot be explained by nucleoplasmic interactions with diffusible protein factors, but rather with transient chromatin associations that can easily account for this differential diffusional behaviour. These data supported the previously proposed model in which the interaction between Spp1 and Mer2 brings potential meiotic DSB sites to the axis, thereby allowing their cleavage by Spo11 at axis-proximal regions that are depleted in nucleosomes [132], [133], [229]. The model integrated in meiotic steps of budding yeasts is shown in **Figure 32**. It demonstrates that Spp1 switches function in the early phase of meiosis and binds H3K4me3 in the nucleosome depleted regions independently from COMPASS. It is possible that there are similar meiosis-specific activities in the mammalian chromatin as well. In mammals, the position of hotspots is mainly defined by the presence of a consensus sequence for Prdm9 methyltransferase binding that trimethylates H3K4 and H3K36 at these sites [186]. There may also be a PHD finger protein that reads H3K4me3 in meiotic cells and interacts with the axis-

associated DSB proteins to trigger DSB formation. One candidate might be Cxxc1 (also known as Cfp1) which is the closest homolog of Spp1 in mammals and a reported interacting partner of Prdm9 [198], and Iho1 (ortholog of yeast Mer2) [230]. Oocyte-specific inhibition of Cxxc1 or abrogation of H3K4 methylation in oocytes causes a delay of meiotic resumption as well as metaphase I arrest owing to defective spindle assembly and chromosome misalignment [231]. Interestingly, male Cxxc1 knockout mice are fertile, and the loss of Cxxc1 in spermatocytes had no effect on Prdm9 hotspot trimethylation, DSB formation or repair [232]. This suggests that other direct Prdm9 interactors, such as Ewsr1, Ehmt2, Cdyl, Pih1d1 [198], [233] and Ctcf [193], could also be involved in hotspot association with the chromosome axis. The protein interactions of Prdm9 suggest new experimental directions and these experiments could answer what brings the homologous hotspot down to the axis in mammals.

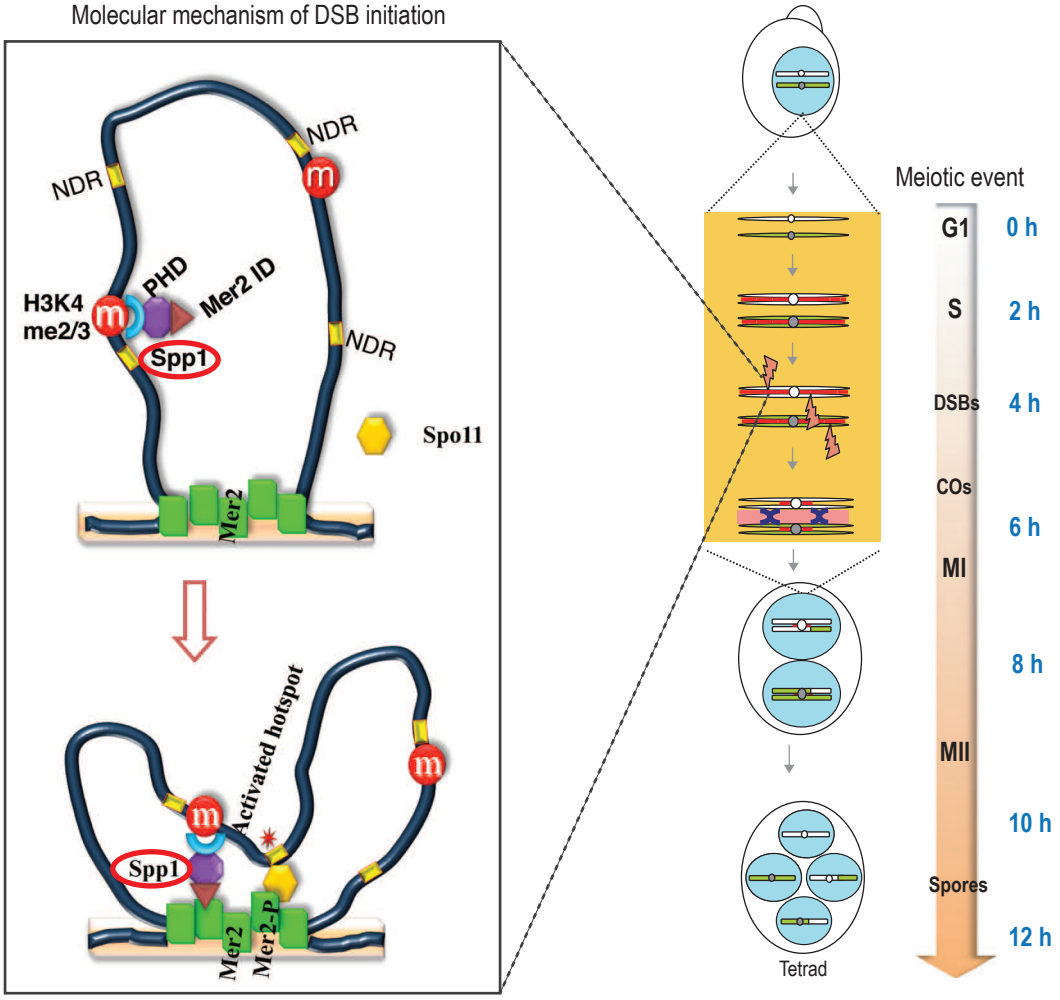

Figure 32. *The loop-axis model of recombination initiation in budding yeast meiosis. The left side shows the proposed spatial interaction that forms during DSB formation in the prophase I of meiosis. The role of Spp1 is crucial in this mechanism and based on our experiments it works independently from COMPASS. NDR: nucleosome depleted region, Mer ID: Zn finger (CxxC) domain of Spp1 that interacts with Mer2, PHD: PHD finger domain of Spp1 that interacts with trimethylated H3K4, COs: crossing overs, MI and MII: First and second meiotic divisions. Modified from* [234], [235].

FRAP and FCS are common methods for studying protein-DNA binding interactions at single cell level. These approaches provide information about how the protein diffuses in the nucleus

and interacts with DNA. However, our data from the FCS and FRAP experiments contributed to the understanding of Spp1 dynamic with suitable temporal resolving power, the spatial resolution of these measurements was limited. Genome-wide competition ChIP-Seq was an excellent approach to investigate Spp1-DNA dynamics and to complete our biophysical results with binding site turnover across the entire genome. Recent publications demonstrated that this method has the ability to measure dynamic nuclear events [211], [236]. Also, it is well described in yeast experimental systems [212]. The performed c-ChIP experiments concluded that distinction between different functional types of Spp1 binding sites could be possible based on turnover rate. Differential turnover of COMPASS-associated and COMPASS-independent Spp1 peaks prove the presence of two kinetic Spp1 pools that distribute differentially between the Set1 complex and meiotic DSB proteins. We can see the different binding characteristics of these Spp1 populations in **Figure 31/E-G**. The distributions show that there is an Spp1 population with prolonged Mer2 binding, but not with Bre2/COMPASS. This association of Spp1 with Mer2 axial sites reduces *bona fide* turnover rates of Spp1 upon chromatin binding. This increased residence time was also supported by the reduced nuclear dynamics of Spp1 seen in our FCS measurements. The increased residence time raises the question, whether it is due to prolonged Mer2-Spp1 interaction, which is crucial regarding proper DSB formation [133], or due to tethering mechanisms of the chromatin loop following H3K4me3 binding of Spp1. Noteworthy, Mer2 is a multifunctional protein that is evolutionarily conserved from fungi to plants (ortholog: PRD3/PAIR1) and mammals (ortholog: IHO1) [237], [238]. Consequently, the interplay between Spp1 and Mer2 might play a role in other Mer2-dependent mechanisms as well. In our studies, we focused on the DSB initiation and how the activated DSB hotspots tether to the chromosome axis preceding DSB formation, but Mer2 participates in mechanisms such as maintenance and releasing of the recombination complex or post-recombination chiasma development following recombination [237]. Perhaps the Spp1 population with

prolonged Mer2 binding is involved in these meiotic events as well. It would also be intriguing to examine this interaction and its effect on the meiotic chromatin structures by chromosome conformation capture (3C) methodology [239]–[241]. The study of the local conformations near DSB hotspots could reveal further functions of this Spp1 population. It is conceivable that the elimination of the appearing Spp1 population could alter the local genome organization through a perturbed tethering mechanism. These methods could reveal the fine-scale structures of the hotspots and complete the hotspot-centric view with other possible hierarchies.

In conclusion, the binding kinetics measured by c-ChIP was in accordance with the FCS estimates and with the hypothesized loop axis model. The model proposes that Spp1 mediates the tethering of DSB sites independently from COMPASS. It delineates the multi-functionality of Spp1: in vegetative state, Spp1 associates with COMPASS and colocalizes with highly transcribed genes, but in the early phase of meiosis its function is switched and Spp1 mediates the tethering of DSB sites to the chromosome axes for DSB formation. The pivotal question whether similar mechanism helps DSB formation in mammal remains open. Presumably, the mammalian orthologs of the yeast DSB machinery play an essential role in the DSB activation. Unraveling of the molecular strategies of these orthologs and the adaptation of the yeast loop axis model to the mammalian taxa will certainly be an interesting avenue to pursue.

7. SUMMARY

H3K27M histone mutation defines clinically and biologically distinct subgroups of high-grade gliomas. The molecular biological consequences of this driver mutation and how the substitution affects pathways contributing tumor initiation and progression are not well understood yet. In the present thesis, we investigated the H3K27M mutation using *in vivo* and *in vitro* experimental systems and determined its biophysical characteristics at chromatin, nucleosome and nuclear diffusion levels. We were also interested in Ezh2 protein, which is the catalytic subunit of the PRC2 and interacts with the K27M residue. Furthermore, we examined the diffusional properties of COMPASS protein complex which belongs to the trithorax group proteins and its mammalian homolog is involved in hematological and brain malignancies as well. We observed that Spp1 switches to COMPASS-independent function in meiosis and it helps to prepare potential recombination initiation sites.

We found that H3.3K27M histones follow similar diffusion kinetics as histone H3.3 and the mutant nucleosomes maintain the wild type molecular architecture and chromatin incorporation profile. Additionally, the K27M mutation does not manifest in growth defect in budding yeast strains bearing H3K27M histone pool. We demonstrated for the first time the *in vivo* nuclear mobility of H3.3 histone variant in various time and spatial resolution and estimated the diffusional parameters of Ezh2 observed transcription dependent mobility. The experiments on COMPASS subunits revealed differences between Set1 and Spp1 diffusion. These results support our hypothesis that Spp1 might have a COMPASS-independent regulatory role and collaborates with high molecular weight macromolecular complexes such as chromosome axial sites. We revealed that dynamic turnover of Spp1 is important in the establishment of transient chromatin changes during meiosis and prepare potential recombination initiation sites for DNA break formation.

8. ÖSSZEFOGLALÁS

A H3K27M irányító (driver) mutációjának molekuláris biológiai következményei, valamint a szubsztitúció tumor iniciációra és progresszióra kifejtett hatásai tisztázatlanok. Jelen disszertációban megvizsgáltuk a H3K27M mutációt *in vivo* és *in vitro* kísérleti rendszerek alkalmazásával, és meghatároztuk biofizikai jellemzőit kromatin, nukleoszóma és nukleáris diffúzió szinten. Ezenkívül tanulmányoztuk az Ezh2 fehérjét, amelyről közismert, hogy a PRC2 fehérje komplex katalitikus alegysége és a K27M mutáció metioninjával kialakított kölcsönhatás révén megváltoztatja a tumorsejtek epigenetikai mintázatát. Végezetül megvizsgáltuk a COMPASS fehérje komplex diffúziós tulajdonságait, amelynek emlős homológja hematológiai és agyi malignus folyamatokban is érintett. Megfigyeltük, hogy a COMPASS Spp1 alegysége a meiózisban COMPASS-független működésre vált, és elősegíti a lehetséges rekombinációt iniciáló helyek kialakulását.

Megállapítottuk, hogy a H3.3K27M hisztonok hasonló diffúziós kinetikával rendelkeznek, mint a vad típusú megfelelőik, valamint a mutáns nukleoszómák fenntartják a vad típusú molekuláris architektúrát és kromatin beépülési profilt. Ezenkívül a K27M mutáció nem eredményez növekedési defektusokat H3K27M hisztonkészlettel rendelkező élesztőtörzsekben. Első alkalommal mutattuk be a H3.3 hiszton variáns *in vivo* nukleáris mobilitását különböző időbeli és térbeli felbontásban, és becsültük meg az Ezh2 transzkripció-függő mobilitását és diffúziós paramétereit. A COMPASS alegységeken végzett kísérletek különbségeket mutattak a Set1 és az Spp1 diffúziós tulajdonságai között. Ezek az eredmények alátámasztják azt a hipotézisünket, hogy az Spp1 COMPASS-független szabályozó szerepet kaphat, és együttműködik a nagy molekulatömegű makromolekuláris komplexekkel, például a kromoszóma axiális részeivel. Kimutattuk, hogy az Spp1 dinamikus turnover rátája fontos szerepet tölt be a meiózis során bekövetkező tranziens kromatinváltozások kialakulásában és a DNS-rekombináció iniciációjának kialakításában.

9. KEYWORDS

histone, histone modification, H3K27M, glioblastoma, Ezh2, recombination, COMPASS, Spp1, double-strand break.

10. PUBLICATIONS

UNIVERSITY of DEBRECEN

UNIVERSITY AND NATIONAL LIBRAY
UNIVERSITY OF DEBRECEN
H-4002 Egyetem tér 1, Debrecen
Phone: +3652/410-443, email: publikaciok@lib.unideb.hu

Registry number: DEENK/277/2018.PL
Subject: PhD Publikációs Lista

Candidate: Szabolcs Hetey
Neptun ID: CNDDBL
Doctoral School: Doctoral School of Molecular Cellular and Immune Biology

List of publications related to the dissertation

1. Karányi, Z., Halász, L., Acquaviva, L., Jonás, D., **Hetey, S.**, Boros-Oláh, B., Peng, F., Chen, D., Klein, F., Géli, V., Székvölgyi, L.: Nuclear dynamics of the Set1C subunit Spp1 prepares meiotic recombination sites for break formation.
   J. Cell Biol. [Epub ahead of print], 2018.
   DOI: http://dx.doi.org/10.1083/jcb.201712122
   IF: 8.784 (2017)
2. **Hetey, S.**, Boros-Oláh, B., Kuik-Rózsa, T., Li, Q., Karányi, Z., Szabó, Z., Roszik, J., Szalóki, N., Vámosi, G., Tóth, K. Á., Székvölgyi, L.: Biophysical characterization of histone H3.3 K27M point mutation.
   Biochem. Biophys. Res. Commun. 490 (3), 868-875, 2017.
   DOI: http://dx.doi.org/10.1016/j.bbrc.2017.06.133
   IF: 2.559

Total IF of journals (all publications): 11,343
Total IF of journals (publications related to the dissertation): 11,343

The Candidate's publication data submitted to the iDEa Tudóstér have been validated by DEENK on the basis of Web of Science, Scopus and Journal Citation Report (Impact Factor) databases.

03 August, 2018

DEBRECENI EGYETEM Egyetemi és Nemzeti Könyvtár

11. ACKNOWLEDGEMENTS

I would like to express my sincere gratitude to my supervisor, Dr. Lóránt Székvölgyi, for the excellent training, continuous support, motivation, immense knowledge and for scientific discussions during my Ph.D. I am also grateful to Dr. Katalin Tóth (Division Biophysics of Macromolecules, DKFZ, Heidelberg, Germany) who was my tutor in Heidelberg and introduced me into FRET and FCS experiments. Their guidance helped me through all aspects of research, writing this thesis and the related papers.

I am grateful to Professor Dr. József Tőzsér, head of the Department of Biochemistry and Molecular Biology, and my advisory committee: Dr. Laszló Fesüs and Dr. Attila Bácsi.

Special thanks to Professor Dr. Gábor Szabó, Dr. György Vámosi, Dr. László Imre and to our colleagues from Cell biology research group of Department of Biophysics and Cell Biology for the valuable and constructive suggestions.

My gratitude also goes to all the past and current members of Genome architecture and recombination research group for their help and scientific discussions, specially to Zsolt Karányi and to my lab mates, László Halász, Dr. Éva Sipos and Dr. Ágnes Mosolygó-Lukács.

I should also acknowledge the endless help I received from technicians: Adél Nagy Vezendiné and Ibolya Fürtös.

I am especially thankful to Zsolt Karányi who performed the bioinformatics analysis of c-ChIP data, to Éva Nagy, Ibolya Fürtös and Beáta Boros-Oláh for their special help in sampling and validation of c-ChIP samples, and to Tímea Kuik-Rózsa and Beáta Boros-Oláh for calculating the Manders colocalization parameters of CLSM images.

Last but not least, I would like to express my deepest gratitude to my beloved family, who have supported me throughout the entire process.

12. REFERENCES

[1] E. I. Campos and D. Reinberg, “Histones: Annotating Chromatin,” *Annu. Rev. Genet.*, vol. 43, no. 1, pp. 559–599, Dec. 2009.

[2] P. Trojer and D. Reinberg, “Facultative Heterochromatin: Is There a Distinctive Molecular Signature?,” *Mol. Cell*, vol. 28, no. 1, pp. 1–13, Oct. 2007.

[3] R. Buning and J. van Noort, “Single-pair FRET experiments on nucleosome conformational dynamics.,” *Biochimie*, vol. 92, no. 12, pp. 1729–40, Dec. 2010.

[4] R. D. Kornberg, “Chromatin structure: a repeating unit of histones and DNA.,” *Science*, vol. 184, no. 4139, pp. 868–71, May 1974.

[5] A. L. Olins and D. E. Olins, “Spheroid chromatin units (v bodies).,” *Science*, vol. 183, no. 4122, pp. 330–2, Jan. 1974.

[6] K. Luger, A. W. Mäder, R. K. Richmond, D. F. Sargent, and T. J. Richmond, “Crystal structure of the nucleosome core particle at 2.8 Å resolution,” *Nature*, vol. 389, no. 6648, pp. 251–260, Sep. 1997.

[7] J. D. McGhee and G. Felsenfeld, “Nucleosome Structure,” *Annu. Rev. Biochem.*, vol. 49, no. 1, pp. 1115–1156, Jun. 1980.

[8] N. P. Nurse, I. Jimenez-Useche, I. T. Smith, and C. Yuan, “Clipping of flexible tails of histones H3 and H4 affects the structure and dynamics of the nucleosome,” *Biophys. J.*, vol. 104, no. 5, pp. 1081–1088, 2013.

[9] S. Khorasanizadeh, “The nucleosome: from genomic organization to genomic regulation.,” *Cell*, vol. 116, no. 2, pp. 259–72, Jan. 2004.

[10] D. J. Tremethick, “Higher-Order Structures of Chromatin: The Elusive 30 nm Fiber,” *Cell*, vol. 128, no. 4, pp. 651–654, Feb. 2007.

[11] O. Bell, V. K. Tiwari, N. H. Thomä, and D. Schübeler, “Determinants and dynamics of genome accessibility,” *Nat. Rev. Genet.*, vol. 12, no. 8, pp. 554–564, Jul. 2011.

[12] K. Luger, M. L. Dechassa, and D. J. Tremethick, “New insights into nucleosome and chromatin structure: an ordered state or a disordered affair?,” *Nat. Rev. Mol. Cell Biol.*, vol. 13, no. 7, pp. 436–447, Jun. 2012.

[13] J. Schwartzentruber *et al.*, “Driver mutations in histone H3.3 and chromatin remodelling genes in paediatric glioblastoma.,” *Nature*, vol. 482, no. 7384, pp. 226–31, Feb. 2012.

[14] A. Flaus and T. Owen-Hughes, “Mechanisms for nucleosome mobilization,”

Biopolymers, vol. 68, no. 4, pp. 563–578, Apr. 2003.

[15] K. Luger, "Dynamic nucleosomes," *Chromosom. Res.*, vol. 14, no. 1, pp. 5–16, Feb. 2006.

[16] F.-T. Chien and J. van Noort, "10 years of tension on chromatin: results from single molecule force spectroscopy.," *Curr. Pharm. Biotechnol.*, vol. 10, no. 5, pp. 474–85, Aug. 2009.

[17] W. J. a Koopmans, a Brehm, C. Logie, T. Schmidt, and J. van Noort, "Single-pair FRET microscopy reveals mononucleosome dynamics.," *J. Fluoresc.*, vol. 17, no. 6, pp. 785–95, Nov. 2007.

[18] D. Lovullo, D. Daniel, J. Yodh, D. Lohr, and N. W. Woodbury, "A fluorescence resonance energy transfer-based probe to monitor nucleosome structure," *Anal. Biochem.*, vol. 341, no. 1, pp. 165–172, Jun. 2005.

[19] D. A. Hoch, J. J. Stratton, and L. M. Gloss, "Protein–Protein Förster Resonance Energy Transfer Analysis of Nucleosome Core Particles Containing H2A and H2A.Z," *J. Mol. Biol.*, vol. 371, no. 4, pp. 971–988, Aug. 2007.

[20] T. Ha, T. Enderle, D. F. Ogletree, D. S. Chemla, P. R. Selvin, and S. Weiss, "Probing the interaction between two single molecules: fluorescence resonance energy transfer between a single donor and a single acceptor.," *Proc. Natl. Acad. Sci. U. S. A.*, vol. 93, no. 13, pp. 6264–8, Jun. 1996.

[21] M. Tomschik, H. Zheng, K. van Holde, J. Zlatanova, and S. H. Leuba, "Fast, long-range, reversible conformational fluctuations in nucleosomes revealed by single-pair fluorescence resonance energy transfer," *Proc. Natl. Acad. Sci.*, vol. 102, no. 9, pp. 3278–3283, Mar. 2005.

[22] A. Gansen *et al.*, "Nucleosome disassembly intermediates characterized by single-molecule FRET.," *Proc. Natl. Acad. Sci. U. S. A.*, vol. 106, no. 36, pp. 15308–13, Sep. 2009.

[23] V. Böhm *et al.*, "Nucleosome accessibility governed by the dimer/tetramer interface.," *Nucleic Acids Res.*, vol. 39, no. 8, pp. 3093–102, Apr. 2011.

[24] A. Gansen *et al.*, "Reversible transitions in nucleosomes on the microsecond to minute time scale revealed by high precision single-molecule FRET," *Nat. Commun.*, vol. under revi, no. 2018, pp. 1–13, 2018.

[25] A. Kossel, "Ueber einen peptoartigen bestandheil des zellkerns," *Z. Physiol. Chem*, vol. 8, pp. 511–515, 1884.

[26] D. M. Phillips and E. W. Johns, "A fractination of the histones of group F2A from calf

tyhmus," *Biochem. J.*, vol. 94, no. 1, pp. 127–30, Jan. 1965.

[27] R. J. DeLange, D. M. Fambrough, E. L. Smith, and J. Bonner, "Calf and pea histone IV. II. The complete amino acid sequence of calf thymus histone IV; presence of epsilon-N-acetyllysine.," *J. Biol. Chem.*, vol. 244, no. 2, pp. 319–34, Jan. 1969.

[28] R. Hancock, "Conservation of histones in chromatin during growth and mitosis in vitro.," *J. Mol. Biol.*, vol. 40, no. 3, pp. 457–66, Mar. 1969.

[29] K. Luger, "Crystal structure of the nucleosome core particle at 2.8 A resolution." 1997.

[30] S. Smith and B. Stillman, "Stepwise assembly of chromatin during DNA replication in vitro.," *EMBO J.*, vol. 10, no. 4, pp. 971–80, Apr. 1991.

[31] O. I. Kulaeva, F.-K. Hsieh, and V. M. Studitsky, "RNA polymerase complexes cooperate to relieve the nucleosomal barrier and evict histones.," *Proc. Natl. Acad. Sci. U. S. A.*, vol. 107, no. 25, pp. 11325–30, Jun. 2010.

[32] R. D. Kornberg and J. O. Thomas, "Chromatin structure; oligomers of the histones.," *Science*, vol. 184, no. 4139, pp. 865–8, May 1974.

[33] J. D. Hackett *et al.*, "Insights into a dinoflagellate genome through expressed sequence tag analysis.," *BMC Genomics*, vol. 6, no. 1, p. 80, May 2005.

[34] W. F. Marzluff, P. Gongidi, K. R. Woods, J. Jin, and L. J. Maltais, "The human and mouse replication-dependent histone genes," *Genomics*, vol. 80, no. 5, pp. 487–498, 2002.

[35] W. F. Marzluff, E. J. Wagner, and R. J. Duronio, "Metabolism and regulation of canonical histone mRNAs: life without a poly(A) tail.," *Nat. Rev. Genet.*, vol. 9, no. 11, pp. 843–54, Nov. 2008.

[36] Z. Dominski and W. F. Marzluff, "Formation of the 3' end of histone mRNA.," *Gene*, vol. 239, no. 1, pp. 1–14, Oct. 1999.

[37] P. R. Eriksson, D. Ganguli, V. Nagarajavel, and D. J. Clark, "Regulation of histone gene expression in budding yeast.," *Genetics*, vol. 191, no. 1, pp. 7–20, May 2012.

[38] M. M. Smith and K. Murray, "Yeast H3 and H4 histone messenger RNAs are transcribed from two non-allelic gene sets.," *J. Mol. Biol.*, vol. 169, no. 3, pp. 641–61, Sep. 1983.

[39] L. Hereford, K. Fahrner, J. Woolford, M. Rosbash, and D. B. Kaback, "Isolation of yeast histone genes H2A and H2B.," *Cell*, vol. 18, no. 4, pp. 1261–71, Dec. 1979.

[40] K. Fahrner, J. Yarger, and L. Hereford, "Yeast histone mRNA is polyadenylated.," *Nucleic Acids Res.*, vol. 8, no. 23, pp. 5725–37, Dec. 1980.

[41] M. A. Osley, "The Regulation of Histone Synthesis in the Cell Cycle," *Annu. Rev.*

Biochem., vol. 60, no. 1, pp. 827–861, Jun. 1991.

[42] M. E. Harris, R. Böhni, M. H. Schneiderman, L. Ramamurthy, D. Schümperli, and W. F. Marzluff, "Regulation of histone mRNA in the unperturbed cell cycle: evidence suggesting control at two posttranscriptional steps.," *Mol. Cell. Biol.*, vol. 11, no. 5, pp. 2416–24, May 1991.

[43] P. B. Talbert and S. Henikoff, "Histone variants - ancient wrap artists of the epigenome," *Nat Rev Mol Cell Biol*, vol. 11, no. 4, pp. 264–275, 2010.

[44] C. Bönisch, S. M. Nieratschker, N. K. Orfanos, and S. B. Hake, "Chromatin proteomics and epigenetic regulatory circuits," *Expert Rev. Proteomics*, vol. 5, no. 1, pp. 105–119, Feb. 2008.

[45] H. Tagami, D. Ray-Gallet, G. Almouzni, and Y. Nakatani, "Histone H3.1 and H3.3 complexes mediate nucleosome assembly pathways dependent or independent of DNA synthesis.," *Cell*, vol. 116, no. 1, pp. 51–61, Jan. 2004.

[46] C. Jin and G. Felsenfeld, "Nucleosome stability mediated by histone variants H3.3 and H2A.Z," *Genes Dev.*, vol. 21, no. 12, pp. 1519–1529, Jun. 2007.

[47] R. E. Branson, S. R. Grimes, G. Yonuschot, and J. L. Irvin, "The histones of rat testis.," *Arch. Biochem. Biophys.*, vol. 168, no. 2, pp. 403–12, Jun. 1975.

[48] O. Witt, W. Albig, and D. Doenecke, "Testis-Specific Expression of a Novel Human H3 Histone Gene," *Exp. Cell Res.*, vol. 229, no. 2, pp. 301–306, Dec. 1996.

[49] Y. Jiao *et al.*, "DAXX/ATRX, MEN1, and mTOR Pathway Genes Are Frequently Altered in Pancreatic Neuroendocrine Tumors," *Science (80-.).*, vol. 331, no. 6021, pp. 1199–1203, Mar. 2011.

[50] D. S. Dunican, P. McWilliam, O. Tighe, A. Parle-McDermott, and D. T. Croke, "Gene expression differences between the microsatellite instability (MIN) and chromosomal instability (CIN) phenotypes in colorectal cancer revealed by high-density cDNA array hybridization.," *Oncogene*, vol. 21, no. 20, pp. 3253–7, May 2002.

[51] D. Rangasamy, I. Greaves, and D. J. Tremethick, "RNA interference demonstrates a novel role for H2A.Z in chromosome segregation," *Nat. Struct. Mol. Biol.*, vol. 11, no. 7, pp. 650–655, Jul. 2004.

[52] R. D. Phair, S. A. Gorski, and T. Misteli, "Measurement of Dynamic Protein Binding to Chromatin In Vivo, Using Photobleaching Microscopy," *Methods Enzymol.*, vol. 375, no. 2000, pp. 393–414, 2004.

[53] R. D. Phair and T. Misteli, "High mobility of proteins in the mammalian cell nucleus," *Nature*, vol. 404, no. 6778, pp. 604–609, Apr. 2000.

[54] T. Misteli, A. Gunjan, R. Hock, M. Bustin, and D. T. Brown, “Dynamic binding of histone H1 to chromatin in living cells.,” *Nature*, vol. 408, no. 6814, pp. 877–881, Dec. 2000.

[55] T. Misteli, “Protein dynamics: implications for nuclear architecture and gene expression.,” *Science*, vol. 291, no. 5505, pp. 843–7, Feb. 2001.

[56] R. D. Phair *et al.*, “Global nature of dynamic protein-chromatin interactions in vivo: three-dimensional genome scanning and dynamic interaction networks of chromatin proteins.,” *Mol. Cell. Biol.*, vol. 24, no. 14, pp. 6393–402, Jul. 2004.

[57] H. Kimura and P. R. Cook, “Kinetics of Core Histones in Living Human Cells : Little Exchange of H3 and H4 and Some Rapid Exchange of H2B,” vol. 153, no. 7, pp. 1341–1353, 2001.

[58] H. Kimura, “Histone dynamics in living cells revealed by photobleaching,” *DNA Repair (Amst).*, vol. 4, no. 8, pp. 939–950, Jul. 2005.

[59] V. Jackson, “In vivo studies on the dynamics of histone-DNA interaction: evidence for nucleosome dissolution during replication and transcription and a low level of dissolution independent of both.,” *Biochemistry*, vol. 29, no. 3, pp. 719–31, Jan. 1990.

[60] D. C. Kraushaar, W. Jin, A. Maunakea, B. Abraham, M. Ha, and K. Zhao, “Genome-wide incorporation dynamics reveal distinct categories of turnover for the histone variant H3.3,” *Genome Biol.*, vol. 14, no. 10, p. R121, 2013.

[61] A. P. Wolffe and J. J. Hayes, “Chromatin disruption and modification.,” *Nucleic Acids Res.*, vol. 27, no. 3, pp. 711–20, Feb. 1999.

[62] R. Mandel and G. D. Fasman, “Chromatin and nucleosome structure.,” *Nucleic Acids Res.*, vol. 3, no. 8, pp. 1839–55, Aug. 1976.

[63] A. J. Bannister and T. Kouzarides, “Regulation of chromatin by histone modifications,” *Cell Res.*, vol. 21, no. 3, pp. 381–395, Mar. 2011.

[64] P. Tessarz and T. Kouzarides, “Histone core modifications regulating nucleosome structure and dynamics.,” *Nat. Rev. Mol. Cell Biol.*, vol. 15, no. 11, pp. 703–708, 2014.

[65] F. Xu, K. Zhang, and M. Grunstein, “Acetylation in Histone H3 Globular Domain Regulates Gene Expression in Yeast,” *Cell*, vol. 121, no. 3, pp. 375–385, May 2005.

[66] T. Kouzarides, “Chromatin Modifications and Their Function,” *Cell*, vol. 128, no. 4, pp. 693–705, 2007.

[67] J. Dover *et al.*, “Methylation of Histone H3 by COMPASS Requires Ubiquitination of Histone H2B by Rad6,” *J. Biol. Chem.*, vol. 277, no. 32, pp. 28368–28371, Aug. 2002.

[68] S. D. Briggs *et al.*, “Gene silencing: Trans-histone regulatory pathway in chromatin,”

Nature, vol. 418, no. 6897, pp. 498–498, Aug. 2002.

[69] D. E. Sterner and S. L. Berger, "Acetylation of histones and transcription-related factors.," *Microbiol. Mol. Biol. Rev.*, vol. 64, no. 2, pp. 435–59, Jun. 2000.

[70] Y. Zhang and D. Reinberg, "Transcription regulation by histone methylation: interplay between different covalent modifications of the core histone tails," *Genes Dev.*, vol. 15, no. 18, pp. 2343–2360, Sep. 2001.

[71] S. J. Nowak and V. G. Corces, "Phosphorylation of histone H3: a balancing act between chromosome condensation and transcriptional activation," *Trends Genet.*, vol. 20, no. 4, pp. 214–220, Apr. 2004.

[72] A. Shilatifard, "Chromatin Modifications by Methylation and Ubiquitination: Implications in the Regulation of Gene Expression," *Annu. Rev. Biochem.*, vol. 75, no. 1, pp. 243–269, Jun. 2006.

[73] D. Nathan *et al.*, "Histone sumoylation is a negative regulator in *Saccharomyces cerevisiae* and shows dynamic interplay with positive-acting histone modifications," *Genes Dev.*, vol. 20, no. 8, pp. 966–976, Apr. 2006.

[74] P. O. Hassa, S. S. Haenni, M. Elser, and M. O. Hottiger, "Nuclear ADP-Ribosylation Reactions in Mammalian Cells: Where Are We Today and Where Are We Going?," *Microbiol. Mol. Biol. Rev.*, vol. 70, no. 3, pp. 789–829, Sep. 2006.

[75] G. L. Cuthbert *et al.*, "Histone Deimination Antagonizes Arginine Methylation," *Cell*, vol. 118, no. 5, pp. 545–553, Sep. 2004.

[76] C. J. Nelson, H. Santos-Rosa, and T. Kouzarides, "Proline Isomerization of Histone H3 Regulates Lysine Methylation and Gene Expression," *Cell*, vol. 126, no. 5, pp. 905–916, Sep. 2006.

[77] E. Metzger *et al.*, "LSD1 demethylates repressive histone marks to promote androgen-receptor-dependent transcription.," *Nature*, vol. 437, no. 7057, pp. 436–9, Sep. 2005.

[78] M. M. Steward, J.-S. Lee, A. O'Donovan, M. Wyatt, B. E. Bernstein, and A. Shilatifard, "Molecular regulation of H3K4 trimethylation by ASH2L, a shared subunit of MLL complexes," *Nat. Struct. Mol. Biol.*, vol. 13, no. 9, pp. 852–854, Sep. 2006.

[79] M. G. Lee, C. Wynder, N. Cooch, and R. Shiekhattar, "An essential role for CoREST in nucleosomal histone 3 lysine 4 demethylation," *Nature*, vol. 437, no. 7057, pp. 432–5, Aug. 2005.

[80] M. Shogren-Knaak, H. Ishii, J.-M. Sun, M. J. Pazin, J. R. Davie, and C. L. Peterson, "Histone H4-K16 Acetylation Controls Chromatin Structure and Protein Interactions," *Science (80-.).*, vol. 311, no. 5762, pp. 844–847, Feb. 2006.

[81] X.-J. Yang and E. Seto, “HATs and HDACs: from structure, function and regulation to novel strategies for therapy and prevention,” *Oncogene*, vol. 26, no. 37, pp. 5310–5318, Aug. 2007.

[82] Y. Wei, C. A. Mizzen, R. G. Cook, M. A. Gorovsky, and C. D. Allis, “Phosphorylation of histone H3 at serine 10 is correlated with chromosome condensation during mitosis and meiosis in Tetrahymena.,” *Proc. Natl. Acad. Sci. U. S. A.*, vol. 95, no. 13, pp. 7480–4, Jun. 1998.

[83] M.-M. Zhou *et al.*, “Structure and ligand of a histone acetyltransferase bromodomain.,” *Nature*, vol. 399, no. 6735, pp. 491–496, Jun. 1999.

[84] K. S. Champagne and T. G. Kutateladze, “Structural insight into histone recognition by the ING PHD fingers.,” *Curr. Drug Targets*, vol. 10, no. 5, pp. 432–41, May 2009.

[85] S. Maurer-Stroh, N. J. Dickens, L. Hughes-Davies, T. Kouzarides, F. Eisenhaber, and C. P. Ponting, “The Tudor domain ‘Royal Family’: Tudor, plant Agenet, Chromo, PWWP and MBT domains,” *Trends Biochem. Sci.*, vol. 28, no. 2, pp. 69–74, Feb. 2003.

[86] Y. Xu, C. Kanagaratham, and D. Radzioch, “Chromatin Remodelling During Host-Bacterial Pathogen Interaction,” *Chromatin Remodel.*, pp. 173–198, 2013.

[87] G. Schotta *et al.*, “A silencing pathway to induce H3-K9 and H4-K20 trimethylation at constitutive heterochromatin,” *Genes Dev.*, vol. 18, no. 11, pp. 1251–1262, Jun. 2004.

[88] S. C. Dillon, X. Zhang, R. C. Trievel, and X. Cheng, “The SET-domain protein superfamily: protein lysine methyltransferases.,” *Genome Biol.*, vol. 6, no. 8, p. 227, 2005.

[89] Q. Feng *et al.*, “Methylation of H3-lysine 79 is mediated by a new family of HMTases without a SET domain.,” *Curr. Biol.*, vol. 12, no. 12, pp. 1052–8, Jun. 2002.

[90] R. J. Klose and Y. Zhang, “Regulation of histone methylation by demethylimination and demethylation,” *Nat. Rev. Mol. Cell Biol.*, vol. 8, no. 4, pp. 307–318, Apr. 2007.

[91] A. J. Bannister and T. Kouzarides, “Reversing histone methylation,” *Nature*, vol. 436, no. 7054, pp. 1103–1106, Aug. 2005.

[92] E. M. Duncan *et al.*, “Cathepsin L Proteolytically Processes Histone H3 During Mouse Embryonic Stem Cell Differentiation,” *Cell*, vol. 135, no. 2, pp. 284–294, Oct. 2008.

[93] A. Barski *et al.*, “High-Resolution Profiling of Histone Methylations in the Human Genome,” *Cell*, vol. 129, no. 4, pp. 823–837, 2007.

[94] J. Cheng *et al.*, “A Role for H3K4 Monomethylation in Gene Repression and Partitioning of Chromatin Readers,” *Mol. Cell*, vol. 53, no. 6, pp. 979–992, Mar. 2014.

[95] B. E. Bernstein *et al.*, “Genomic maps and comparative analysis of histone modifications in human and mouse.,” *Cell*, vol. 120, no. 2, pp. 169–81, Jan. 2005.

[96] H. Santos-Rosa *et al.*, “Active genes are tri-methylated at K4 of histone H3,” *Nature*, vol. 419, no. 6905, pp. 407–411, Sep. 2002.

[97] T. Kim and S. Buratowski, “Dimethylation of H3K4 by Set1 Recruits the Set3 Histone Deacetylase Complex to 5′ Transcribed Regions,” *Cell*, vol. 137, no. 2, pp. 259–272, Apr. 2009.

[98] D. K. Pokholok *et al.*, “Genome-wide Map of Nucleosome Acetylation and Methylation in Yeast,” *Cell*, vol. 122, no. 4, pp. 517–527, Aug. 2005.

[99] S. L. Berger, “The complex language of chromatin regulation during transcription,” *Nature*, vol. 447, no. 7143, pp. 407–412, May 2007.

[100] V. Borde, N. Robine, W. Lin, S. Bonfils, V. Géli, and A. Nicolas, “Histone H3 lysine 4 trimethylation marks meiotic recombination initiation sites.,” *EMBO J.*, vol. 28, no. 2, pp. 99–111, 2009.

[101] Y. Liu, R. Subrahmanyam, T. Chakraborty, R. Sen, and S. Desiderio, “A Plant Homeodomain in Rag-2 that Binds Hypermethylated Lysine 4 of Histone H3 Is Necessary for Efficient Antigen-Receptor-Gene Rearrangement,” *Immunity*, vol. 27, no. 4, pp. 561–571, Oct. 2007.

[102] T. Miller *et al.*, “COMPASS: A complex of proteins associated with a trithorax-related SET domain protein.”

[103] J. R. Whetstine *et al.*, “Reversal of Histone Lysine Trimethylation by the JMJD2 Family of Histone Demethylases,” *Cell*, vol. 125, no. 3, pp. 467–481, May 2006.

[104] H. H. Ng, D. N. Ciccone, K. B. Morshead, M. A. Oettinger, and K. Struhl, “Lysine-79 of histone H3 is hypomethylated at silenced loci in yeast and mammalian cells: A potential mechanism for position-effect variegation,” *Proc. Natl. Acad. Sci.*, vol. 100, no. 4, pp. 1820–1825, Feb. 2003.

[105] D. Schubeler *et al.*, “The histone modification pattern of active genes revealed through genome-wide chromatin analysis of a higher eukaryote,” *Genes Dev.*, vol. 18, no. 11, pp. 1263–1271, Jun. 2004.

[106] Z. Farooq, S. Banday, T. K. Pandita, and M. Altaf, “The many faces of histone H3K79 methylation.,” *Mutat. Res. Rev. Mutat. Res.*, vol. 768, pp. 46–52, 2016.

[107] G. A. Shanower, M. Muller, J. L. Blanton, V. Honti, H. Gyurkovics, and P. Schedl, “Characterization of the grappa Gene, the Drosophila Histone H3 Lysine 79 Methyltransferase,” *Genetics*, vol. 169, no. 1, pp. 173–184, Oct. 2004.

[108] A. H. F. M. Peters *et al.*, “Partitioning and plasticity of repressive histone methylation states in mammalian chromatin.,” *Mol. Cell*, vol. 12, no. 6, pp. 1577–89, Dec. 2003.

[109] R. Cao and Y. Zhang, “The functions of E(Z)/EZH2-mediated methylation of lysine 27 in histone H3,” *Curr. Opin. Genet. Dev.*, vol. 14, no. 2, pp. 155–164, Apr. 2004.

[110] W. Fischle, Y. Wang, S. A. Jacobs, Y. Kim, C. D. Allis, and S. Khorasanizadeh, “Molecular basis for the discrimination of repressive methyl-lysine marks in histone H3 by Polycomb and HP1 chromodomains,” *Genes Dev.*, vol. 17, no. 15, pp. 1870–1881, Aug. 2003.

[111] J. Min, Y. Zhang, and R.-M. Xu, “Structural basis for specific binding of Polycomb chromodomain to histone H3 methylated at Lys 27,” *Genes Dev.*, vol. 17, no. 15, pp. 1823–1828, Aug. 2003.

[112] T. S. Mikkelsen *et al.*, “Genome-wide maps of chromatin state in pluripotent and lineage-committed cells,” *Nature*, vol. 448, no. 7153, pp. 553–560, Aug. 2007.

[113] B. E. Bernstein *et al.*, “A Bivalent Chromatin Structure Marks Key Developmental Genes in Embryonic Stem Cells,” *Cell*, vol. 125, no. 2, pp. 315–326, Apr. 2006.

[114] L. Ringrose and R. Paro, “Epigenetic Regulation of Cellular Memory by the Polycomb and Trithorax Group Proteins,” *Annu. Rev. Genet.*, vol. 38, no. 1, pp. 413–443, Dec. 2004.

[115] V. Pirrotta, “Polycombing the genome: PcG, trxG, and chromatin silencing.,” *Cell*, vol. 93, no. 3, pp. 333–6, May 1998.

[116] V. Orlando, “Polycomb, epigenomes, and control of cell identity.,” *Cell*, vol. 112, no. 5, pp. 599–606, Mar. 2003.

[117] R. S. Jones and W. M. Gelbart, “Genetic analysis of the enhancer of zeste locus and its role in gene regulation in Drosophila melanogaster.,” *Genetics*, vol. 126, no. 1, pp. 185–99, Sep. 1990.

[118] F. Pelegri and R. Lehmann, “A role of polycomb group genes in the regulation of gap gene expression in Drosophila.,” *Genetics*, vol. 136, no. 4, pp. 1341–53, Apr. 1994.

[119] H. Richly, L. Aloia, and L. Di Croce, “Roles of the Polycomb group proteins in stem cells and cancer,” *Cell Death Dis.*, vol. 2, no. 9, p. e204, 2011.

[120] C. Kandoth *et al.*, “Mutational landscape and significance across 12 major cancer types,” *Nature*, vol. 502, no. 7471, pp. 333–339, Oct. 2013.

[121] R. C. Rao and Y. Dou, “Hijacked in cancer: the MLL/KMT2 family of methyltransferases.”

[122] P. L. Nagy, J. Griesenbeck, R. D. Kornberg, and M. L. Cleary, “A trithorax-group

complex purified from *Saccharomyces cerevisiae* is required for methylation of histone H3," *Proc. Natl. Acad. Sci.*, vol. 99, no. 1, pp. 90–94, Jan. 2002.

[123] A. Roguev *et al.*, "The *Saccharomyces cerevisiae* Set1 complex includes an Ash2 homologue and methylates histone 3 lysine 4.," *EMBO J.*, vol. 20, no. 24, pp. 7137–48, Dec. 2001.

[124] S. Ziemin-van der Poel *et al.*, "Identification of a gene, MLL, that spans the breakpoint in 11q23 translocations associated with human leukemias.," *Proc. Natl. Acad. Sci. U. S. A.*, vol. 88, no. 23, pp. 10735–9, Dec. 1991.

[125] Y. Gu *et al.*, "The t(4;11) chromosome translocation of human acute leukemias fuses the ALL-1 gene, related to Drosophila trithorax, to the AF-4 gene.," *Cell*, vol. 71, no. 4, pp. 701–8, Nov. 1992.

[126] C. M. Hughes *et al.*, "Menin associates with a trithorax family histone methyltransferase complex and with the hoxc8 locus.," *Mol. Cell*, vol. 13, no. 4, pp. 587–97, Feb. 2004.

[127] A. Shilatifard, "The COMPASS Family of Histone H3K4 Methylases: Mechanisms of Regulation in Development and Disease Pathogenesis," *Annu. Rev. Biochem.*, vol. 81, no. 1, pp. 65–95, 2012.

[128] J. Dover *et al.*, "Methylation of Histone H3 by COMPASS Requires Ubiquitination of Histone H2B by Rad6," *J. Biol. Chem.*, vol. 277, no. 32, pp. 28368–28371, Aug. 2002.

[129] P.-M. Dehé and V. Géli, "The multiple faces of Set1," *Biochem. Cell Biol.*, vol. 84, no. 4, pp. 536–548, Aug. 2006.

[130] P. M. Dehé *et al.*, "Protein interactions within the Set1 complex and their roles in the regulation of histone 3 lysine 4 methylation," *J. Biol. Chem.*, vol. 281, no. 46, pp. 35404–35412, 2006.

[131] A. Kirmizis *et al.*, "Arginine methylation at histone H3R2 controls deposition of H3K4 trimethylation," *Nature*, vol. 449, no. 7164, pp. 928–932, Oct. 2007.

[132] V. Sommermeyer, C. Béneut, E. Chaplais, M. E. Serrentino, and V. Borde, "Spp1, a Member of the Set1 Complex, Promotes Meiotic DSB Formation in Promoters by Tethering Histone H3K4 Methylation Sites to Chromosome Axes," *Mol. Cell*, vol. 49, no. 1, pp. 43–54, 2013.

[133] L. Acquaviva *et al.*, "The COMPASS Subunit Spp1 Links Histone Methylation to Initiation of Meiotic Recombination," *Science (80-.).*, vol. 339, no. 6116, pp. 215–218, Jan. 2013.

[134] P. A. Lawrence and G. Morata, "Homeobox genes: their function in Drosophila

segmentation and pattern formation.," *Cell*, vol. 78, no. 2, pp. 181–9, Jul. 1994.

[135] B. D. Yu, J. L. Hess, S. E. Horning, G. A. J. Brown, and S. J. Korsmeyer, "Altered Hox expression and segmental identity in Mll-mutant mice," *Nature*, vol. 378, no. 6556, pp. 505–508, Nov. 1995.

[136] B. Schuettengruber and G. Cavalli, "Recruitment of Polycomb group complexes and their role in the dynamic regulation of cell fate choice," *Development*, vol. 136, no. 21, pp. 3531–3542, Nov. 2009.

[137] S. Aranda, G. Mas, and L. Di Croce, "Regulation of gene transcription by Polycomb proteins.," *Sci. Adv.*, vol. 1, no. 11, p. e1500737, 2015.

[138] R. Margueron and D. Reinberg, "The Polycomb complex PRC2 and its mark in life.," *Nature*, vol. 469, no. 7330, pp. 343–9, Jan. 2011.

[139] R. Cao and Y. Zhang, "SUZ12 Is Required for Both the Histone Methyltransferase Activity and the Silencing Function of the EED-EZH2 Complex," *Mol. Cell*, vol. 15, no. 1, pp. 57–67, Jul. 2004.

[140] C. J. Woo, P. V. Kharchenko, L. Daheron, P. J. Park, and R. E. Kingston, "Variable Requirements for DNA-Binding Proteins at Polycomb-Dependent Repressive Regions in Human HOX Clusters," *Mol. Cell. Biol.*, vol. 33, no. 16, pp. 3274–3285, Aug. 2013.

[141] A. Sing *et al.*, "A Vertebrate Polycomb Response Element Governs Segmentation of the Posterior Hindbrain," *Cell*, vol. 138, no. 5, pp. 885–897, Sep. 2009.

[142] R. R. Pandey *et al.*, "Kcnq1ot1 Antisense Noncoding RNA Mediates Lineage-Specific Transcriptional Silencing through Chromatin-Level Regulation," *Mol. Cell*, vol. 32, no. 2, pp. 232–246, Oct. 2008.

[143] K. J. Ferrari *et al.*, "Polycomb-dependent H3K27me1 and H3K27me2 regulate active transcription and enhancer fidelity.," *Mol. Cell*, vol. 53, no. 1, pp. 49–62, Jan. 2014.

[144] K. Cui *et al.*, "Chromatin Signatures in Multipotent Human Hematopoietic Stem Cells Indicate the Fate of Bivalent Genes during Differentiation," *Cell Stem Cell*, vol. 4, no. 1, pp. 80–93, Jan. 2009.

[145] J. K. Stock *et al.*, "Ring1-mediated ubiquitination of H2A restrains poised RNA polymerase II at bivalent genes in mouse ES cells," *Nat. Cell Biol.*, vol. 9, no. 12, pp. 1428–1435, Dec. 2007.

[146] B. Shi *et al.*, "Integration of Estrogen and Wnt Signaling Circuits by the Polycomb Group Protein EZH2 in Breast Cancer Cells," *Mol. Cell. Biol.*, vol. 27, no. 14, pp. 5105–5119, 2007.

[147] J. A. Simon and C. A. Lange, "Roles of the EZH2 histone methyltransferase in cancer

epigenetics," *Mutat. Res. Mol. Mech. Mutagen.*, vol. 647, no. 1–2, pp. 21–29, Dec. 2008.

[148] M. A. Dawson and T. Kouzarides, "Cancer Epigenetics: From Mechanism to Therapy," *Cell*, vol. 150, pp. 12–27, 2012.

[149] M. L. Suva, N. Riggi, and B. E. Bernstein, "Epigenetic Reprogramming in Cancer," *Science (80-.).*, vol. 339, no. 6127, pp. 1567–1570, Mar. 2013.

[150] G. van Haaften *et al.*, "Somatic mutations of the histone H3K27 demethylase gene UTX in human cancer," *Nat. Genet.*, vol. 41, no. 5, pp. 521–523, May 2009.

[151] N. Avvakumov and J. Côté, "The MYST family of histone acetyltransferases and their intimate links to cancer," *Oncogene*, vol. 26, no. 37, pp. 5395–5407, Aug. 2007.

[152] G. Wu *et al.*, "Somatic histone H3 alterations in pediatric diffuse intrinsic pontine gliomas and non-brainstem glioblastomas," *Nat. Genet.*, vol. 44, no. 3, pp. 251–253, Jan. 2012.

[153] C. Orillac *et al.*, "Pilocytic astrocytoma and glioneuronal tumor with histone H3 K27M mutation.," *Acta Neuropathol. Commun.*, vol. 4, no. 1, p. 84, 2016.

[154] G. Wu *et al.*, "Somatic histone H3 alterations in pediatric diffuse intrinsic pontine gliomas and non-brainstem glioblastomas," *Nat. Genet.*, vol. 44, no. 3, pp. 251–253, Jan. 2012.

[155] D.-A. Khuong-Quang *et al.*, "K27M mutation in histone H3.3 defines clinically and biologically distinct subgroups of pediatric diffuse intrinsic pontine gliomas.," *Acta Neuropathol.*, vol. 124, no. 3, pp. 439–47, Sep. 2012.

[156] D. Sturm *et al.*, "Hotspot Mutations in H3F3A and IDH1 Define Distinct Epigenetic and Biological Subgroups of Glioblastoma," *Cancer Cell*, vol. 22, no. 4, pp. 425–437, Oct. 2012.

[157] L. Bjerke *et al.*, "Histone H3.3 mutations drive pediatric glioblastoma through upregulation of MYCN," *Cancer Discov.*, vol. 3, no. 5, pp. 512–519, 2013.

[158] R. R. Lulla, A. M. Saratsis, and R. Hashizume, "Mutations in chromatin machinery and pediatric high-grade glioma.," *Sci. Adv.*, vol. 2, no. 3, p. e1501354, Mar. 2016.

[159] P. Drane, K. Ouararhni, A. Depaux, M. Shuaib, and A. Hamiche, "The death-associated protein DAXX is a novel histone chaperone involved in the replication-independent deposition of H3.3," *Genes Dev.*, vol. 24, no. 12, pp. 1253–1265, Jun. 2010.

[160] P. W. Lewis, S. J. Elsaesser, K.-M. Noh, S. C. Stadler, and C. D. Allis, "Daxx is an H3.3-specific histone chaperone and cooperates with ATRX in replication-independent

chromatin assembly at telomeres," *Proc. Natl. Acad. Sci.*, vol. 107, no. 32, pp. 14075–14080, Aug. 2010.

[161] P. W. Lewis *et al.*, "Inhibition of PRC2 activity by a gain-of-function H3 mutation found in pediatric glioblastoma.," *Science*, vol. 340, no. 6134, pp. 857–61, May 2013.

[162] S. Bender *et al.*, "Reduced H3K27me3 and DNA Hypomethylation Are Major Drivers of Gene Expression in K27M Mutant Pediatric High-Grade Gliomas," *Cancer Cell*, vol. 24, pp. 660–672, 2013.

[163] S. Venneti *et al.*, "Evaluation of histone 3 lysine 27 trimethylation (H3K27me3) and enhancer of Zest 2 (EZH2) in pediatric glial and glioneuronal tumors shows decreased H3K27me3 in H3F3A K27M mutant glioblastomas.," *Brain Pathol.*, vol. 23, no. 5, pp. 558–64, Sep. 2013.

[164] K.-M. Chan *et al.*, "The histone H3.3K27M mutation in pediatric glioma reprograms H3K27 methylation and gene expression.," *Genes Dev.*, vol. 27, no. 9, pp. 985–90, May 2013.

[165] B. T. K. Yuen and P. S. Knoepfler, "Histone h3.3 mutations: a variant path to cancer.," *Cancer Cell*, vol. 24, no. 5, pp. 567–74, Nov. 2013.

[166] K. Chan *et al.*, "The histone H3 . 3K27M mutation in pediatric glioma reprograms H3K27 methylation and gene expression," pp. 985–990, 2013.

[167] P. W. Lewis and C. D. Allis, "Poisoning the histone code in pediatric gliomagenesis.," *Cell Cycle*, vol. 12, no. 20, pp. 3241–2, Oct. 2013.

[168] D. Sanders *et al.*, "Histone lysine-to-methionine mutations reduce histone methylation and cause developmental pleiotropy," *Plant Physiol.*, vol. 173, no. April, p. pp.01499.2016, 2017.

[169] K. Funato, T. Major, P. W. Lewis, C. D. Allis, and V. Tabar, "Use of human embryonic stem cells to model pediatric gliomas with H3.3K27M histone mutation," *Science (80-.).*, vol. 346, no. 6216, pp. 1529–1533, Dec. 2014.

[170] K. M. Chan, J. Han, D. Fang, H. Gan, and Z. Zhang, "A lesson learned from the H3.3K27M mutation found in pediatric glioma," *Cell Cycle*, vol. 12, no. 16, pp. 2546–2552, Aug. 2013.

[171] D. W. Parsons *et al.*, "The Genetic Landscape of the Childhood Cancer Medulloblastoma," *Science (80-.).*, vol. 331, no. 6016, pp. 435–439, Jan. 2011.

[172] M. Gallo *et al.*, "A tumorigenic MLL-homeobox network in human glioblastoma stem cells," *Cancer Res.*, vol. 73, no. 1, pp. 417–427, 2013.

[173] J. M. Heddleston *et al.*, "Hypoxia-induced mixed-lineage leukemia 1 regulates glioma

stem cell tumorigenic potential," *Cell Death Differ.*, vol. 19, no. 3, pp. 428–439, 2012.

[174] I. Lam and S. Keeney, "Mechanism and control of meiotic recombination initiation.," *Cold Spring Harb Perspet Biol*, vol. 52, pp. 1–53, 2015.

[175] S. Keeney, J. Lange, and N. Mohibullah, "Self-Organization of Meiotic Recombination Initiation: General Principles and Molecular Pathways," *Annu. Rev. Genet.*, vol. 48, no. 1, pp. 187–214, 2014.

[176] S. Keeney, C. N. Giroux, and N. Kleckner, "Meiosis-specific DNA double-strand breaks are catalyzed by Spo11, a member of a widely conserved protein family.," *Cell*, vol. 88, no. 3, pp. 375–84, Feb. 1997.

[177] Y. Blat, R. U. Protacio, N. Hunter, and N. Kleckner, "Physical and functional interactions among basic chromosome organizational features govern early steps of meiotic chiasma formation," *Cell*, vol. 111, no. 6, pp. 791–802, 2002.

[178] S. Panizza *et al.*, "Spo11-accessory proteins link double-strand break sites to the chromosome axis in early meiotic recombination," *Cell*, vol. 146, no. 1097–4172 (Electronic), pp. 372–383, Aug. 2011.

[179] J. Sollier *et al.*, "Set1 is required for meiotic S-phase onset, double-strand break formation and middle gene expression," *EMBO J.*, vol. 23, no. 9, pp. 1957–1967, May 2004.

[180] K. Yamashita, M. Shinohara, and A. Shinohara, "Rad6-Bre1-mediated histone H2B ubiquitylation modulates the formation of double-strand breaks during meiosis," *Proc. Natl. Acad. Sci.*, vol. 101, no. 31, pp. 11380–11385, Aug. 2004.

[181] S. E. Tischfield and S. Keeney, "Scale matters: the spatial correlation of yeast meiotic DNA breaks with histone H3 trimethylation is driven largely by independent colocalization at promoters," *Cell Cycle*, vol. 11, no. 8, pp. 1496–1503, Apr. 2012.

[182] N. Robine *et al.*, "Genome-Wide Redistribution of Meiotic Double-Strand Breaks in *Saccharomyces cerevisiae*," *Mol. Cell. Biol.*, vol. 27, no. 5, pp. 1868–1880, Mar. 2007.

[183] T. Fukuda, K. Kugou, H. Sasanuma, T. Shibata, and K. Ohta, "Targeted induction of meiotic double-strand breaks reveals chromosomal domain-dependent regulation of Spo11 and interactions among potential sites of meiotic recombination," *Nucleic Acids Res.*, vol. 36, no. 3, pp. 984–997, Feb. 2008.

[184] C. Grey, F. Baudat, and B. de Massy, "PRDM9, a driver of the genetic map," *PLOS Genet.*, vol. 14, no. 8, p. e1007479, 2018.

[185] T. Hohenauer and A. W. Moore, "The Prdm family: expanding roles in stem cells and development," *Development*, vol. 139, no. 13, pp. 2267–2282, Jul. 2012.

[186] F. Baudat *et al.*, “PRDM9 is a major determinant of meiotic recombination hotspots in humans and mice.,” *Science*, vol. 327, no. 5967, pp. 836–40, 2010.

[187] K. Hayashi, K. Yoshida, and Y. Matsui, “A histone H3 methyltransferase controls epigenetic events required for meiotic prophase,” *Nature*, vol. 438, no. 7066, pp. 374–378, Nov. 2005.

[188] N. R. Powers, E. D. Parvanov, C. L. Baker, M. Walker, P. M. Petkov, and K. Paigen, “The Meiotic Recombination Activator PRDM9 Trimethylates Both H3K36 and H3K4 at Recombination Hotspots In Vivo,” *PLOS Genet.*, vol. 12, no. 6, p. e1006146, Jun. 2016.

[189] E. D. Parvanov, P. M. Petkov, and K. Paigen, “Prdm9 Controls Activation of Mammalian Recombination Hotspots,” *Science (80-.).*, vol. 327, no. 5967, pp. 835–835, Feb. 2010.

[190] F. Smagulova, I. V Gregoretti, K. Brick, P. Khil, R. D. Camerini-Otero, and G. V Petukhova, “Genome-wide analysis reveals novel molecular features of mouse recombination hotspots (suppl.),” *Nature*, vol. 472, no. 7343, pp. 375–8, Apr. 2011.

[191] K. Brick, F. Smagulova, P. Khil, R. D. Camerini-Otero, and G. V. Petukhova, “Genetic recombination is directed away from functional genomic elements in mice,” *Nature*, vol. 485, no. 7400, pp. 642–645, 2012.

[192] M. Walker *et al.*, “Affinity-seq detects genome-wide PRDM9 binding sites and reveals the impact of prior chromatin modifications on mammalian recombination hotspot usage,” *Epigenetics Chromatin*, vol. 8, no. 1, p. 31, Dec. 2015.

[193] C. Grey *et al.*, “In vivo binding of PRDM9 reveals interactions with noncanonical genomic sites,” *Genome Res.*, vol. 27, no. 4, pp. 580–590, Apr. 2017.

[194] J. Lange *et al.*, “The Landscape of Mouse Meiotic Double-Strand Break Formation, Processing, and Repair,” *Cell*, vol. 167, no. 3, p. 695–708.e16, Oct. 2016.

[195] N. Kleckner, “Chiasma formation: chromatin/axis interplay and the role(s) of the synaptonemal complex,” *Chromosoma*, vol. 115, no. 3, pp. 175–194, Jun. 2006.

[196] R. Kumar, H.-M. Bourbon, and B. de Massy, “Functional conservation of Mei4 for meiotic DNA double-strand break formation from yeasts to mice,” *Genes Dev.*, vol. 24, no. 12, pp. 1266–1280, Jun. 2010.

[197] R. Kumar *et al.*, “MEI4 - a central player in the regulation of meiotic DNA double-strand break formation in the mouse,” *J. Cell Sci.*, vol. 128, no. 9, pp. 1800–1811, May 2015.

[198] E. D. Parvanov *et al.*, “PRDM9 interactions with other proteins provide a link between

recombination hotspots and the chromosomal axis in meiosis," *Mol. Biol. Cell*, vol. 28, no. 3, pp. 488–499, 2017.

[199] K. Luger, T. J. Rechsteiner, and T. J. Richmond, "Preparation of nucleosome core particle from recombinant histones.," *Methods Enzymol.*, vol. 304, pp. 3–19, 1999.

[200] P. . Lowary and J. Widom, "New DNA sequence rules for high affinity binding to histone octamer and sequence-directed nucleosome positioning," *J. Mol. Biol.*, vol. 276, no. 1, pp. 19–42, Feb. 1998.

[201] A. Gansen, K. Tóth, N. Schwarz, and J. Langowski, "Structural Variability of Nucleosomes Detected by Single-Pair Förster Resonance Energy Transfer: Histone Acetylation, Sequence Variation, and Salt Effects," *J. Phys. Chem. B*, vol. 113, no. 9, pp. 2604–2613, Mar. 2009.

[202] A. Gansen, K. Toth, N. Schwarz, and J. Langowski, "Opposing roles of H3- and H4-acetylation in the regulation of nucleosome structure--a FRET study," *Nucleic Acids Res.*, vol. 43, no. 3, pp. 1433–1443, Feb. 2015.

[203] L. Imre *et al.*, "Nucleosome stability measured in situ by automated quantitative imaging.," *Sci. Rep.*, vol. 7, no. 1, p. 12734, Oct. 2017.

[204] R. S. Sikorski and P. Hieter, "A system of shuttle vectors and yeast host strains designed for efficient manipulation of DNA in *Saccharomyces cerevisiae*.," *Genetics*, vol. 122, pp. 19–27, 1989.

[205] E. Delbarre, B. M. Jacobsen, A. H. Reiner, A. L. Sørensen, and P. Collas, "Chromatin Environment of Histone Variant H3.3 Revealed by Quantitative Imaging and Genome-scale Chromatin and DNA Immunoprecipitation," vol. 21, pp. 1872–1884, 2010.

[206] P. A. Longo, J. M. Kavran, M.-S. Kim, and D. J. Leahy, "Transient mammalian cell transfection with polyethylenimine (PEI).," *Methods Enzymol.*, vol. 529, pp. 227–40, 2013.

[207] F. P. Bolte, S., Cordelieres, "A guided tour into subcellular colocalization analysis in light microscopy," *J. Microsc.*, vol. 224, pp. 213–232, 2006.

[208] N. Dross *et al.*, "Mapping eGFP Oligomer Mobility in Living Cell Nuclei," *PLoS One*, vol. 4, no. 4, 2009.

[209] L. Halász *et al.*, "RNA-DNA hybrid (R-loop) immunoprecipitation mapping: an analytical workflow to evaluate inherent biases," *Genome Res.*, vol. 27, no. 6, pp. 1063–1073, Jun. 2017.

[210] R. B. Deal, J. G. Henikoff, and S. Henikoff, "Genome-Wide Kinetics of Nucleosome Turnover Determined by Metabolic Labeling of Histones," *Science (80-.).*, vol. 328,

no. 5982, pp. 1161–1165, 2010.

[211] M. F. Dion, T. Kaplan, M. Kim, S. Buratowski, N. Friedman, and O. J. Rando, "Dynamics of Replication-Independent Histone Turnover in Budding Yeast," *Science (80-.).*, vol. 315, no. 5817, pp. 1405–1408, Mar. 2007.

[212] C. R. Lickwar, F. Mueller, and J. D. Lieb, "Genome-wide measurement of protein-DNA binding dynamics using competition ChIP," *Nat. Protoc.*, vol. 8, no. 7, pp. 1337–1353, Jun. 2013.

[213] L. Jiao and X. Liu, "Structural basis of histone H3K27 trimethylation by an active polycomb repressive complex 2 A tripartite gene silencing complex," *Science (80-.).*, 2015.

[214] R. S. Sikorski and J. D. Boeke, "In Vitro Mutagenesis and Plasmid Shuffling: From Cloned Gene to Mutant Yeast," *Methods Enzymol.*, vol. 194, no. 1989, pp. 302–318, 1991.

[215] K. W. Dunn, M. M. Kamocka, and J. H. McDonald, "A practical guide to evaluating colocalization in biological microscopy.," *Am. J. Physiol. Cell Physiol.*, vol. 300, no. 4, pp. C723-42, Apr. 2011.

[216] S. Bolte and F. P. Cordelieres, "A guided tour into subcellular colocalisation analysis in light microscopy," *J. Microsc.*, vol. 224, no. 3, pp. 13–232, 2006.

[217] M. Dundr *et al.*, "A kinetic framework for a mammalian RNA polymerase in vivo," *Science (80-.).*, vol. 298, no. 5598, pp. 1623–1626, 2002.

[218] R. D. Phair, S. A. Gorski, and T. Misteli, "Measurement of dynamic protein binding to chromatin in vivo, using photobleaching microscopy.," *Methods Enzymol.*, vol. 375, pp. 393–414, 2004.

[219] B. L. Sprague and J. G. McNally, "FRAP analysis of binding: Proper and fitting," *Trends Cell Biol.*, vol. 15, no. 2, pp. 84–91, 2005.

[220] M. V. Blagosklonny, "Flavopiridol, an inhibitor of transcription: Implications, problems and solutions," *Cell Cycle*, vol. 3, no. 12, pp. 1537–1542, 2004.

[221] P. Brazda *et al.*, "Ligand Binding Shifts Highly Mobile Retinoid X Receptor to the Chromatin-Bound State in a Coactivator-Dependent Manner, as Revealed by Single-Cell Imaging," *Mol. Cell. Biol.*, vol. 34, no. 7, pp. 1234–1245, Apr. 2014.

[222] 4 Michael F. Dion, Tommy Kaplan, Minkyu Kim, Stephen Buratowski and O. J. R. Nir Friedman, "Dynamics of Replication-Independent\nHistone Turnover in Budding Yeast," *Science (80-.).*, no. March, pp. 1405–1408, 2007.

[223] H. Ferreira, J. Somers, R. Webster, A. Flaus, and T. Owen-Hughes, "Histone Tails and

the H3 N Helix Regulate Nucleosome Mobility and Stability," *Mol. Cell. Biol.*, vol. 27, no. 11, pp. 4037–4048, 2007.

[224] K. Lehmann *et al.*, "Effects of charge-modifying mutations in histone H2A α3-domain on nucleosome stability assessed by single-pair FRET and MD simulations," *Sci. Rep.*, vol. 7, no. 1, p. 13303, 2017.

[225] R. K. Yadav *et al.*, "Histone H3G34R mutation causes replication stress, homologous recombination defects and genomic instability in S. pombe," 2017.

[226] K. Xu *et al.*, "EZH2 oncogenic activity in castration-resistant prostate cancer cells is Polycomb-independent.," *Science*, vol. 338, no. 6113, pp. 1465–9, Dec. 2012.

[227] R. Tatavosian *et al.*, "Live-cell single-molecule dynamics of PcG proteins imposed by the DIPG H3.3K27M mutation.," *Nat. Commun.*, vol. 9, no. 1, p. 2080, 2018.

[228] J. Buard, P. Barthès, C. Grey, and B. de Massy, "Distinct histone modifications define initiation and repair of meiotic recombination in the mouse.," *EMBO J.*, vol. 28, no. 17, pp. 2616–24, Sep. 2009.

[229] I. Lam and S. Keeney, "Mechanism and Regulation of Meiotic Recombination Initiation," *Cold Spring Harb. Perspect. Biol.*, vol. 7, no. 1, p. a016634, Jan. 2015.

[230] Y. Imai, F. Baudat, M. Taillepierre, M. Stanzione, A. Toth, and B. de Massy, "The PRDM9 KRAB domain is required for meiosis and involved in protein interactions.," *Chromosoma*, vol. 126, no. 6, pp. 681–695, Dec. 2017.

[231] Q. Q. Sha *et al.*, "CFP1 coordinates histone H3 lysine-4 trimethylation and meiotic cell cycle progression in mouse oocytes," *Nat. Commun.*, vol. 9, no. 1, pp. 1–17, 2018.

[232] H. Tian, T. Billings, and P. M. Petkov, "CXXC1 is not essential for normal DNA double-strand break formation and meiotic recombination in mouse," *PLOS Genet.*, vol. 14, no. 10, p. e1007657, Oct. 2018.

[233] Y. Imai, F. Baudat, M. Taillepierre, M. Stanzione, A. Toth, and B. de Massy, "The PRDM9 KRAB domain is required for meiosis and involved in protein interactions," *Chromosoma*, vol. 126, no. 6, pp. 681–695, Dec. 2017.

[234] L. Székvölgyi and A. Nicolas, "From meiosis to postmeiotic events: Homologous recombination is obligatory but flexible," *FEBS J.*, vol. 277, no. 3, pp. 571–589, 2010.

[235] L. Acquaviva, J. Drogat, P. M. Dehé, C. de La Roche Saint-André, and V. Géli, "Spp1 at the crossroads of H3K4me3 regulation and meiotic recombination," *Epigenetics*, vol. 8, no. 4, pp. 355–360, 2013.

[236] C. R. Lickwar, F. Mueller, S. E. Hanlon, J. G. McNally, and J. D. Lieb, "Genome-wide protein-DNA binding dynamics suggest a molecular clutch for transcription factor

function," *Nature*, vol. 484, no. 7393, pp. 251–255, 2012.

[237] S. Tessé *et al.*, "Asy2/Mer2: An evolutionarily conserved mediator of meiotic recombination, pairing, and global chromosome compaction," *Genes Dev.*, vol. 31, no. 18, pp. 1880–1893, 2017.

[238] M. Stanzione *et al.*, "Meiotic DNA break formation requires the unsynapsed chromosome axis-binding protein IHO1 (CCDC36) in mice," *Nat. Cell Biol.*, vol. 18, no. 11, pp. 1208–1220, 2016.

[239] Z. Duan *et al.*, "A three-dimensional model of the yeast genome.," *Nature*, vol. 465, no. 7296, pp. 363–7, May 2010.

[240] J. Dekker, K. Rippe, M. Dekker, and N. Kleckner, "Capturing Chromosome Conformation," *Science (80-.).*, vol. 295, no. 5558, pp. 1306–1311, Feb. 2002.

[241] M. Simonis *et al.*, "Nuclear organization of active and inactive chromatin domains uncovered by chromosome conformation capture–on-chip (4C)," *Nat. Genet.*, vol. 38, no. 11, pp. 1348–1354, Nov. 2006.